Thesis for the Degree of Doctor of Philosophy

Electrocatalyst Materials for Low-Temperature Hydrogen Fuel Cells

Gerard Montserrat Sisó

CHALMERS

Department of Physics

CHALMERS UNIVERSITY OF TECHNOLOGY

Gothenburg, Sweden 2023

Electrocatalyst materials for low-temperature hydrogen fuel cells

GERARD MONTSERRAT SISÓ

ISBN 978-91-7905-773-2

Doktorsavhandlingar vid Chalmers tekniska högskola
Ny serie nr 5239
ISSN 0346-718X

Department of Physics

Chalmers University of Technology

SE-412 96 Gothenburg

Sweden

Telephone +46 (0)31-772 1000

Cover: Cyclic voltammetry responses for Pd (orange) and PdNi annealed (blue) evaporated thin films in alkaline media with a Ni-rich surface needed to catalyze the hydrogen oxidation reaction (left) and a Pd with a Ni subsurface used to catalyze the oxygen reduction reaction.

Printed at Chalmers Reproservice

Göteborg, Sweden 2023

Electrocatalyst materials for low-temperature hydrogen fuel cells

Gerard Montserrat Sisó
Department of Physics, Division of Chemical Physics
Chalmers University of Technology

ABSTRACT

Fuel cells have emerged as an alternative to satisfy the need of energy systems with net-zero emissions. Although fuel cells date back to the 1800s, it is only during the last decades that research and development has enabled true commercialization. The growing interest in fuel cells implementation goes hand in hand with the decrease in green H_2 production cost, which makes fuel cells a cornerstone in promising energy systems based on H_2. It is crucial that the transport sector shifts towards inexpensive carbon-free fuel alternatives, which is possible with H_2 owing to its high energy density. A broad implementation of fuel cells is, however, impeded by the high cost of fuel cell systems, which can be attributed to the Pt-based catalyst currently used in low-temperature hydrogen fuel cells. As Pt is a scarce expensive material, development of new efficient and inexpensive electrocatalysts is essential for large-scale fuel cells implementation.

Although many strategies have been explored to reduce the amount of Pt without compromising the power output and lifetime, electrocatalyst development is currently hindered by the lack of mechanistic understanding. In order to gain a better understanding of the mechanisms behind the electrochemical reactions in proton exchange membrane fuel cells (PEMFC) and anion exchange membrane fuel cells (AEMFC), this thesis delves into both the fabrication and the characterization of electrocatalysts. A versatile platform was established to study model system catalysts with the aim to test electrocatalytic materials and provide reliable comparisons, making their performance rationalizable in terms of geometric and electronic structure. Pt-rare earth metal (REM) alloys were studied with respect to both their activity and stability towards the oxygen reduction reaction (ORR) in PEMFCs. Measurements with different model systems indicated an overall increase in their specific activity, but it was found that the addition of REM could compromise their stability. Different Ag alloys were studied for the ORR in alkaline conditions. It was found that alloying could improve the binding energy of oxygenated species, which enhances their ORR activity. Hydrogen oxidation reaction (HOR) and ORR activity of PdNi annealed thin films in alkaline media were investigated to pinpoint the mechanism behind the increased activity. This provides insights to the fundamental principles that lead to a good catalyst efficiency, which was also tested with the addition of different ionomers. By providing additional insights on the mechanistic aspects of fuel cell reactions, the presented work takes a step in tailoring new electrocatalytic materials that could eventually outperform bare Pt in terms of both activity and stability while reducing the total fuel cell cost.

Keywords: Fuel Cell, PEMFC, AEMFC, Model System, Electrode, Thin Film, Catalyst, Oxygen Reduction, Hydrogen Oxidation, Nanofabrication, Alloys.

List of Appended Papers

This thesis is based on the work presented in the following papers:

Paper I

Enhanced Oxygen Reduction Activity with Rare Earth Metal Alloy Catalysts in Proton Exchange Membrane Fuel Cells

B. Eriksson, G. Montserrat-Sisó, R. Brown, T. Skála, R. W. Lindström, G. Lindbergh, B. Wickman, C. Lagergren

*Electrochimica Acta 387 (**2021**) 138454*

Paper II

PdNi Thin Films for Hydrogen Oxidation Reaction and Oxygen Reduction Reaction in Alkaline Media

G. Montserrat-Sisó and B. Wickman

*Electrochimica Acta 420 (**2022**) 140425*

Paper III

Tunning the Activity of Silver Alloy Electrocatalysts for the Oxygen Reduction Reaction in Alkaline Media

G. Montserrat-Sisó, B. Wickman

Submitted

Paper IV

Oxygen Reduction Reaction on Pt_3Y Thin Film Catalysts in Gas Diffusion Electrode Cells

G. Montserrat-Sisó*, R. Mohan*, K. Ehelebe, A.W. Jensen, R. Brown, V. Shokhen, M. Escudero-Escribano, S. Cherevko, B. Wickman

In manuscript

Paper V

Oxygen Reduction Reaction Kinetics on a Pt Thin Layer Electrode in AEMFC

E. Marra, H. Grimler, G. Montserrat-Sisó, R. Wreland Lindström, B. Wickman

*Electrochimica Acta 435 (**2022**) 141376*

Paper VI

Core–shell and heterostructured silver–nickel nanocatalysts fabricated by γ-radiation induced synthesis for oxygen reduction in alkaline media

Y. Yang, G. Montserrat-Sisó, B. Wickman, P. Nikolaychuk, I. Soroka

*Dalton Trans., **2022**, 51, 3604*

Paper VII

Fuel Cell Aging and Stability Tests of Pt_3Y Thin Films for Polymer Exchange Membrane Fuel Cells

E. S. Marra, B. Eriksson, G. Montserrat-Sisó, B. Wickman, G. Lindbergh, C. Lagergren

In manuscript

Paper VIII

Ionomer-Catalyst Interactions and the Effect of Solvent Ratio on Oxygen Reduction and Hydrogen Oxidation Reactions

R. Mohan, G. Montserrat-Sisó, D. Pan, V. Shokhen, P. Jannasch, B. Wickman

In manuscript

My contribution to the appended papers

Paper I: I performed the SEM and XPS measurements with the related quantitative and qualitative analysis. I wrote the experimental part of the manuscript as well as part of the analysis section.

Paper II: I fabricated the samples, performed XPS and SEM measurements, as well as qualitative and quantitative XPS analysis, and electrochemical evaluation. I wrote the manuscript.

Paper III: I performed the XPS and XRD measurements and their analysis. I performed all electrochemical evaluation and analysis and I wrote the manuscript.

Paper IV: I performed half of the electrochemical measurements, the EDX and XPS measurements and the corresponding analysis and participated in writing of the manuscript.

Paper V: I performed the SEM analysis and participated in the electrochemical evaluation. I participated in the writing of the manuscript.

Paper VI: I performed the XPS measurements and the corresponding qualitative analysis and assisted with the electrochemical evaluation. I participated in the writing of the manuscript.

Paper VII: I performed the EDX and XPS measurements and the corresponding quantitative and qualitative analysis and assisted with the electrochemical evaluation. I participated in the writing of the manuscript.

Paper VIII: I performed the initial electrochemical measurements, SEM and XPS analysis and participated in the writing of the manuscript.

Related publications not included in this thesis

Paper IX

Hydrogen Evolution Reaction for Vacancy-Ordered i-MXenes and the Impact of Proton Absorption into the Vacancies

H. Lind, B. Wickman, J. Halim, G. Montserrat-Sisó, A. Hellman, J. Rosen

Advanced Sustainable Systems **5**, 2000158 (2021)

Paper X

Tuning Morphology, Composition and Oxygen Reduction Reaction (ORR) Catalytic Performance of Manganese Oxide Particles Fabricated by γ-radiation Induced Synthesis

Z. Li, Y. Yang, A. Relefors, X. Kong, G. Montserrat-Sisó, B. Wickman, Y. Kiros, I. L. Soroka

Journal of Colloid and Interface Science **583**, 71-79 (2021)

Table of Contents

1. Introduction

The Industrial Revolution is a turning point in the history of mankind, which transformed economies based on agriculture and handicrafts into large-scale industry-based economies. Modern civilization has seen thenceforth a tremendous and fast-growing industrialization that, accompanied by growth in human population, has raised the energy demand to unprecedented levels. As society develops and energy consumption grows, concerns for future energy supply and sustainability issues emphasize the need for shifting away from fossil fuels. Combustion of this finite resource is strongly contributing to emissions of anthropogenic greenhouse gases (GHG), which represent an imminent threat to public health and the environment [1]. This, together with the depletion of viable fossil fuel reserves, evidences the necessity of rapid improvements in energy efficiency and the adoption of low-carbon energy alternatives, as well as policies that implement the alternatives effectively.

As a result of the European Green Deal, the European Union (EU) aims to be an economy with net-zero greenhouse gas emissions by 2050 [2]. At the same time, the European Commission estimates that a continuation of the current trends would result in only a 40% reduction in GHG emissions by the same year [3]. This implies that renewable energy sources need to be expeditiously implemented in Europe if the clean energy goals should be met by 2050. Nevertheless, there are uncertainties and constrains involved in a shift towards renewable energies, such as high equipment cost or spatial and temporal mismatch between availability and demand. The problem with the equipment cost may be mitigated by an increase in production volumes together with the simultaneous increase of fossil fuel prices, which will make green fuels competitive. On the other hand, the availability problem may be solved by converting excess energy that cannot be utilized immediately to energy carriers that can be stored, transported and converted to useful forms of energy.

An energy carrier that satisfies the requirements is hydrogen, the most abundant chemical substance in the universe and third most abundant element in the Earth's crust [4]. Hydrogen represents a promising energy carrier thanks to its potential to be used as a power supply for almost all devices using fuel-based energy. Moreover, it also presents

the advantage of long-term energy storage, long distance transport, high energy density and light weight [5]. However, there are still challenges such as hydrogen storage, cost of production and infrastructure that have to be overcome. Besides the mentioned problems with hydrogen as an energy carrier, challenges also arise in the production of hydrogen. Currently, around 95% of hydrogen is produced from fossil fuels (grey hydrogen) [6], which gives rise to significant amounts of CO_2. Net-zero emissions hydrogen production can also be carried out by splitting natural gas with an additional CO_2 capture process (blue hydrogen), although it only provides a short-term solution [7]. Thus, in the long-term, carbon-neutral hydrogen sources must be considered to make hydrogen a clean energy alternative.

Water is one of the most abundant and inexhaustible raw materials in Earth and can be used for H_2 production through water-splitting processes, of which electrolysis is the most effective [8]. Water electrolysis is a commercially available electrochemical technology that can produce hydrogen from electricity with oxygen as the only by-product, making this hydrogen the cleanest energy carrier that could be used provided that the electricity is produced in a sustainable way (green hydrogen) [9]. Hydrogen obtained from water electrolysis presents the advantage of high purity after removal of oxygen impurities, which is a critical feature in several applications [10]. More importantly, the integration of large-scale water electrolysis into the power grid can mitigate the discordance between clean energy availability and demand by immediately converting renewable electricity into hydrogen that can be stored and used on-demand [11]. However, power-to-power electricity storage based on hydrogen requires an efficient energy conversion (both from electricity to hydrogen and vice versa) in order to make the storage of renewable energy profitable.

Hydrogen produced via water electrolysis is one of the potential applications of the fundamental electrochemical mechanism through which energy carriers can be produced. However, electrochemical methods involving hydrogen are not limited to green hydrogen production. Numerous electrochemical devices are used for storage of energy carriers, such as batteries [12] and supercapacitors [13]. However, other electrochemical devices such as fuel cells commonly use high-purity hydrogen as a fuel from electrolysis. In fact, hydrogen fuel cells operate like an electrolyzer in reverse: they combine hydrogen and oxygen to produce electricity and water (Fig. 1.1). Although they are often compared to batteries because both convert energy produced by a chemical reaction into usable electric power, fuel cells have the additional feature of producing electricity as long as fuel, i.e. hydrogen, is supplied. Thus, fuel cells present the advantage over batteries in that they do not run down or need recharging. More importantly, fuel cells use a

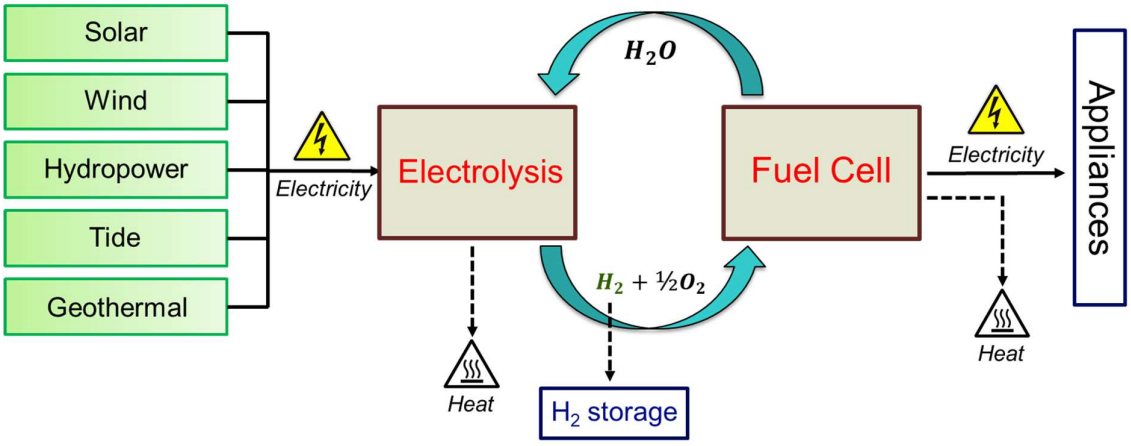

Figure 1.1 Schematic illustration of the production of green hydrogen and its use in carbon-free power generation.

renewable energy source and they do not release any harmful substances, which make them highly sustainable power generators.

There are many types of fuel cells considered for a wide range of applications, from small portable devices to large-scale stationary power generation systems. They all consist of an anode, a cathode and an electrolyte that allows the transport of charge carriers, i.e. ions, from the anode to the cathode. At the same time, an electron flow produced by a chemical reaction occurring inside the fuel cell travels from the anode to the cathode through an external circuit, which generates an electric current. The different fuel cell types have intrinsic differences in their operating conditions, components and fuel. They are often classified by the type of electrolyte they use, which dictates their operating temperature range. This temperature, as well as the useful life of the fuel cell, commands the properties of the other materials used in the cell components. Low-temperature hydrogen fuel cells, which is the topic of this thesis, are the most viable option for vehicles, portable devices and small stationary power.

Proton exchange membrane fuel cells (PEMFCs), which operate at low temperatures, is the most widely studied category of fuel cells. The PEMFC was invented during the 1960s and since then has been considered a promising candidate as a power source due to its low operating temperature and high power density. However, it has not been until the last two decades that the PEMFC has reached wide commercialization [14]. Today there are commercially available systems that use PEMFC technology within transport, as well as stationary and portable power generation. Examples of vehicles that use fuel cells as a source of power (FCV), are Toyota Mirai, Honda Clarity and Hyundai Nexo, as well as busses fleets [15]. Similarly, PEMFCs are also currently used for small-scale power demands (<10 kW) in for example domestic applications [16]. However, the world-wide commercialization of PEMFC has not come yet owing to two major technical

barriers: durability and cost. Durability issues arise from the degradation that fuel cell components, such as the membrane electrode assembly (MEA), suffer during long-term operation. For transportation powered with direct hydrogen fuel cell systems, the U.S. Department of Energy (DOE) has set a target of 8,000 hours of durability in automotive load cycles with a 65% peak energy efficiency by 2025 [17]. For state-of-the-art PEM fuel cells, however, lifetime decreases with decreasing platinum group metal (PGM) loading in the catalyst layer, which accounts for approximately 40% of the total fuel cell cost at high volume production. The high cost of the catalyst layer arises from the scarcity of Pt, which is commonly used as electrocatalyst [18]. Thus, both the lifetime and cost issues that hinder the large-scale commercialization of PEMFCs are related to the metal that catalyzes the fuel cell electrochemical reactions. Along these lines, the DOE has established a cost target of 30 \$/kW with a total PGM content of ≤ 0.10 g_{PGM}/kW at high volume production by 2025 [17,19]. Several strategies have been adopted with the aim to decrease the cost of the catalyst layer and, thus, facilitate the wide-spread implementation of PEMFCs, including better Pt utilization through material optimization or alloying with less expensive metals [20–22]. Nonetheless, state-of-the-art PEM systems are still far from the ultimate desired cost and durability set by the DOE and other alternatives started gaining prominence.

The anion exchange membrane fuel cell (AEMFC) has recently gained increased attention in the fuel cell research community motivated by the intrinsic advantages over their acidic analog, including more facile cathode kinetics, minimized corrosion problems and a wider range of materials stable in the fuel cell environment [23]. The most prominent merit of AEMFCs is the possibility to use non-noble metal electrocatalysts thanks to milder alkaline conditions, which opens up new possibilities of finding less expensive catalyst materials without compromising the power density of the fuel cell. Thus, during the last decade, much fuel cell research has focused on finding efficient inexpensive catalytic materials that could potentially bring the AEMFC technology to the frontline of the low-temperature fuel cell market [24]. Although there are a number of major issues that still remain to be resolved for the AEMFC technology, such as MEA poor performance [25], their successful application can already be foreseen with continuous industrial and policy support.

To summarize, there are currently numerous issues that impede the global implementation of carbon-free technologies with net-zero GHG emissions for energy utilization. However, during the last decades, the awareness of the need for green energy sources and sustainable energy utilization to palliate the sequels of human activities has grown hand in hand with the development of devices that could (and can) make it happen. The successful implementation of the already existing technologies demonstrates

the feasibility of such technologies and, together with competent policies, provides the impetus needed to shift towards a development completely independent from fossil fuels. In this way, the eventual deployment of efficient and profitable electrolysis and fuel cell systems will certainly lead to a turning point as revolutionary for modern civilization as the Industrial Revolution.

1.1 Scope of this thesis

The overall aim of this thesis is to contribute to the development of low-temperature fuel cell systems and thus accomplish a sustainable and resource-efficient energy supply without GHG net emissions. By providing a better understanding of the mechanisms through which the electrochemical reactions occur in fuel cells, new inexpensive and efficient catalysts can be tailored. In this way, the cost and durability barriers on widespread commercialization of low-temperature fuel cells can be overcome, thereby facilitating the implementation of a sustainable fossil-free energy system.

In this thesis, which is partly based on previous work published by the same author [26], physical vapor deposition methods such as thermal deposition and sputtering are employed to fabricate thin-film catalysts for both PEMFCs and AEMFCs. The electrocatalytic materials have been used to study the hydrogen oxidation (anode) and oxygen reduction (cathode) reactions. A major part of this work has been focused on increasing the understanding of the reaction mechanisms in both alkaline and acidic media, providing key knowledge for the unclear mechanism of the reaction in alkaline conditions. Another part of this work has been dedicated to the fabrication of thin-film model electrodes that have been evaluated in a fuel cell system with the aim to study the thin-film catalysts under realistic fuel cell conditions. These model systems have been used to isolate the catalyst contribution and provide a reliable comparison between catalyst materials and thus bridge the gaps between fundamental and applied fuel cell research. Thin-film catalyst fabrication and electrochemical evaluation in liquid half-cell have been conducted at Chalmers, as well as physical characterization by spectroscopy (X-ray Photoelectron Spectroscopy [XPS] and energy-dispersive X-ray spectroscopy [EDX]), microscopy (SEM) and X-ray diffraction (XRD). Fruitful collaborations with the Applied Electrochemistry Department at the Royal Institute of Technology (KTH) in Stockholm resulted in measurements of both activity and stability, as well as kinetic reaction studies, of Pt and Pt-based alloy thin-film catalysts fabricated at Chalmers, whose physical characterization was also carried out at Chalmers. As a result of a collaboration with both University of Erlangen–Nuremberg and the University of Copenhagen, the catalytic performance of a Pt-Y thin-film alloy was further investigated in gas diffusion electrode (GDE) half-cell setups, whose inter-lab comparison shortened

the gap between lab-scale and applied fuel cell Pt-Y catalyst research. Another collaboration with the Applied Physical Chemistry Department at KTH allowed the electrochemical characterization of nanoparticles-based catalysts produced via radiation synthesis which, together with X-ray diffraction (XRD) and XPS measurements. Lastly, ionomers synthesized at the Center for Analysis and Synthesis in Lund University were both electrochemically evaluated and physically characterized at Chalmers in order to further provide insights on the best practices to obtain the utmost beneficial effect from ionomer addition.

2. Electrochemistry

The *Journal of Natural Philosophy, Chemistry and the Arts*, which was the first monthly independent scientific journal, had one of the earliest references to electrochemistry back in 1829. It was defined as 'one of the connecting branches between remote divisions of the Philosophy of Nature' [27]. Thus, although electrochemistry is often labelled as a discipline within Physical Chemistry, the truth is that it is not solely physics nor chemistry, but actually encompasses a vast range of science from biology to material science. In fact, the birth of electrochemistry was marked by a discovery in the field of biology back in the 18th century.

In 1786, the Italian anatomist Luigi Galvani discovered that the leg muscles of a dead frog twitched when struck by an electrical spark, which he termed as 'animal electricity'. Shortly after, another Italian scientist Alessandro Volta refuted Galvani's finding by proposing that electricity was generated because of two dissimilar metals in contact with each other through a moist conductor. He further proved his hypothesis by reproducing Galvani's system with pairs of zinc and silver disks connected by brine-soaked cardboard, which generated electricity. This became the first example of a practical battery, the so-called 'Voltaic pile'. During the same time, English researchers Nicholson and Carlisle used Volta's configuration to separate water into its constituent elements by passing electricity through it, which is now known as "electrolysis". They published their findings in 1800 in the *Journal of Natural Philosophy, Chemistry and the Arts*, where Nicholson was the editor [28]. Using the same concept, Humphrey Davy used the electricity generated by the pile to separate different compounds into their constituents and realized that the electricity produced depended on the occurrence of chemical reactions. In this way, he discovered several new elements such as potassium, sodium, calcium and magnesium. Davy's student and successor, Michael Faraday, pursued the relationship between electricity and magnetism and invented the electric motor and the dynamo. He also predicted the relationship between the applied current and the amount of chemical product generated through a process that he named "electrolysis". His two laws of electrolysis were published in 1834 and are still fundamental to industrial electrolytic production of chemicals [27,29].

The laws of electrolysis established by Faraday back in 1834 set the bases of the modern definition of electrochemistry: 'a branch of chemistry concerned with the relations between chemical and electrical phenomena, especially with reactions occurring at the point of contact of an electrical conductor and a conducting liquid' [30]. Thus, electrochemistry can be defined as the study of interfaces, where interactions between phases containing electrons (electrode) and phases containing ions (electrolyte) take place. The chemical processes that occur between these phases involve an electron transfer to or from an ion changing its oxidation state, either through the application of an external voltage (electrolytic cell) or through the release of chemical energy in a spontaneous reaction (galvanic cell). These electron transfer reactions are known as 'redox', which stands for reduction-oxidation, being *reduction* the gain of electrons (i.e. decrease of the oxidation state) and *oxidation* the loss of electrons (i.e. increase in the oxidation state) of an atom. Similar to acid-base reactions, these processes occur simultaneously and cannot occur independently of one another. Hence, both reduction and oxidation processes are considered "half-reactions" and redox constitutes the "whole reaction".

As all reactions, redox reactions are driven by the difference between the energy states of their reactants and products, which in the case of electron transfer reactions, corresponds to the difference in electrochemical potential. Once the potential difference is balanced out, the reaction is considered to be in thermodynamic equilibrium and there is no net flux of electrons. Thus, as in any other chemical reaction, the rate of redox reactions is governed by the principles of thermodynamics.

2.1 Thermodynamics: Equilibrium and Nernst Equation

Thermodynamic equilibrium is of special interest for electrochemical reactions in both galvanic and electrolytic cells, which require the non-equilibrium of the redox reaction to produce electrical and chemical energy respectively. Hence, determination of electrochemical equilibrium is crucial for the study of electron transfer reactions [31].

Considering the following redox reaction with n electrons transferred:

$$Ox + n\,e^- \rightleftharpoons Red$$

thermodynamics dictate that the Gibbs free energy (ΔG) of a reaction is related to the free energy change under standard conditions (ΔG^o), i.e. 1 atm and 273.15 K, by:

$$\Delta G = \Delta H - T\Delta S = \Delta G^o + RTlnQ_r \tag{2.1}$$

where Q_r is the reaction quotient, R the gas constant and T absolute temperature.

For an electrochemical system, the maximum possible voltage of the cell is at zero current, which is used to calculate the maximum possible electrical energy that could be obtained from a chemical reaction ($W_{electrical}$). Thus, since ΔG is the maximum amount of work that can be extracted from a system, it can be expressed as:

$$W_{max} = W_{electrical} = \Delta G = -nFE_{cell} \tag{2.2}$$

being F the Faraday constant (96485 C/mol). ΔG is also related to the cell potential (E_{cell}) under general conditions (standard or not). Similarly, ΔG^o and E^o are related by the same relation. Hence, combining Eq. 2.1 and Eq. 2.2 gives:

$$-nFE_{cell} = -nFE^o_{cell} + RTlnQ_r \tag{2.3}$$

by dividing by the amount of charge transferred (i.e. $-nF$) leads to the Nernst equation for a redox reaction:

$$E_{cell} = E^o_{cell} - \frac{RT}{nF} lnQ_r \tag{2.4}$$

which relates the reduction potential of an electrochemical reaction to the standard electrode potential.

The Nernst equation states that the E_{cell} depends on the relative amount of products and reactants (i.e. Q_r). As the redox reaction proceeds, reactants are consumed and product concentration increases. The potential of the cell gradually decreases until the reaction is at equilibrium, at which $\Delta G = 0$ and $Q_r = K_{eq}$, so $E_{cell} = 0$. As shown in Eq. 2.2, positive cell potential gives a negative ΔG, indicating spontaneous electrochemical reaction. Thus, a positive cell potential is needed for the generation of electric current, which is the basis of batteries and fuel cells. Conversely, a positive ΔG indicates a non-spontaneous reaction ($E_{cell} < 0$) and thus electric current should be applied for the redox to occur, which is the principle of electrolytic cells [31,32].

Since the cell potential corresponds to the difference between cathode (reduction) and anode (oxidation) potentials:

$$E_{cell} = E_{red} - E_{ox} \tag{2.5}$$

the Nernst equation can also be used to study half-cell reactions with:

$$E_{red} = E^o_{red} - \frac{RT}{nF} ln \frac{a_{red}}{a_{ox}} \tag{2.6}$$

Essentially, the Nernst equation relates the reduction potential of a half or full cell reaction to the concentrations of the chemical species being reduced or oxidized, i.e. the position of the redox reaction equilibrium. However, the Nernst equation does not describe how fast the system reaches equilibrium and, since reactions could be prevented from reaching equilibrium by their kinetic limitations, the study of the reaction kinetics at the electrode surface is of crucial importance for electrochemical reactions.

2.2 Electrode Kinetics and Overpotential

The kinetics of electrode reactions can be treated in a completely analogous way to solution-phase reactions, but with the added dimension of electric potential.

Again, considering the following reversible one-step redox reaction:

$$Ox + n\,e^- \underset{k_{ox}}{\overset{k_{red}}{\rightleftharpoons}} Red \tag{2.7}$$

the dependence of the reaction rate constants on temperature can be described by the Eyring-Polanyi equation, an Arrhenius-like equation that define the transition state theory [33]:

$$k_{red} = \frac{k_B T}{h} e^{\frac{-\Delta G^{\ddagger}_{red}}{RT}}; k_{ox} = \frac{k_B T}{h} e^{\frac{-\Delta G^{\ddagger}_{ox}}{RT}} \tag{2.8}$$

Where $\Delta G^{\ddagger}$ is the Gibbs free energy of activation, which corresponds to the free energy of the transition state (TS), as depicted in Fig. 2.1.

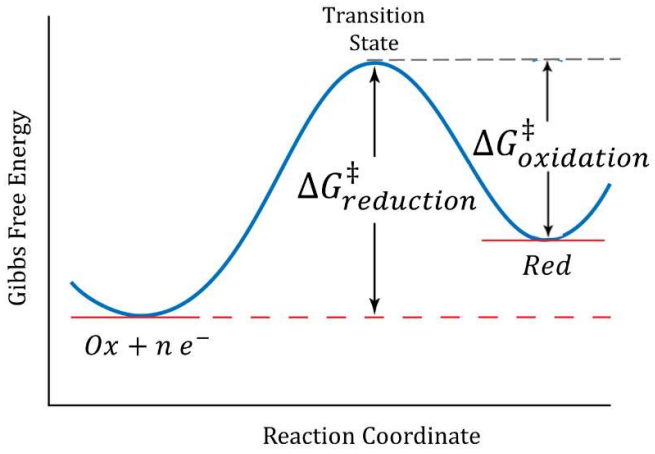

Figure 2.1 Gibbs free energy curve for a redox reaction. $\Delta G^{\ddagger}_{ox}$ represents the minimum amount of free energy required to transform *Ox* into *Red* (i.e. reduction) and $\Delta G^{\ddagger}_{red}$ for oxidation. The value of $\Delta G^{\ddagger}$ is equivalent to the difference in free energy between the initial state and the transition state.

The forward and backward reaction rates (r_{red} and r_{ox}) can be taken as the expressions for first-order chemical reactions. However, reaction rates for redox reactions must bring in a measurable voltage, which is when the Faraday's law of electrolysis comes in (i.e. the current is directly related to the rate of the reaction):

$$r_{red} = k_{ox}c_{Red} = \frac{j_{red}}{nF} \;\; ; \;\; r_{ox} = k_{ox}c_{Red} = \frac{j_{ox}}{nF} \tag{2.9}$$

Where j_{red} and j_{ox} are the reduction and oxidation current densities respectively. Henceforth, we will be referring to *current* as a faradaic current, i.e. current generated by any chemical reaction involving an electron transfer. The net rate of the redox reaction (r) and net current density (j) can be written as:

$$r = r_{ox} - r_{red} = k_{ox}c_{Red} - k_{ox}c_{Red} = \frac{j_{ox} - j_{red}}{nF} = \frac{j}{nF} \tag{2.10}$$

The oxidation reaction dominates if $r>0$ and the reduction command the net rate if $r<0$. In electrochemistry, an additional electrode potential relative to the equilibrium potential, i.e. beyond the thermodynamic requirement, is needed to drive reactions at a certain rate. The magnitude of the deviation of the potential (E) from the equilibrium value ($E_{eq.}$) is known as *overpotential*:

$$\eta = E - E_{eq.} \tag{2.11}$$

If the electrode is polarized to a greater potential than at equilibrium, η is positive and oxidation occurs. If instead the electrode is polarized to a smaller potential than at equilibrium, then η is negative and reduction takes place. Thus, application of an E greater than $E_{eq.}$, so that $\eta>0$, reduces the activation barrier of the oxidation ($\Delta G_{ox}^{\ddagger}$) by $(1-\alpha)F(E-E_{eq.})$ and that for the reduction increases by $\alpha F(E-E_{eq.})$. α where the TS is along the reaction coordinate. Since the current density depends on the Gibbs free energy of the TS, α determines the dependence of the current density on overpotential. Hence, the value of α is between 0 and 1, being α=0.5 when the TS lies symmetrically with respect to *Ox* and *Red* and, thus, j_{ox} and j_{red} have the same absolute value at the same overpotential [32].

Under the application of an overpotential, the Gibbs free energies of activation for cathodic (reduction) and anodic (oxidation) reactions become:

$$\Delta G_c^{\ddagger} = \Delta G_{0,c}^{\ddagger} - \alpha F\big(E - E_{eq.}\big) \tag{2.12a}$$

$$\Delta G_a^{\ddagger} = \Delta G_{0,a}^{\ddagger} - (1-\alpha)F(E - E_{eq.}) \tag{2.12b}$$

bringing these expressions into the reduction and oxidation rate constants (Eq. 2.8) leads to:

$$k_{red} = \frac{k_B T}{h} e^{(-\frac{\Delta G^{\ddagger}_{0,c}}{RT})} e^{[-\frac{\alpha F}{RT}(E - E_{eq.})]} \tag{2.13a}$$

$$k_{ox} = \frac{k_B T}{h} e^{(-\frac{\Delta G^{\ddagger}_{0,a}}{RT})} e^{[\frac{(1-\alpha) F}{RT}(E - E_{eq.})]} \tag{2.13b}$$

where $\Delta G^{\ddagger}_{0,c}$ and $\Delta G^{\ddagger}_{0,a}$ are the activation Gibbs free energies of the TS when the reaction is at equilibrium (i.e. no overpotential). Since at equilibrium the net current is 0 (η=0 and $E = E_{eq.}$) and both oxidation and reduction rate constants have the same value, Eq 2.13a and 2.13b can be written as:

$$k_{red} = \frac{k_B T}{h} e^{(-\frac{\Delta G^{\ddagger}_{0,c}}{RT})} = k_0 \tag{2.14a}$$

$$k_{ox} = \frac{k_B T}{h} e^{(-\frac{\Delta G^{\ddagger}_{0,a}}{RT})} = k_0 \tag{2.14b}$$

where the constant k_0 is the standard rate constant, which brings all the non-electrochemical terms together.

Accordingly, if we merge Eq. 2.10. 2.11 and 2.13, we can now write an equation relating the electrode potential (E) to the observed current density (j) as:

$$j = j_{ox} - j_{red} = nF[c_{red} k_{ox} - c_{ox} k_{red}] = nF k_0 [c_{red} e^{\left(\frac{(1-\alpha)F\eta}{RT}\right)} - c_{ox} e^{\left(-\frac{\alpha F \eta}{RT}\right)}] \tag{2.15}$$

Even though $j = 0$ at the equilibrium potential, the oxidation and reduction current densities are not. The value of the oxidation (and reduction) current density is called the exchange current density (j_0), which is the current at zero overpotential and, from Eq. 2.15, it can be written in terms of either reduction or oxidation as:

$$j_0 = j_{ox} = j_{red} = nF k_0 c_{red} e^{\left(\frac{(1-\alpha)F\eta}{RT}\right)} = nF k_0 c_{ox} e^{\left(-\frac{\alpha F \eta}{RT}\right)} \tag{2.16}$$

The j_0 greatly determines the overall kinetics, with large values of j_0 indicating that high current densities are already reached at small overpotentials and thus fast electrode kinetics. Inserting Eq. 2.16 into Eq. 2.15 leads to the Butler-Volmer reaction for $n = 1$ reactions:

$$j = j_{ox} - j_{red} = j_0 [e^{\left(\frac{(1-\alpha)F\eta}{RT}\right)} - e^{\left(-\frac{\alpha F \eta}{RT}\right)}] \tag{2.17}$$

which show that anodic and cathodic current densities will increase or decrease exponentially with overpotential and the slope will depend on α.There are two limiting cases in the Butler-Volmer equation (Fig. 2.2a):

A) The low overpotential region ($|\eta|$ < ca. 10 mV):

At such small values of η, the exponents in Eq. 2.17 are small enough to allow for the expansion of both exponential terms according to $e^x \approx 1+x$ for very small x. We can thus linearize the exponential terms to obtain:

$$j = j_{ox} - j_{red} = j_0 \left[1 + \frac{(1-\alpha)F\eta}{RT} - \left(1 - \frac{\alpha F\eta}{RT}\right)\right] = j_0 \frac{F\eta}{RT} = \eta R_{ct} \qquad (2.18)$$

where $R_{ct} = j_0 F/RT$, the charge-transfer resistance. Hence, in this region, a linear current-voltage dependence in the form of Ohm's law is found, which can be used to determine the exchange current density.

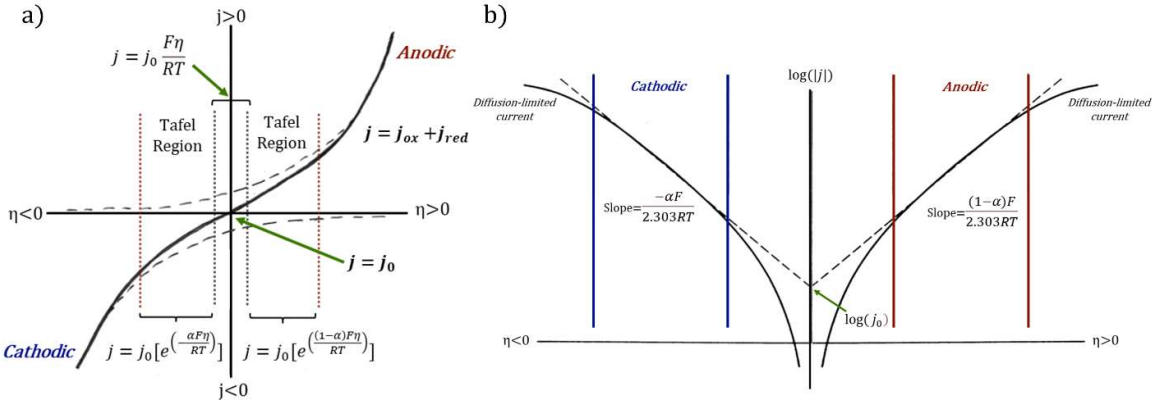

Figure 2.2 (a) Current-overpotential curve for a system with one electron transfer (n=1) and α=0.5 with the two regions for the limiting cases of the Butler-Volmer equation and **(b)** Tafel plots for anodic and cathodic branches for the same system**.** Adapted from [32].

B) The high overpotential region ($|\eta|$ > ca. 100 mV):

For large values of $|\eta|$, one of the partial current densities dominates so that the opposite reaction in Eq. 2.17 becomes small enough to be considered negligible. The two possibilities are:

B.1) Cathodic currents dominate:

Then $\eta \ll 0$ and thus: $j \approx j_{red}$ and $j_{ox} \approx 0$, leading to: $j = j_0[e^{\left(-\frac{\alpha F\eta}{RT}\right)}]$ (2.19a)

B.2) Anodic currents dominate:

Then $\eta \gg 0$ and thus: $j \approx j_{ox}$ and $j_{red} \approx 0$, becoming: $j = j_0\left[e^{\left(\frac{(1-\alpha)F\eta}{RT}\right)}\right]$ (2.19b)

Taking logarithms to the base 10 in Eq. 2.19a and 2.19b, we can write:

$$(cathodic) \qquad \log(j) = \log(j_0) - \frac{\alpha F \eta}{2.303RT} \tag{2.20a}$$

$$(anodic) \qquad \log(j) = \log(j_0) + \frac{(1-\alpha) F \eta}{2.303RT} \tag{2.20b}$$

for cathodic and anodic currents respectively. If we want to express Eq. 2.20a and 2.20b in terms of overpotential, at for instance high cathodic currents, it becomes:

$$(cathodic) \qquad \eta = \left(\frac{2.303RT}{\alpha F}\right) \log(j_0) - \left(\frac{2.303RT}{\alpha F}\right) \log(|j|) \tag{2.21a}$$

$$(anodic) \qquad \eta = \left(\frac{2.303RT}{(1-\alpha) F}\right) \log(j_0) - \left(\frac{2.303RT}{(1-\alpha) F}\right) \log(|j|) \tag{2.21b}$$

These equations can also be written in the form of:

$$\eta = A + B \log(|j|) \tag{2.22}$$

which is known as the Tafel equation, which also gives name to the Tafel region (Fig. 2.2a), This equation expresses how the current varies exponentially with overpotential. By plotting $\log(|j|)$ vs. η, we can extract the α from the slope of the plot and the value of j_0 from the intercept with the ordinate (Fig. 2.2b).

As shown in Fig. 2.2b, the current-overpotential plots deviate sharply from linear behavior as η approaches zero. The deviation from linear behavior arises because the back reactions cannot be considered negligible and, thus, the reaction cannot longer be treated as irreversible. At high values of η, the net current density reaches a limiting value because the reaction rates become limited by diffusion of reactants to the electrode. Hence, transport of reactants to the electrode surface where the charge transfer takes place is of crucial importance for heterogeneous electron transfer reactions [31–33].

2.3 The Electrochemical Double Layer

The charge transfer processes that give rise to the current are governed by the properties of the interface formed by a charged electrode surface immersed in an electrolyte, which influences the electrochemical response of the electrolyte/electrode system. Aqueous electrochemical interfaces differ from other interfaces in that they are governed by potential-dependent interactions between water molecules and species found in the so-called *electrical double layer* (EDL) [34]. Two types of physicochemical interactions control the structure of the double layer in aqueous electrolytes: interactions between adsorbates and the electrode, which are chemical in nature (chemisorption and electron transfer), and electrostatic metal-ion forces that attract ions in the vicinity of the

electrode but do not involve metal-adsorbate bonding. The first layer, governed by chemical interactions, is a two-dimensional surface with a non-zero electric charge (either positive or negative depending on the applied potential) and it is known as the *Helmholtz layer*. The second layer, which arises from long-range Coulombic forces, is made of free solvated ions whose movement is driven by electrostatic attractions and is called the *diffuse layer*. These two regions at the electrode/electrolyte interface form the double layer (Fig. 2.3, top) [35,36].

Since the conception of the EDL in the 19th century by Helmholtz, it has been refined to describe the details. Nowadays the Goüy-Chapman-Stern model (GCS) is the most commonly used model to explain the structures involved in the EDL [37]. In this model, the EDL is divided into the same two layers explained above, but they incorporated the electric potential response as a function of distance from the electrode surface: a first layer formed by ions of opposite charge to those on the electrode in which the potential drop is linear, and a second layer of solvated ions after which the potential decreases exponentially (Fig. 2.3, bottom) [32].

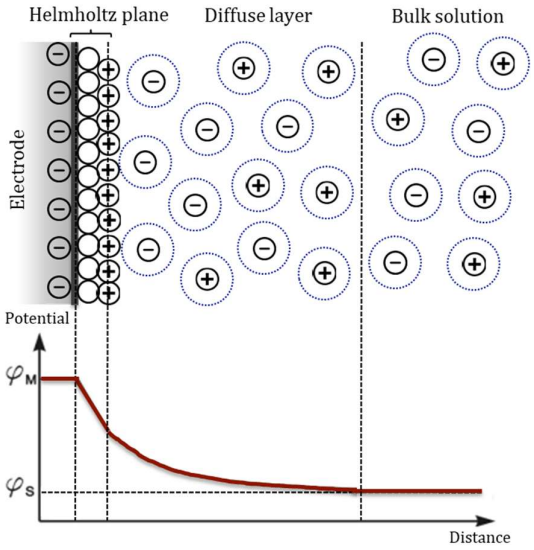

Figure 2.3 Schematic illustration of the structure (top) and potential distribution (bottom) of the electrical double layer according to the Goüy-Chapman-Stern model. ϕ_M and ϕ_S represent the metal and solution electric potentials respectively [36].

Although the EDL is always composed of two layers, the charge of the ions in the vicinity of the electrode surface depends on the electrode potential. If a potential is applied across an electrolyte (i.e. between two electrodes), the ions in the electrolyte migrate along the electric field, resulting in the polarization of the electrolyte and the build-up of the EDL at each electrode. If the potential is reversed, the electrodes will switch over their charge and ions will migrate towards the opposite electrode. However, at short timescales the ions do not have time to move from one electrode to the other and the electrolyte acts

like a dielectric material with a uniform potential drop over the electrolyte. With a continuous change of the electrode potentials, the EDLs build-up along the interface and the potential drop becomes more pronounced within the EDL. At longer timescales, if a constant changing potential is applied long enough to establish a steady state condition, the potential drop will become completely concentrated at the EDLs, where the electric field is very high [31,36]. Thus, the double layer behaves as a conventional capacitor, in which the stored electrical charge is linearly dependent on voltage. The electrical double layer capacitance is given by:

$$C = \frac{\partial Q}{\partial E} \tag{2.23}$$

where Q is the stored charge, E the applied potential. Capacitance is usually measured in μF/cm^2. Applying a potential difference in an electrode/electrolyte system results in charge accumulation within the electrical double layer, which gives rise to non-Faradaic (capacitive) currents [31].

2.4 Transport

As explained in the previous sections, the generated faradaic current is a direct measure of the rate of the electrochemical reaction at the electrode surface, which depends on the applied potential. The current itself is dependent upon two rates [38]:

(i) the rate at which electrons transfer occurs across the interface between the electrode and the solution, known as *charge transfer* rate.
(ii) the rate at which reactants are provided from the bulk solution to the electrode and products removed from the electrode, known as *mass transport* rate.

As in any other chemical reaction influenced by its kinetics, the slowest of these rates will determine the rate of the overall reaction. Thus, both mass transport and charge transfer rates will dictate the concentrations of the reactants (O) and products (R) at the electrode surface, which at the same time are dictated by them (Fig. 2.4).

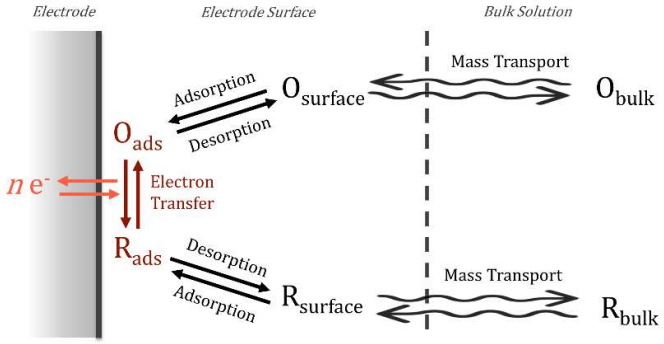

Figure 2.4 Schematic illustration of the different steps during an electrochemical reaction as a function of the distance from the electrode surface.

Charge Transfer

Although the term *charge transfer* is used in electrochemistry to refer to electron transfer processes at the electrode, in galvanic cells this term is often used to denote both the flux of electrons within the electrode and the flux of ions in the electrolyte. This rate is governed by the applied potential across the electrodes, as evidenced by the proportionality between potential and current derived in the preceding section.

In electrochemical systems, such as fuel cells, the voltage responsible for the charge transfer represents a loss which obeys Ohm's law (i.e. Ohmic loss): $V = iR$. This Ohmic loss depends on both the current that flows through the electrode and the resistance of the conducting media (e.g. electrolyte for ions). Hence, the total voltage loss in an electrochemical system is the summation of all Ohmic resistances, including electrodes and electrolyte resistance. However, for the majority of systems, the ionic conductivity in the electrolyte is generally the major contributor to the Ohmic resistance. The overall Ohmic resistance can be mitigated by: i) using electrolytes with high ionic conductivity, ii) using highly conductive electrodes, and iii) reducing the distance between electrodes [33,38].

Mass Transport

Since the generation of current needs the constant addition of reactants and constant removal of products, the transport of these from the bulk solution to the electrode surface is essential for any electron transfer reaction. There are three basic mechanisms of mass transport:

a) *Diffusion*: random movement of molecules driven by the concentration gradient between a region of high concentration of molecules and a region with low concentration. The rate of diffusion therefore depends on the concentration gradient and on the diffusion coefficient.
b) *Migration*: movement of charged particles (e.g. protons) in response to an electric field. It depends on the applied potential and is proportional to the charge of the ions, their diffusion coefficient and the ion concentration.
c) *Convection*: forced movement of the species in solution by an external mechanical force, e.g. stirring.

Although the utilization of the Butler-Volmer equation (Eq. 2.17) in electrochemistry is broad, it assumes that the concentrations at the electrode surface are the same as that of the bulk solution. In this way, by assuming that the charge transfer is much faster than mass transport, current can be expressed only in terms of potential. However, concentrations of reactants and products can be incorporated in the Butler-Volmer equation and thus obtain current as a function of both the bulk and surface

concentrations, which in turn depend on the potential as well. Hence, mass transport effects may also be taken into account in the extended Butler-Volmer reaction [31,38]:

$$j = j_0[\frac{c_O(0,t)}{c_O^*} e^{\left(\frac{(1-\alpha)F\eta}{RT}\right)} - \frac{c_R(0,t)}{c_R^*} e^{\left(-\frac{\alpha F\eta}{RT}\right)}] \tag{2.24}$$

where c_O^* and c_R^* are the bulk concentrations of the species to be oxidized and to be reduced respectively and $c(0,t)$ is the time-dependent concentration at a distance 0 from the electrode surface. In this form, the Butler-Volmer equation expresses the concentration dependence of the current, which becomes entirely dependent on mass transport when the electron transfer rate is very fast (i.e. O and R are being converted at a faster rate than their mass transport rate to the electrode). This current is known as the *limiting current density* (j_L) and relates to the concentration of O/R by:

$$c(0,t) = c^* \frac{j_L - j}{j_L} \tag{2.25}$$

Eq. 2.22 can now be written as a function of the limiting current:

$$j = j_0[(1 - \frac{j}{j_{ox,L}}) e^{\left(\frac{(1-\alpha)F\eta}{RT}\right)} - (1 - \frac{j}{j_{red,L}}) e^{\left(-\frac{\alpha F\eta}{RT}\right)}] \tag{2.26}$$

where $j_{ox,L}$ and $j_{red,L}$ correspond to the anodic and cathodic limiting current densities.

2.5 Electrochemical Methods

There are many experimental designs and methods to study electrical and chemical transport properties by means of potential, current or charge. These are often classified into either *static* methods, in which there is no current flowing between electrodes, and *dynamic* methods, in which current passes and concentrations change as a result of a redox reaction at the solution-electrode interface. Dynamic methods can be further subdivided into: i) measuring potential while controlling current or ii) measuring current under potential control. As this thesis delves into the study of electrochemical reactions taking place at fuel cell electrodes, only dynamic methods with potential control will be considered [32,38].

Most dynamic electrochemical techniques in which current is measured are carried out using a potentiostat to control the voltage difference between electrodes in an electrochemical cell, in which the controlled variable is the cell potential and the measured variable is the cell current. This cell typically contains three electrodes:

i) *Working electrode* (WE), in which the reaction to be studied is occurring.

ii) *Reference electrode* (RE), through which no current flows and whose potential remains constant. This electrode is used to measure the electrode potential.

iii) *Counter electrode* (CE), which completes the electric circuit and through which current is allowed to flow. It is usually an inert conductor like platinum or graphite.

By measuring the resulting current when applying a varying potential between the working and reference electrode, the reduction potential of an analyte and its electrochemical reactivity can be revealed. Thus, in this section, electrochemical techniques used for the study of mechanistic, kinetic and structural properties of electrodes will be discussed.

Cyclic Voltammetry

In voltammetry, a time-dependent potential is applied linearly to the WE (changing its potential relative to the stable potential of the RE) and the current that flows between the WE and CE is measured. In cyclic voltammetry (CV), after the limit potential is reached, the WE potential is ramped in the opposite direction to return to the initial potential, repeating this cycle as many times as needed. By convention, negative currents obtained in the region where potential is scanned negatively (i.e. towards negative potentials) are known as *cathodic* currents (reduction) and, positive currents generated by scanning positively are known as *anodic* currents (oxidation) The current measured between WE and CE is then plotted versus the applied potential at the WE to give a cyclic voltammogram. The CV parameters that are under the control of the experimenter are: i) the lower and upper potential limits (E_1 and E_2 in Fig. 2.5) and the direction of the initial scan, ii) the potential scan rate (ν), i.e. the rate of potential change over time and iii) number of cycles.

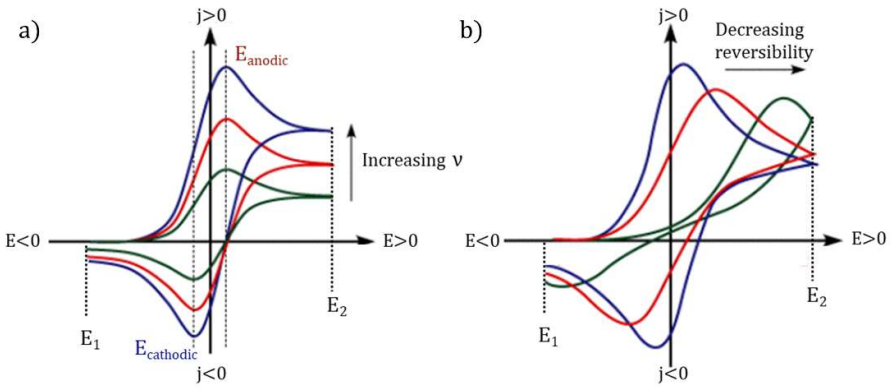

Figure 2.5 Typical cyclic voltammetry for (a) a reversible and (b) a kinetically slow redox reaction couple.

CV provides a rather fast qualitative interpretation of a redox reaction without need for any calculations. However, in order to gain the knowledge needed for the correct

interpretation of the electrochemical process, the following parameters should be properly monitored:

a) Number of peaks in the forward and reverse scans, with each peak corresponding to current generation through an electron transfer process (i.e. faradaic current).

b) The shape of the peaks, which, among other experimental factors, depend on whether convection is included in mass transport or not. In the absence of external stirring, the current will pass through a maximum and will thereafter decrease as the concentration of analyte on the electrode surface is depleted. Conversely, in the case of a continuous supply of reactants to the electrode by convection, the current will increase as a response of the applied potential until it reaches a limiting current, thereby showing a current plateau.

c) Peak potentials, which indicate the potential at which the reaction occurs. In the case of a reversible redox reaction, the cathodic and anodic peak positions are similar (Fig. 2.3a). If instead the redox is not reversible, the cathodic and anodic peaks are found at different potentials (Fig. 2.5b).

d) Peak current densities, which are proportional to the charge being transferred during an electrochemical process.

e) Difference between cycles, since different behavior through cycling between E_1 and E_2 relates to the nature of the electron transfer reaction, e.g. formation of a monolayer.

Cyclic voltammograms are presented in a form that allows the rapid qualitative interpretation of a current-generating process. Thus, the insights gained from a CV may immediately be used in the design of the next experiment, for instance, a polarization curve [31,33,38].

Polarization Curves

Although polarization curves can be plotted in numerous ways, the most common representation follows the same principle as the cyclic voltammetry: current vs. applied potential. Since by changing the overpotential, the free energy barrier of a given electron transfer reaction is either lowered or raised, they are often obtained by recording the current density as a function of the overpotential. They are determined after the open-circuit electrode potential, i.e. potential at which there is no current, has reached a steady-state value. Then, by recording the current generated when a potential that differs from the equilibrium potential is applied, a polarization curve is obtained [32,40].

Electrochemical Impedance Spectroscopy

Like resistance, impedance is a measure of the ability of an alternating current circuit to resist the flow of electrical current. In electrochemical impedance spectroscopy (EIS), the impedance of the circuit of the electrochemical cell is measured by applying an AC potential and measuring the current through the cell. Although there are many interpretations of EIS data, a common analysis is carried out by interpreting the Nyquist plot, which plots the real and imaginary parts of the impedance. The uncompensated resistance (i.e. solution resistance, R_u) of the cell can be found from the Nyquist plot at the high frequency intercept and the charge transfer resistance (R_{ct} in Eq. 2.18) can be obtained from the difference between the high frequency intercept and low frequency intercept [32,33].

3. Catalysis

By the end of the 18th and the beginning of the 19th centuries, experimental data across the globe reported the modification of chemical reactions by the presence of small amounts of foreign substances was enough to indicate a common, but then unknown, phenomena [41]. The explanation of this phenomena was first proposed by Jöns Jakob Berzelius in 1835, who established the relation between the otherwise disparate studies [42]. He described those reactions in a frame outside the theory of chemical affinity and termed the process as *catalysis*, a term derived from Greek meaning down (*kata*) and loosen (*lyein*) [43]. These early experimental observations were the genesis of what we know now as the field of catalysis, which endorses many of the chemical processes conducted by modern civilization [44]. In fact, approximately 35% of world's GDP relies on catalysts [45]. Examples of these applications are commonplace in everyday life, from catalytic converters in the exhaust of vehicles to mitigate pollution, to catalysts in ammonia synthesis for fertilizer production to increase global food production [46,47].

Nowadays we have a somewhat clearer understanding of how a catalytic process works, which the IPUAC describes as: '*A substance that increases the rate of a reaction without modifying the overall standard Gibbs energy change in the reaction; the process is called catalysis'* [48]. In this way, any material which accelerates a chemical reaction without being consumed in the process is called a *catalyst* and, correspondingly, the process of converting substrate molecules to products using a catalyst is called *catalysis*. There are two key roles that catalysts play in chemical reactions: enhancing the reaction rate and increasing selectivity towards desired products. An enhanced reaction rate makes slow reactions more economically viable and improved selectivity reduces the energy required to separate a desired product from the reaction mixture. Thus, catalysis research is of crucial importance to improve the sustainability of chemical industries.

Depending on the phase at which a catalytic process occurs, catalysis is often subdivided in two groups: homogeneous and heterogeneous catalysis. Homogeneous catalysis entails those catalytic processes in which the catalyst and the reactants are dispersed in the same phase (usually gaseous or liquid). In heterogeneous catalysis, instead, the reaction

components are at least in two phases. The present work is focused on heterogeneous catalysis, in particular reactions taking place at the solid-liquid interface.

3.1 Heterogeneous Catalysis

The vast majority of materials that we encounter in our day-to-day lives have been produced, at least partially, using catalytic processes. Most of the largest processes for industrial applications are based on heterogenous catalysis, which include crude oil cracking, methane steam reforming, ammonia synthesis, sulfuric acid production, polymerizations and water-gas shift reaction [49]. In fact, catalytic reactions are used in around 90% of the processes in chemical industry, most of which take place on heterogeneous catalysts [50]. These catalysts are not only used to increase the effectiveness of an industrial process, they also contribute to the environmental protection by lowering the energy needed to drive the chemical reactions, as well as reducing waste products that are harmful for the environment. Three-way catalysts are a very good example of the latter, which are used to remove NO, CO and hydrocarbons from the exhaust of combustion engine vehicles [49,51].

It is well known that the underlying mechanism behind the enhancement of a certain chemical reaction relies on its intermediate states. More precisely, catalysts increase the reaction rate by lowering the activation energy of a reaction (E_a). This is achieved by providing alternative routes to overcome to the potential energy barrier between reactants and products, which are energetically more favorable compared to the uncatalyzed reaction (Fig. 3.1). The preferred route involves the formation of lower energy transition states, which result in a decrease of the overall activation energy [50].

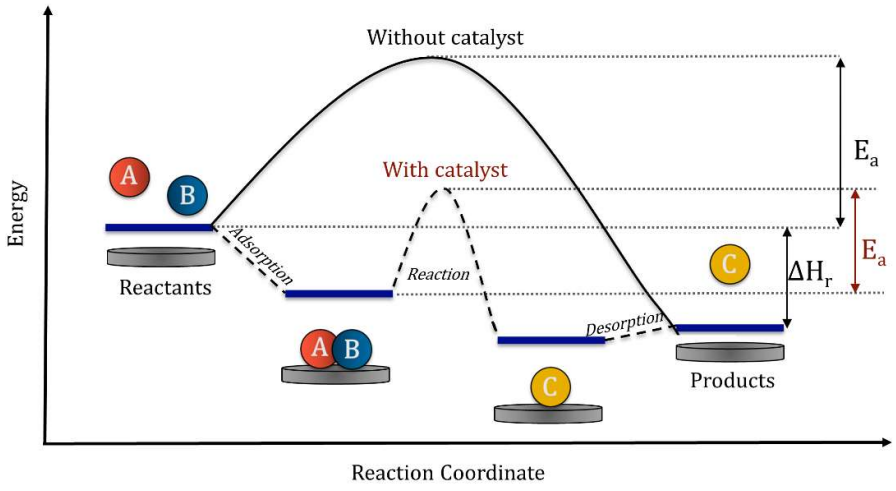

Figure 3.1 Energy diagram of an exothermic reaction of reactants A and B to produce C in the presence and absence of a heterogeneous catalyst, which changes the energy landscape by adding more favorable reaction pathways and thus lowering the activation energy (E_a).

Considering that most reactions in heterogeneous catalysis are between gaseous reactants on a solid surface, the catalyzed reaction can be broken down into four elementary steps: adsorption of reactants on the catalyst, the diffusion of adsorbed species along the surface, the surface reaction and the desorption of the products back into the gas phase [50,52]. How fast each elementary step can proceed is determined by the activation energy.

The dependence of the reaction rate with the adsorption/desorption of reactants and products is given by the *Sabatier's principle*. This principle states that, if the interaction between catalyst and reactants is too weak, then the activation of the reactant would be the rate-determining step. On the contrary, a too strong interaction will make the adsorbed species unable to desorb from the catalyst surface, blocking the active sites and thus stopping other reactants from being adsorbed. In this case, the rate-determining step would be the regeneration of the catalyst surface [50,53]. This principle can be shown graphically by plotting the overall reaction rate against the adsorption energy, which leads to a triangle-shaped plot known as the Volcano plot (Fig. 3.2). The Volcano curve describes the relation between the interaction reactant-catalytic surface and the catalytic activity of a catalyst for a given reaction. A reaction catalyzed by the catalyst laying on the left part of the curve (strong adsorption) will be limited by the product desorption and those placed at the right (weak adsorption) will be limited by the adsorption of reactants. Thus, an ideal catalyst would be located at the top of the Volcano plot.

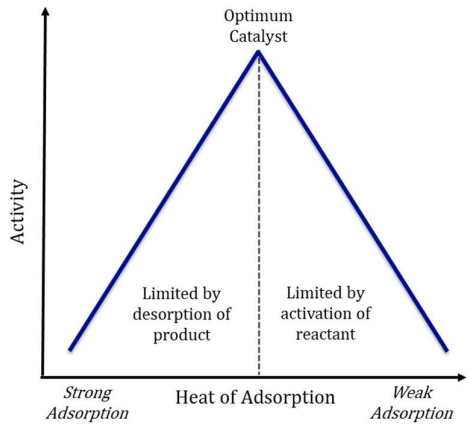

Figure 3.2 Typical Volcano plot representing the Sabatier principle [53].

Even though the correct balance between catalyst adsorption and desorption of reaction intermediates is applicable to all heterogeneous catalysts, strategies to find optimal catalysts often vary depending on their end-use, which in turn dictates the suitable catalytic properties. Thus, since this work focuses on catalysts for electrochemical

devices, the insights of catalyst research described hereafter will solely target electrocatalysts.

3.2 Electrocatalysis

In electrochemistry the reactants are adsorbed at the surface of the electrode where the electrochemical reaction occurs. Electrocatalysis can therefore be seen as the heterogeneous catalysis of electrochemical reactions, which occur at the electrode–electrolyte interface and where the electrode plays both the role of electron donor/acceptor and of catalyst. The activation energy in electrochemical processes is related to the potential, at which the reaction takes place. Thus, electrocatalysts usually enhance the reaction rate by changing the potential at which oxidation and reduction are observed. Moreover, since electrochemical reactions occur when electrons are passed from one chemical species to another, the potential at which those reactions occur highly depend on the favorable interactions at the electrode surface.

As many other heterogeneous catalysts, the development of electrocatalysts is based on the optimization of three key factors that determine their performance [54]:

i) *Activity*, which is evaluated by how much current density is generated at a given potential, as described in Eq. 2.22.
ii) *Selectivity*, which is evaluated by comparing the response of the electrocatalyst to a desired analyte with the response to others.
iii) *Stability*, which is assessed qualitatively by their ability to withstand potentials at which reactions occur, as well as fast potential changes.

The three figures of merit mentioned above, together with cost and abundance, are the most important parameters taken into account when searching for an optimal electrocatalyst. The electrocatalyst research therefore involves finding better materials that could potentially improve the efficiency of the main processes that they are used for, such as water splitting [55], fuel cells [56] and electrochemical carbon dioxide reduction [57]. Nevertheless, difficulties arise when trying to achieve the correct optimization of the three performance key factors due to the numerous parameters of the electrocatalytic system that should be taken into account.

3.1.1 Electrocatalyst Design

The ability to break and create new chemical bonds dictates the ability of a metal surface to act as an electrocatalyst. However, as explained in the previous section, most catalysts bind reaction intermediates either too weakly or too strongly, hence limiting the electrochemical reaction rate. Thus, in order to develop more efficient catalysts and

achieve an optimal catalytic activity, a rational design of heterogeneous catalysts (including electrocatalysts) is a crucial step. Ready-to-use electrocatalysts are systems with a very high complexity, whose performance depends on many parameters: surface and bulk composition, crystal facets, structural defects, interaction with the support material, size (in the case of nanoparticles), coordination number, etc. (Fig. 3.3)[58]. Hence, given the great deal of parameters that control the catalytic properties of an electrocatalyst, the use of simplified model systems is essential to reduce complexity, isolate the contribution of a certain parameter and thus facilitate the development of the new electrocatalyst generation. Whereas this gives rise to numerous approaches that can be adopted to reach the highest electroactivity, two main development strategies are commonly used in electrocatalyst research [59]: (i) increasing the total number of active sites, and (ii) increasing the intrinsic catalytic activity of the electrode material.

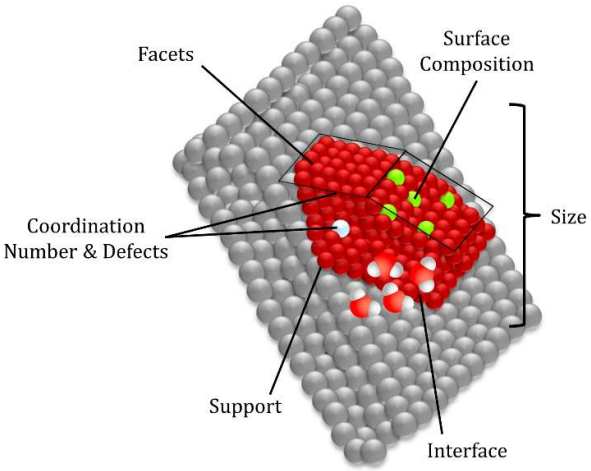

Figure 3.3 Schematic illustration of a high surface area nanoparticulate electrocatalyst and the parameters and factors that control its surface area. Adapted from [58].

A vast portion of electrocatalyst research has focused on increasing the total number of active sites, which is carried out by either increasing the electrochemical surface area (ECSA), or by increasing the catalyst loading. Whereas the catalyst loading is undesired because it would imply a major cost increase of the often-used noble metal electrocatalyst, as well as the arising of charge and mass transport limitations; several strategies have focused on increasing the catalyst surface area. The ECSA can be improved, for instance, through the optimization of high surface-to-bulk ratio structures, such as nanoparticles or nanofibers [60,61], or by using highly porous substrates [62]. The impact of these strategies on the reaction rate is, however, limited due to the linear relationship between activity and number of active sites. Another strategy to increase both the ECSA and the intrinsic activity is to use modified carbon-based supports with properties that can both boost the catalyst activity by means of synergetic effects and

enhance its stability, thereby optimizing the material use by enabling single-atom (or clusters) dispersion with high specific activity [63,64].

A strategy that can be employed to increase overall electroactivity is through tailoring the intrinsic activity of the electrode material, i.e. its specific activity, which can lead to several orders of magnitude enhancement [65]. In order to do so, the binding energy of the electrode surface needs to be modified in a way that results in the optimal adsorption/desorption balance, which in turn requires atomic-scale tuning of the catalyst electronic structure. A common practice to induce changes in a catalyst electronic structure is through alloying, whose effect is highly dependent on both structure and composition. Moreover, as some metals used in catalysis such as platinum are scarce and expensive, alloying is regarded as a good strategy for tailoring new inexpensive catalyst that could potentially improve the activity, selectivity and stability of the current scarce metals used in electrocatalysis.

Alloying of different metals and metal oxides induces a change in the intrinsic catalytic properties of a material by two electronic effects: ligand and strain effects. The *ligand effect* is caused by the atomic vicinity of two dissimilar atoms that induces an electronic modification of the alloy components, resulting in a change of the binding energies of reactants and intermediates and thus a change in the catalytic activity [66,67]. On the other hand, the *strain effect* originates from the alteration of a metal lattice when metals with different atomic radii are alloyed together. The incorporation of a metal with a different radius results in either a compressed structure (compressive strain) or an expanded structure (tensile strain) [68,69]. In either case, a modification of the lattice structure results in a change of the electronic structure, whose extend and nature will be given by the difference in atomic radii between the alloy components. Although electronic effects have been demonstrated to be advantageous on tuning the binding energy of catalyst materials, it is usually very difficult to deconvolute the interplay between strain and ligand effects.

A useful descriptor to predict trends in reactivity among alloys is the d-band model, which correlates the interaction strength of adsorbate-metal surface with the average energy of the d-electrons [70]. This model is a convenient tool to describe the bond formation at a metal surface, which can be used to predict the origin of catalytic trends for transition metals in heterogeneous catalysis [71]. A transition metal surface has a continuum of energy levels with electrons filling the states from the lowest energy level until the highest occupied electronic level formed by the valence states of the surface atoms, i.e. the Fermi level. When adsorption on the metal surface takes place, the electronic states of the transition metal interact with the adsorbate energy levels, which can be divided into two interactions: the interactions with the s-band of the metal, and

the d-band interaction. This gives rise to the formation of separate bonding and anti-bonding states, with the strength of the bonding depending on the electron filling and the orbital overlap. Filled antibonding states will results in a weak bond and vice versa. At the same time, the splitting of the bonding and anti-bonding states depends on the energy of the d-band center (ϵ_d) relative to the energy of the adsorbed species (ϵ_a). The closer the d-band center is to the adsorbates energy, the larger is the splitting (Fig. 3.4). However, since the strength of the metal-adsorbate bond also depends on the overlap between the orbitals, it will also depend on the metal structure [70,72]. Based on this so-called d-band model, the d-band center of the metal can be used to predict changes in adsorption strength upon, for example, alloying, and thus the adsorption strength can be adjusted.

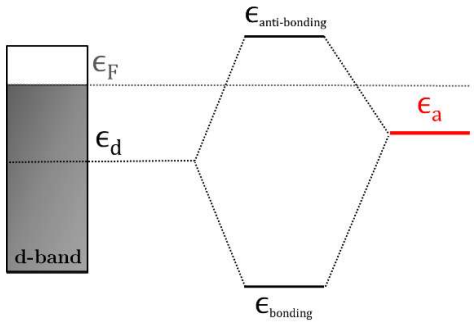

Figure 3.4 Schematic model regarding the whole d-band located at its center and interacting with an adsorbate, together with the resulting bonding and anti-bonding states.

The incorporation of an additional metal to a monometallic catalyst, however, may also be beneficial without the need of alloy formation. Since most of the catalytically carried out reactions involve several reaction steps and therefore numerous reaction intermediates, the assembly of two metals together on the surface can potentially boost the reaction kinetics through *ensemble effects*. In this configuration, one metal is suitable for a certain reaction step whereas the other metal is very active on catalyzing the remaining steps. Thus, the bifunctionality of the surface can be of great service to catalyze reactions that the original metals alone would not be capable of handling. Even though the mere presence of two surface metals with different properties might be enough to observe an activity enhancement, a certain degree of mixture and spatial arrangement is often required in order to observe ensemble effects [73]. However, alloying of these metals may further improve the overall activity by changing their respective electronic structures (i.e. ligand effects) and thus exhibit a two-way enhancement [74]. It is important to note, however, that all the effects explained in this section usually require a deep understanding of the reaction mechanism if a more detailed and rational electrocatalysts design is meant to be accomplished. Hence, mechanistic studies must be concomitant with electrocatalyst research and are of equal importance.

4. Hydrogen Fuel Cells

Modern society will face severe challenges if our lifestyle does not shift away from the use of fossil fuels to meet the ever-growing energy demand. There is no doubt that GHG emissions are responsible for several serious environmental issues, which manifests the need for harness carbon-free renewable energy sources. Many alternatives have been proposed to take over the highly efficient conventional combustion engines, but only a few represent a stable, cost-effective and efficient candidates for energy generation. Among all those alternatives, fuel cells have emerged as a promising competitor to combustion engines because of their high operating efficiency, environmental-friendly operation and the range of fuels that they can use. Thus, fuel cells are energy converters that could potentially provide a highly efficient energy generation, either at the point of use or on a large scale. However, an energy system based on renewable energy sources must have a storage to match generation and consumer demand. Hence, combination of water electrolysis, H_2 storage and fuel cells could provide a solution to this issue.

Fuel cells convert electrochemically the chemical energy stored in fuels (e.g. H_2) directly to useful electricity. As opposed to combustion engines, fuel cells convert chemical energy directly into electrical energy without the need of mechanical work generation. Moreover, electricity is produced as long as fuels and oxidants, that are stored externally to the cell, are supplied, which is their main difference with batteries. Besides the advantages stated above, fuel cells also present the following assets over other power generation systems [16,75–77]:

- High energy density and high operating energy efficiency, which can attain over 60%.
- Scalable production to a range of sizes.
- Environmental-friendly due to absence of GHG emissions (in case of using green hydrogen as a fuel). If green hydrogen is used as a fuel and oxygen as an oxidant, emissions are only water.
- Ease of hydrogen refueling - almost immediate recharge capability.
- Quality of power generated does not degrade over time.

- Manageability: lighter, compact and no moving parts, which makes them very suitable long operating periods.
- More silent energy production.

Nevertheless, fuel cells currently present technical limitations that are yet to be overcome [16,77,78]:

- Safety and cost issues related to hydrogen storage.
- Most of used hydrogen still comes from fossil fuels (grey hydrogen)
- Lack of infrastructure to support hydrogen distribution, impeding the wide availability of hydrogen.
- Most of currently available fuel cell technology still in a prototype stage.
- Expensive fuel cell production (primarily attributed to the cost of the catalyst layer and its application), which should be reduced to 35 $/kW for automotive applications by 2025 [17].
- Reliability and durability of fuel cell systems still far from 2025 target (8000 h durability in automotive load cycles) [17].
- Specific power density and peak energy efficiency still need improvement if DOE target is meant to be met (900 W/Kg power density and 65 % efficiency) [17].

In this chapter, an introduction to fuel cell technology is given and a glimpse of their history is provided. The basic thermodynamic principles under which fuel cells operate are also explained and the different types of fuel cells are briefly described. Parameters influencing fuel cell performance are then discussed, followed by a description and comparison of the two main low-temperature hydrogen fuel cells: PEMFCs and AEMFCs. Lastly, the current status of the electrocatalysts used in these two types of fuel cells is presented, as well as the state-of-the-art of this technology.

4.1 History

It is no surprise that fuel cell history comes hand in hand with the history of electrochemistry explained in Section 2.1. After the discovery of electrolysis in 1800 and the postulation of Faraday's laws of electrochemistry in 1834, Sir William Grove took the idea of electrolysis in reverse back in 1838 [79]. He discovered that, by placing two platinum electrodes with one end immersed in a beaker with sulfuric acid and each of the other ends sealed in glass tubes containing H_2 and O_2, a constant current flowing between the two electrodes was observed [80]. Over time, Grove noticed that the reaction was consuming both gases as the current flowed. A few years later, he created what he called a "gaseous battery" by combining 26 pairs of tubes in a series circuit, which made

him earn the title of "father of the fuel cell". Ironically, this discovery took place at roughly the same time as the first combustion engines were developed [80,81].

During the upcoming years, several insights on the theoretical understanding of how fuel cells operate were provided by several scientists, including Friedrich Ostwald [81]. However, it took over one hundred years after Grove's discovery before fuel cells were used in applications. Beginning in the late 1930s, F.T Bacon made great advances in alkaline hydrogen fuel cells, which ended up being used for the Britain's Royal Navy submarines during World War II [28]. Although they were very costly, they quickly attracted attention and Bacon's fuel cell was licensed to provide on-board power for the Apollo spacecraft in the mid-1960s. Improvements in fuel cells efficiency and cost were made in dribs and drabs until the 1990s, when environmental concerns regarding the use of fossil fuels for power generation started emerging [28,81]. This growing awareness of environmental and sustainable issues with the usage of a finite and polluting source of energy is what catalyzed the development of hydrogen fuel cell technologies, which has continued to grow until the time being.

4.2 Principle and Thermodynamics

In a low-temperature hydrogen fuel cell, hydrogen is electrochemically oxidized at the anode electrode, which generates electrons. These electrons flow through an external circuit to the cathode electrode, where oxygen is supplied, usually through air, and reduced to eventually form water as a waste product [40]. The overall reaction for a hydrogen fuel cell is:

$$H_2 + \frac{1}{2} O_2 \longrightarrow H_2O \tag{4.1}$$

As the enthalpy of water is lower than the combined enthalpy of the reactants, the reaction is exothermic, thereby producing heat as the only by-product (besides water).

Electrons produced in the anodic electrode are forced to pass through a circuit where they are used to perform electrical work before they are used to reduce oxygen at the cathode. Electricity is therefore generated directly from the electrochemical reaction. However, the two half-cell reactions must be physically separated and electrons must be forced to get through the external circuit to produce an electric current. The spatial separation is achieved by using an electrolyte, whose nature will dictate the operating temperature of the fuel cell. The particularity of the electrolyte is that it allows the conduction of ions but not electrons, which prevents the redox reaction to take place without electrons flowing. The nature of the ions being conducted through the electrolyte

(H^+ or OH^-) will depend on the media in which the half-cell reactions take place (i.e. alkaline or acid), which in turn are also governed by the media in which they occur. Thus, the mechanisms of the anode and cathode reactions will be determined by the pH of the electrolyte [82]. These half-cell reactions are known as hydrogen oxidation reaction (HOR) and oxygen reduction reaction (ORR) respectively. The features of these reactions in acid and alkaline media will be extensively discussed in the upcoming sections of this chapter.

The electrical energy generated from the overall fuel cell reaction depends on the chemical energy of the same reaction. According to thermodynamics, the maximum amount of chemical energy of any system that can be converted into energy (electricity in this case) is given by the change in Gibbs free energy (ΔG):

$$\Delta G = \Delta H - T\Delta S \tag{4.2}$$

Thus, the balance between the enthalpy of the reaction (ΔH) and the minimum heat necessary for entropy production ($T\Delta S$) will determine if the reaction can take place spontaneously ($\Delta G < 0$), if it is in equilibrium ($\Delta G = 0$) or if another driving force is needed ($\Delta G > 0$). Since the fuel cell energy conversion implies the energy generation without the need of any external work, fuel cells -together with batteries- will only involve spontaneous reactions.

From a thermodynamic point of view, it could be mentioned that if all the chemical energy released from a reaction is converted into electrical energy, the efficiency would be 100 %. Nonetheless, not all the chemical energy is used to generate current. The maximum thermodynamic efficiency is therefore used as a theoretical reference point for comparing efficiencies. This parameter is defined as the ratio between the maximum energy available and the total energy of the reactants. Thus, for ideal processes:

$$\eta_{FC} = \frac{\Delta G^o}{\Delta H^o} \tag{4.3}$$

For the hydrogen-oxygen fuel cell, the enthalpy change of the overall process is -2.86 $\cdot 10^5$ J/mole of H_2O formed, which leads to a maximum thermodynamic efficiency of 83% [83]. This efficiency is obviously never reached in practice, so the real energy efficiency must be used instead.

The effectiveness of the fuel cell in converting chemical into electrical energy is reflected by the cell voltage:

$$\Delta E = \Delta E_{cell} - \eta_a - \eta_c - iR \tag{4.4}$$

where η_a and η_c are the anodic and cathodic overpotentials and the final term corresponds to the iR drop through the cell. ΔE_{cell} is the difference in equilibrium potentials of the anode and cathode reactions, as described in Eq. 2.2. As the overpotentials and iR drop must be regarded as inefficiencies lowering the fraction of energy effectively converted, the electrochemical fuel cell efficiency can be written as:

$$\epsilon_{FC} = \frac{maximum\ power\ obtained}{maximum\ power\ possible} = \frac{\Delta E}{\Delta E_{cell}} \tag{4.5}$$

4.3 Fuel Cell Components

In this section, the basic components of a single fuel cell will be explained. For the operation of hydrogen fuel cells, basic components are needed to facilitate the following:

- Fuel and oxidant feeding to the anode and cathode, respectively.
- Electrical charge flow through an external circuit.
- Prevent direct mixing of hydrogen and oxygen.
- Dissipation of heat released during operation.
- Water removal from the cell to ensure an efficient performance.

In order to successfully carry out the operations stated above, the basic components of hydrogen low-temperature fuel cells are: electrolyte, gas diffusion layer, catalyst layer and bipolar plates (Fig. 4.1) [40].

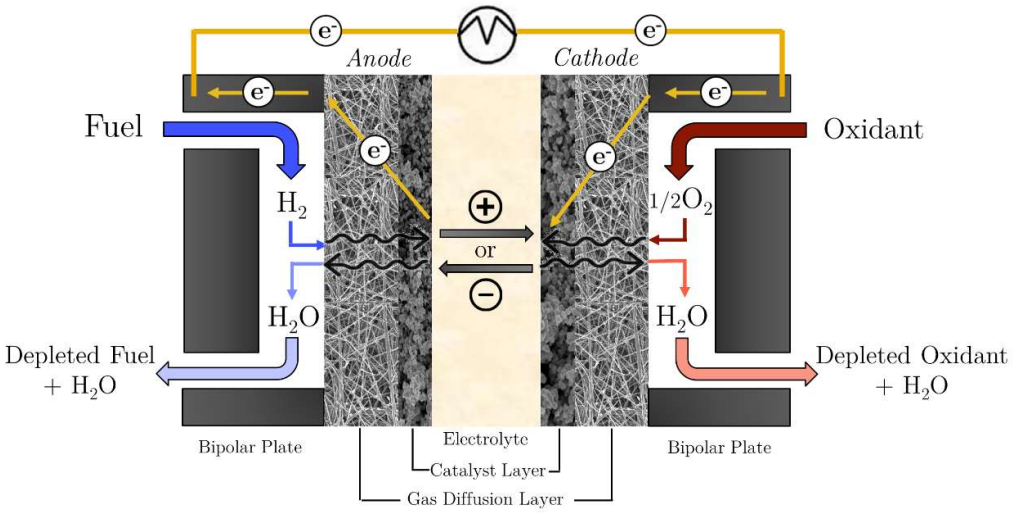

Figure 4.1 Schematic illustration of a single low-temperature hydrogen fuel cell.

In a typical fuel cell, oxidant (often oxygen from air) and fuel (e.g. hydrogen) are fed continuously to the cathode and anode, respectively. Electrochemical reactions take

place at the electrodes to produce an electric current through an external circuit. Thus, on the contrary to batteries, fuel cells produce power as long as fuels are supplied. Among all the areas in a fuel cell where a process occurs, the tiny area at which the actual redox takes place is most likely the most crucial part. This portion of the cell is found where the electrolyte, the electrode and the catalyst sites meet and thus the starting point of all the energy conversion processes. It is named the Three Phase Boundary (TPB) and it must fulfill the following conditions: i) be exposed to the reactant, ii) be in electrical contact with the electrode, iii) be in ionic contact with the electrolyte, and iv) must contain enough catalyst exposed for the reaction to proceed at the desired rate.

The Electrolyte

For all types of fuel cells, the electrolyte constitutes an indispensable component. In fact, the type of electrolyte used determines the name given to a certain fuel cell. The electrolyte not only transports reactants to the electrode but also conducts ionic charge between the electrodes and thus maintain the electroneutrality of the system. Moreover, it also provides a physical barrier to prevent the fuel and oxidant from directly reacting with each other. The desired properties of the electrolyte are therefore: i) high specific ionic conductivity, ii) high electronic resistivity and iii) low reactant permeability [40,82].

There are mainly two types of electrolytes based on their phase: liquid and solid electrolyte. For the low-temperature hydrogen fuel cells considered in this thesis, only polymer membrane electrolytes will be taken into account. These membranes are semipermeable, generally made from ionomers and they are designed to conduct either protons (acid media) or hydroxides (alkaline media) when they are hydrated. Thus, polymeric membranes should be both mechanically and chemically resistant, as well as possess a high water intake [82].

The Gas Diffusion Layer (GDL)

Besides reactants and the ionic conducting medium, a surface for the electrochemical reaction to take place is of crucial importance for the correct operation of the fuel cell. The role of the gas diffusion layer (GDL) will therefore be determined by its specific area, which is, in fact, the number of pores engineered. The GDL plays an essential role inside a fuel cell, namely:

- Even distribution of hydrogen and oxidant to the catalyst layer.
- Proper conduction of electric current
- Effective removal of products generated in the redox reaction.
- Efficient water removal to avoid water flooding.

In order to fulfill the requirements above, a GDL must possess the following features: i) high electronic, ionic and heat conductivity; ii) high corrosion resistance and iii) porous material to ensure proper mass transport. For the latter, carbon cloth or paper are usually chosen as a GDL material, which are also sulphonated to provide hydrophobicity for the correct water removal [40,82].

The Catalyst Layer

The catalyst provides active sites which serve as a platform for the correct occurrence of the two half-cell reactions. The electrocatalysts must provide a high catalytic activity and stability under fuel cell conditions in order to maintain a high reaction rate and thus the desired power output. For this, the requirements that the catalyst layer should fulfill are:

- Large surface area to ensure proper contact in the TPB.
- Proper dispersion to maximize exposed active sites.
- Suitable porosity to ensure proper mass transport.
- Tolerant towards impurities that could potentially poison the catalyst.
- Support with a large area and high electric conductivity.
- High corrosion resistance.

For low-temperature fuel cells, only a few relatively rare and expensive materials provide sufficient electrocatalytic activity, and so such catalysts are deposited in small quantities and properly dispersed to maximize the catalyst utilization. For fuel cells using a polymeric membrane as electrolyte, an ionomer is often added to the catalyst layer to guarantee the ionic transport of reactants and products at the TPB [40,82].

Ionomers

Besides being a main constituent of electrolyte membranes, ionomers are also required in the catalyst layer to provide ionic transport from/to the catalyst active sites and thus improve ion/electron conductivity. Thus, the incorporation of H^+/OH^- conducting ionomers within the catalyst layer may further improve catalyst utilization by extending the TPB and converting physical surface area into electrochemically active area. The amount of ionomer is crucial for the correct ion-transport enhancement, since too much ionomer can hinder mass transport and too little can lead to insufficient ionic transport and poor wetting, i.e. low catalyst utilization [84,85]. Moreover, since the main degradation mechanisms in AEM materials are a result of nucleophilic attack of anion on the cationic head groups, stability is also a major concern [86]. Thus, whereas PEM materials are based on perfluorocarbon-sulfonic acid (PFSA) ionomers (e.g. Nafion®), which are very stable under PEMFC operating conditions, AEM materials are still in need of stable ionomers. Membrane and ionomer durability limit both the lifetime and

maximum operating temperature of AEMFC, for which is considered to require improvement if AEMFC are meant to challenge PEMFC in most applications [87].

Bipolar Plates (BPs)

In order to achieve a higher voltage and power, individual fuel cells are assembled in series forming a fuel cell stack. Bipolar plates (BPs) are a key component in fuel cell stacks because they connect the single fuel cells. They conduct electrical current from cell to cell and provide a uniform distribution of hydrogen and oxygen throughout the fuel cell. Moreover, they contribute to the cooling of the cell by removing the heat generated and prevent leakage of gases and coolant. In order to properly conduct current through the assembly, BPs are usually made of high electrically conductive material, e.g., graphite or stainless steel [40,88].

4.4 Types of Fuel Cells

Fuel cells are applicable in the entire spectrum of energy demand [89]. Their applications are determined by the type of electrolyte they use for ion conduction, which in turn determines the electrochemical reactions, the catalyst type, operating temperature and the fuel used. Most often, their classification is mainly based on the nature of the electrolyte they use and subsequently their typical operating temperature. This temperature, as well as the useful lifetime of the fuel cell, commands the properties of the other materials used in the cell components. The operating temperature also plays an important role in dictating the degree of fuel processing required. In low-temperature fuel cells, for instance, all the fuel must be converted to hydrogen previously to entering the fuel cell. The most common types of fuel cells, their operational strategy, typical applications and their main advantages and limitations are listed in Table 3.1 [40,56,90].

The different types of fuel cells are not exclusive to each other but serve as a complement that broadens their range of applications, which mainly depend on the operating temperature. High-temperature fuel cells, for instance, can achieve high reaction rates without expensive catalysts due to the high temperature at which the reactions take place, as well as being less sensitive to poisoning. Furthermore, natural gas is internally reformed, which can be used directly within the fuel cell without the need for a separate unit. The molten carbonate fuel cell (MCFC) and the solid oxide fuel cell (SOFC) belong to this category and they are mainly considered for stationary power units owing to their waste heat that can be combined with the produced electricity in a combined heat and power (CHP) system. Nevertheless, the high operating temperature implies the use of ceramic materials, which can be difficult to handle and expensive to manufacture. These

systems, moreover, require long startup times, which hinders their applications in vehicles [40,91].

The phosphoric acid fuel cell (PAFC) and the alkaline fuel cell (AFC) operate at medium temperatures and demonstrated excellent thermal and electrochemical stability compared with other fuel cell systems. There are two main commercial uses for PAFC and AFC: small-scale onsite power generation and distributed power using reformed natural gas. However, they both use a liquid electrolyte, which makes manufacturing and handling more difficult [40,92,93].

Lastly, low-temperature fuel cells are remarkably stable and cover a large power range, which include subtypes such as the proton exchange membrane fuel cells (PEMFCs), direct methanol fuel cells (DMFCs), or direct formic acid fuel cells (DFAFCs). PEMFC form the most widely used category of fuel cells, whose main characteristic is the use of a solid polymer membrane as electrolyte. The low temperatures at which PEMFC typically operate (60 to 80 °C) makes them excellent candidates for short start-up applications [94]. This, together with their high-power densities, makes PEMFC the best candidate for small-scale backup power, portable electric devices and automotive applications [40,78,95].

As already explained, there are numerous types of fuel cells that operate under different conditions, which make them suitable for a vast range of applications. However, as previously noted, this chapter will deal only with low-temperature technologies using hydrogen as fuel.

Table 4.1 Key parameters of the main types of fuel cells [40,56,90].

Fuel Cell Type[¥]	**PEMFC**	**AFC**	**PAFC**	**MCFC**	**SOFC**
Electrolyte	Hydrated Polymeric Membrane	$KOH_{(aq)}$	$H_3PO_{4(aq)}$ in SiC	Molten Carbonate in $LiAlO_2$	Ceramic (Perovskites)
Fuel	H_2+H_2O	H_2+H_2O	H_2	H_2+H_2O +CO+CO_2	H_2+H_2O +CO+CO_2
Charge Carrier	$\uparrow H^+$	$\downarrow OH^-$	$\uparrow H^+$	$\downarrow CO_3^{2-}$	$\downarrow O^{2-}$
Oxidant	O_2+H_2O	O_2	O_2+H_2O	CO_2+O_2	O_2
Catalyst	Platinum	Platinum	Platinum	Nickel and Nickel Oxide	Perovskite
Operating T°	40-100 °C	60-220 °C	150-220 °C	650-800 °C	600-1000 °C
Power Range[§]	<1-100 kW	1-100 kW	5-400 kW	300 kW–3 MW	1 kW–2 MW
Primary Contaminant	CO, S and NH_3	CO, CO_2 and S	CO and S	S	S
Primary Cell Components	Carbon-based	Carbon-based	Graphite-based	Stainless-based	Ceramic
Advantages	High power density, quick start-up and low T°	High performance and low-cost components	High CHP efficiency, low-cost and reliable	High efficiency, flexibility of fuels and catalysts and solid electrolyte	High efficiency, fuel flexibility, variety of catalysts and solid electrolyte
Limitations	Expensive catalysts, sensitive to fuel impurities and water management	Sensitive to CO_2, electrolyte management and expensive catalysts	Corrosive electrolyte, expensive catalysts, long start-up times	Expensive materials, corrosion, low power density, degradation and long start-up	Expensive materials, corrosion, long start-up and degradation
Applications	Small-scale back-up power, portab electric devices and transport	Electrical equipment, transportation and stationary	Spacecrafts, military	Stationary	Stationary and heavy-duty transportation

[¥]Only hydrogen fuel cells considered.

[§]Data from US department of Energy – March 2021 [19].

4.5 Fuel Cell Performance

Among other factors, the performance of a hydrogen fuel cell is closely dependent on the capability of hydrogen and oxygen to react at the TPB of their respective electrodes, which in turn is dependent on the morphology, area and structure of the electrode. More importantly, the rate of the half-cell reactions depends on the catalyst used to catalyze the anodic and cathodic reactions. Furthermore, in order to ensure the proper adsorption of reactants on the catalyst active sites, both the electrode and the electrolyte must first provide adequate gas and ionic diffusion respectively.

A commonly used method to measure the fuel cell performance is the current-voltage (I-V) curve or polarization curve, which is usually plotted with current density, i.e. current normalized by the geometric surface area of the electrode, vs. voltage. In this subsection, the polarization curve of the ORR at the cathode of a PEMFC (which uses a Pt catalyst) will be considered for practical reasons (Fig. 4.2). The theoretical open circuit voltage (OCV) of the fuel cell is a function of the Gibbs free energy of the overall reaction. However, the actual OCV is lower than the theoretically predicted value even when no current is drawn due to irreversible voltage loss, which arise from secondary reactions at the cathode [96,97]:

- Reversible O adsorption at the Pt surface:

$$Pt + H_2O \longleftrightarrow PtO + 2H^+ + 2e^- \qquad \text{E°=0.88 V vs. RHE} \qquad (4.6)$$

- Fuel crossover: H_2 permeates across the membrane from the anode to the cathode, where it can be directly oxidized by O_2, i.e. *in situ* electron transfer. This undesirable reaction also generates hydroperoxide radicals, which degrades the membrane and thus reduces the TPB in the catalyst layer.

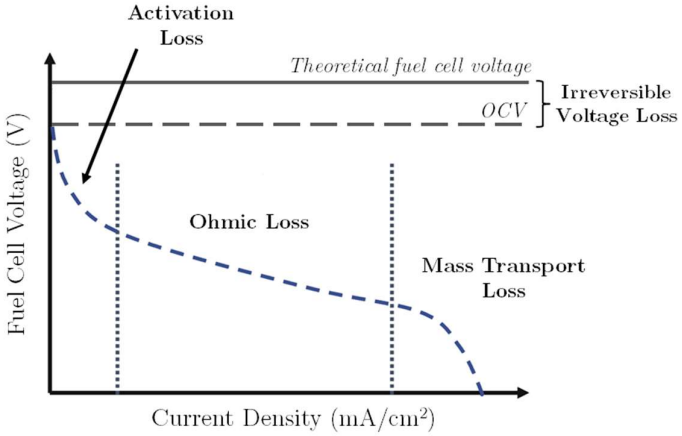

Figure 4.2 Typical fuel cell I-V curve.

Similar to cyclic voltammetry, a qualitive interpretation of an I-V curve requires analysis of the shape of the curve. The total power that can be delivered by the cell is limited by the current generated, which in turn depends on the voltage of the cell. Different fuel cell designs operate at different voltages, but the higher the voltage at a given current density the better. Voltage decreases as the current increases due different losses, which occur at different stages:

I) Activation Loss

Activation overpotential arises from the additional energy required to drive the half-cell reaction compared to the thermodynamically expected value. As explained in Section 2.3, the existence of overpotential implies that less energy is recovered from what is predicted thermodynamically. Thus, activation losses (η_{act}) are associated with the ORR kinetics taking place at the cathode. Even for the same reaction, the value of η_{act} is specific to the design of the cell and operating conditions [40].

II) Ohmic Loss

The linear voltage drop in Fig. 4.2 is related to Ohmic loses (η_{ohmi}), which are caused by the resistance to the electrons flow through the cell components and interconnections, as well as the ion resistance in the electrolyte. The typical fuel cell operating voltage lays in this region [40].

III) Mass Transport Loss

The prompt decay in voltage at high current densities is related to mass transport phenomena ($\eta_{mass\ transport}$), which fails to transport reactant species from the bulk solution to the electrode surface fast enough to keep the electron transfer at a certain rate [40].

Thus, the actual fuel cell voltage will be determined by the contribution of all the voltage losses explained above to the equilibrium potential, i.e. the thermodynamically predicted voltage (E^o):

$$V = E^o - \eta_{act} - \eta_{ohmic} - \eta_{mass\ transport} \tag{4.7}$$

In order to make a reliable comparison among different electrodes, the current in a polarization curve is usually normalized. There are three ways to normalize current: i) geometric current density (A/cm_{geo}^2), which is obtained by using the geometrical area of the electrode; ii) specific current density ($A/cm^2_{catalyst}$), which is normalized by the electrochemical surface area (ECSA) of the catalyst, i.e. area exposed to reactants; and iii) mass activity ($A/mg_{catalyst}$), which gives information about the utilization of the catalyst.

4.6 Electrocatalysts for Low-Temperature Hydrogen Fuel Cells

Platinum and its alloys are currently used as catalyst for most of the commonly used low-temperature fuel cells because its high activity and stability for both electrode reactions. However, Pt demand is growing, which depletes its reservoirs and thus contributes to the increase of its cost [98,99]. In this thesis, Pt will be used as an example of electrocatalyst characterization to illustrate the methods followed for the qualitative and quantitative analysis of catalytic materials for low-temperature hydrogen fuel cells.

As described in Section 2.6, cyclic voltammetry is one of the simplest and most revealing electrochemical methods for electrocatalysts analysis. Thus, insights of the electrochemical behavior of a certain catalytic material can be obtained by looking at the shape and position of the features exhibited in a CV. A typical CV for a Pt electrode in acid media is shown in Fig. 4.3, which shows different types of responses to the applied potential sweep. Each region in the CV reveals different electrochemical surface processes that give rise to faradaic and non-faradaic currents, both in the cathodic region (I and VII) and in the anodic region (II-VI):

I) Underpotential Deposited Hydrogen (H_{UPD}) region at 0-0.4 V, which is dominated by the adsorption of atomic H on Pt right before the equilibrium potential for hydrogen reduction (i.e. hydrogen evolution) at 0 V vs. RHE. The adsorption process involves one electron transfer:

$$Pt + e^- + H^+ \longrightarrow Pt - H \tag{4.8}$$

The peaks at 0.25 and 0.1 V correspond to hydrogen adsorption on Pt (100) and on Pt (110) respectively [100].

II) Also H_{UPD}, but dominated by H desorption during anodic scans:

$$Pt - H \longrightarrow Pt + e^- + H^+ \tag{4.9}$$

III) Double layer region, where only capacitive (non-faradaic) currents arising from a changing potential are seen.

IV) Onset of Pt surface oxidation, which starts with the formation of an adsorbate layer of O-containing species from either OH^- or O^{2-} adsorption, although the former is more commonly accepted [101]:

$$Pt + H_2O \longrightarrow Pt - OH + e^- + H^+ \tag{4.10}$$

V) Formation of a surface oxide layer:

$$Pt - OH \longrightarrow Pt - O + e^- + H^+ \tag{4.11}$$

VI) Growing of the surface oxide to finally form the bulk oxide.

VII) Pt oxide reduction to metallic Pt:

$$Pt - O + 2e^- + 2H^+ \longrightarrow Pt + H_2O \tag{4.12}$$

The exact potential range of the processes mentioned above depend on several experimental parameters, including temperature and scan rate. Moreover, these processes depend also on the catalysts nature and surface morphology. If Pt is alloyed with other elements, new peaks may appear due to either changes in the surface binding energy or reactions in the alloying material [102].

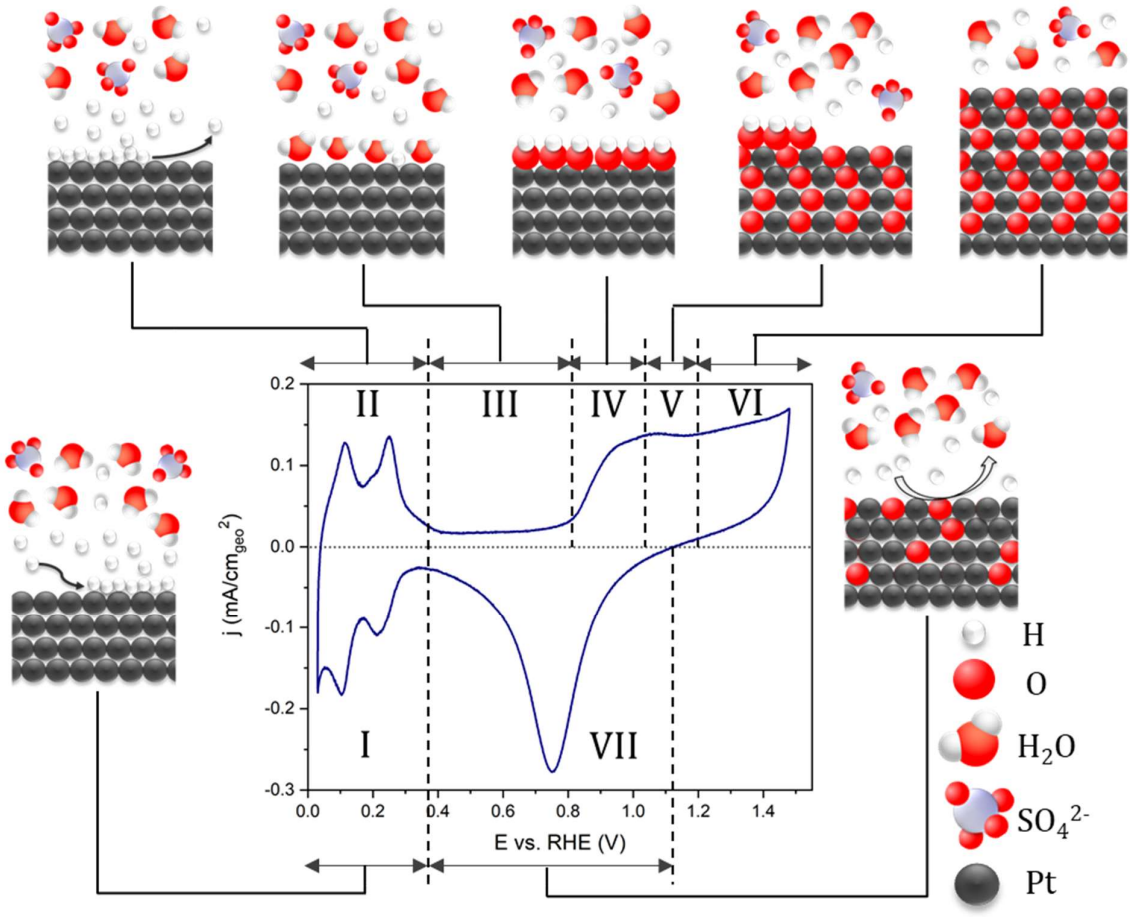

Figure 4.3 Typical cyclic voltammogram of a polycrystalline Pt electrode in Ar-saturated H_2SO_4 0.5 M showing the processes at each potential range (in roman numbers) and an atomistic model of the electrode/electrolyte interface structure in each region. The CV was taken at 50 mV/s with a reversible hydrogen electrode (RHE). Adapted from [82].

4.6.1 Electrochemical Surface Area (ECSA) Quantification

Many of these regions described in the previous section can be used to determine the electrochemical surface area (ECSA) of the electrode and thus allow for a direct comparison between different catalyst, which makes CVs a crucial electrochemical method for electrocatalysts characterization. The ECSA is usually calculated experimentally by using the charge associated with a given surface electrochemical process (Q) and the charge associated with the coverage of one monolayer (θ) by:

$$ECSA = \frac{Q}{\theta} \tag{4.13}$$

and Q is obtained from the integral of the region of interest in the CV by:

$$Q = \int Idt = \int IdE \frac{dt}{dE} \tag{4.14}$$

where $\frac{dt}{dE}$ is the inverse of the scan rate, which evidences the influence of the scan rate on the peak area. This methodology can be applied in several regions of the CV.

Among all electrocatalysts for which the ECSA can be measured, ECSA determination on metals is the most versatile due to the metal surface simplicity and capability of adsorbing various species. This adaptability gives rise to numerous methods that can be employed for ECSA determination, either from the Coulombic charge of a surface adsorption reaction, such as i) H adsorption/desorption, ii) CO stripping, iii) Pb underpotential deposition, and iv) surface redox reactions; or from the v) non-faradaic double layer capacitance. However, most catalysts are not active to all the methods mentioned above and/or the accuracy of the ECSA value varies among different techniques [103]. Hence, special caution should be used when choosing ECSA determination for a certain metal catalyst.

Hydrogen underpotential deposition (H_{UPD})

Charge associated with the adsorption of a hydrogen monolayer is the most commonly used method for ECSA calculation. The area over the two cathodic peaks (region I) after the subtraction of the non-faradaic currents (i.e. double layer) corresponds to 77% coverage of a hydrogen monolayer adsorbed on a polycrystalline Pt [104]. Then, by considering a θ_{Pt-H} of 210 $\mu C/cm_{Pt}^2$, the Pt ECSA can be extracted. This value is based on the assumption that θ of polycrystalline Pt corresponds to the averaged θ value over the three crystal base planes of Pt [104,105]. Besides the error associated with this assumption, the choice of valid integral limits also carries an error due to the presence of the hydrogen evolution peak at potentials close to 0 V vs. RHE. Moreover, the use of

an appropriate baseline for the double-layer region is highly important for accurate determination of the associated charge. Overall, the ECSA determined by this method often corresponds to 90% of the actual ECSA value [105]. Alternatively, the H desorption region may also be used for the calculation of ECSA (region II), but even greater caution should be used when choosing integral limits and scan rate due to both overlapping with the hydrogen evolution region and adsorbing of unwanted species [106,107].

CO stripping

Since CO strongly binds to certain noble metals (e.g. Pt and Rh), the CO stripping quantifies the catalyst ECSA by recording the charge transfer of stripping one CO submonolayer at a metal surface. The adsorption of a CO monolayer is activated by purging CO gas into the electrolyte while applying a mild reducing potential (0.1 V vs. RHE) for a few minutes (depending on CO flow rate and cell volume) [108]. Then, the electrolyte is purged with Ar to remove CO dissolved gas while holding the potential at 0.1 V, followed by slow potential sweeping to ~1.1 V vs. RHE, which triggers the oxidation of the CO monolayer:

$$Pt - CO + H_2O \longrightarrow Pt + CO_2 + 2H^+ + 2e^- \tag{4.15}$$

Whose peaks appears between 0.7-0.9 V vs. RHE. For Pt, the Coulombic charge corresponding to the stripping of this single CO monolayer is converted to surface area assuming a specific charge of 420 $\mu C/cm^2_{Pt}$ [109].

Analogous to the H_{UPD} method, CO stripping is of often the preferred choice of ECSA determination for Pt-based catalysts due to the stronger CO binding to the Pt surface compared to the H adsorption, making CO more resistant to changes in experimental conditions and impurities. However, a few artifacts can make the CO method less accurate than H_{UPD}, namely steric effects and an insufficient O_2 removal, which result in oxidation of the adsorbed CO and thus an ECSA underestimation [110]. Although in general the H adsorption method is more prone to be affected by experimental conditions (e.g. temperature and humidity) than CO stripping [111], the ratio between the ECSAs determined by these two methods tend to be consistent among samples [112]. For that matter, ECSA values from CO stripping are usually reported to be consistently higher than those found from H adsorption (Fig. 4.4a) [103]. Furthermore, since both techniques are surface-specific probes for Pt atoms, the ratio between charge associated with H adsorption (Q_H) and CO stripping charge (Q_{CO}) can also provide information about the surface adsorption energy, whose change with respect to pure metals indicates a different surface electronic structure [113]. The ambiguity caused by alloying is also reported in

CO stripping voltammograms, whose peak position and symmetry may indicate alloying, surface defects and/or crystallographic planes that result in active sites of different nature (Fig. 4.4b) [114,115].

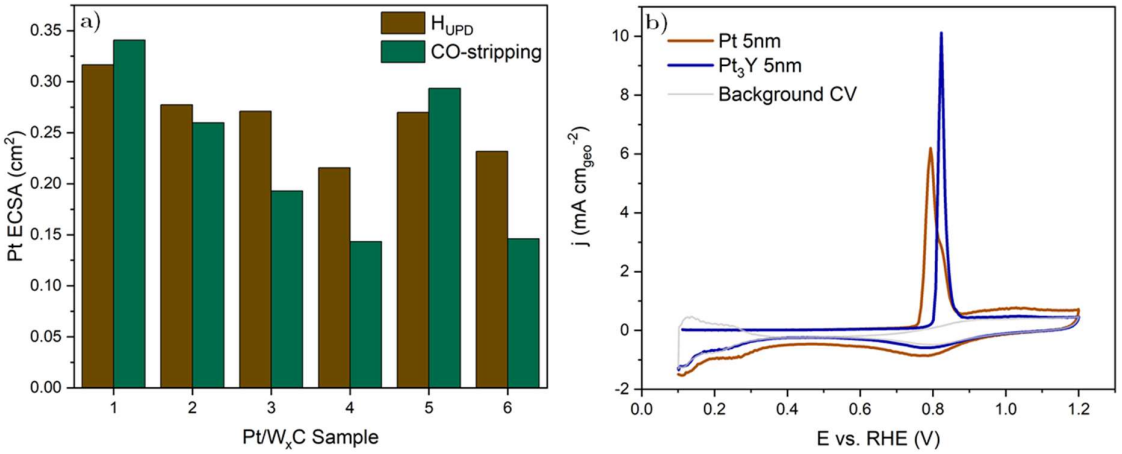

Figure 4.4 (a) Pt ECSA determined by H underpotential deposition and CO-stripping on a set of Pt 3 nm/W_xC samples upon accelerated stress test. The results exhibit a rather consistent Q_H/Q_{CO} ratio, except for samples 1 and 5, which may be indicative a different nature of Pt active sites. (b) CO-stripping voltammograms and baseline CV of 5 nm samples of Pt_3Y acid-treated and Pt thin films measured in a GDE half-cell showing different peak position and shape, which proves the existence of a different Pt in the Pt_3Y sample.

Pb underpotential deposition (Pb_{UPD})

The metal underpotential deposition makes use of the same concept as CO stripping, and it has been well reported to quantify the ECSA of metals such as Ag, Au, Pt and Ru by electrochemically depositing one monolayer of metal atoms (e.g. Cu, Ag or Pb) onto the catalyst surface [112]. However, for metals such as Pt and Ru, the methods described above are preferred since they exhibit more accuracy for the ECSA determination. For metals inactive to other more straightforward methods, such as Ag and Au, the Pb underpotential deposition (Pb_{UPD}) has to be used instead [116]. By holding the potential slightly above the Pb^{2+}/Pb reduction, a submonolayer (i.e. 2/3 monolayers) of Pb deposits onto the metal surface [117]. The potential is then slowly scanned to higher values, which triggers the dissolution of the deposited Pb submonolayer, thereby resulting in an oxidative current. The Pb_{UPD} stripping reaction in alkaline media can be written as:

$$Pb_{UPD} + 3OH^- \longrightarrow HPbO_2^- + H_2O + 2e^- \tag{4.16}$$

The ECSA can therefore be determined by integrating the Pb_{UPD} oxidation peak over a charge density of 280 µC/cm² [118–120].

Although it is well reported that the potential should be held right above the Pb^{2+} reduction (~0.2 V vs. RHE) for several minutes, the potential at which Pb_{UPD} occurs, as well as the voltametric shape, are highly sensitive to crystallographic orientation and morphology of the electrode[120,121]. Hence, for the correct Ag and Au ECSA determination, one should optimize the Pb_{UPD} method according to the system being analyzed. As an example, Fig. 4.5 depicts the Pb_{UPD} stripping on the same AgPd thin film sample, which was held at different potentials for 300 s. As observed, only 10 mV difference in potential holding can induce up to one order of magnitude differences in ECSA values.

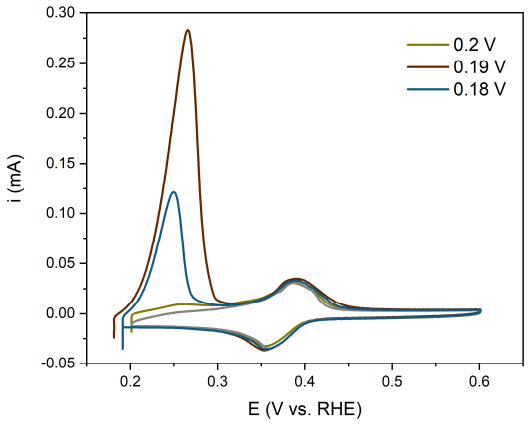

Figure 4.5 Pb_{UPD} stripping on the same AgPd thin film at different potential holds.

It should also be mentioned that, for samples containing more than one metal active to Pb_{UPD} (e.g. CuAg and AgAu), peak overlapping can be dismissed due to the Pb_{UPD} kinetics being much slower on these surfaces and exhibiting stripping peaks at different potentials than that of Ag [122–124]. However, great caution is advised when choosing integral limits and background subtraction on such bimetallic samples.

Metal oxidation and metal oxide reduction

Since the Coulombic charge of the metal surface redox reaction is directly related to its ECSA, metal reduction peaks can be used for ECSA quantification for samples that do not exhibit H adsorption peaks or CO stripping features. For instance, ECSA determination from H_{UPD} may become very inaccurate for metals such as Pd, whose H absorption complicates the integration of the area corresponding to a H monolayer formation [125]. For such metals, the area of the anodic/cathodic peak corresponding to the oxidation/reduction of the metal/metal oxide can be used instead. Table 4.2 summarizes the most typical oxidation/reduction peaks used for ECSA determination of metals commonly used in electrocatalysis.

Table 4.2 Redox reactions used for ECSA determination of common metal electrocatalysts [103,112].

Peak Potential (V vs. RHE)	Anodic/Cathodic reaction	Monolayer specific charge
~0.60 V	$PdO + 2e^- + H_2O \longrightarrow Pd + 2OH^-$	424 $\mu C/cm^2_{Pd}$
~1.25 V	$Ag + OH^- \longrightarrow \frac{1}{2}Ag_2O + \frac{1}{2}H_2O + e^-$	400 $\mu C/cm^2_{Ag}$
~0.60 V	$Cu + OH^- \longrightarrow \frac{1}{2}Cu_2O + \frac{1}{2}H_2O + e^-$	360 $\mu C/cm^2_{Cu}$
~1.10 V	$AuO + 2e^- + H_2O \longrightarrow Au + 2OH^-$	390 $\mu C/cm^2_{Au}$
~0.05 V	$Ni(OH)_2 + 2e^- \longrightarrow Ni + 2OH^-$	514 $\mu C/cm^2_{Ni}$

Since for all the reactions in Table 4.2 the potential range must include the analog redox peak, the CV selected potential window is therefore crucial for a correct ECSA determination using metal redox peaks. However, oxidation at higher potentials may also lead to a higher oxide coverage, which in turn causes a surface rearrangement and thus a fluctuating ECSA during CVs, or induces irreversible surface oxidation [126,127]. Since different metals may also give rise to redox peaks at similar potentials, attention should also be given to bimetallic samples that exhibit overlapping CV peaks. For instance, whereas Pd and Ag redox peaks used for ECSA determination are well-separated (Fig. 4.6a), the Ag anodic peak in a CuAg sample is overlapping the Cu oxidation peak at ~1.2 V vs. RHE and Ag ECSA is thus undeterminable (Fig. 4.6b). Moreover, the Ag cathodic peak at ~1.0 V vs. RHE occurs at different potential in each sample, thereby indicating different Ag oxygen affinity due to alloying [128,129].

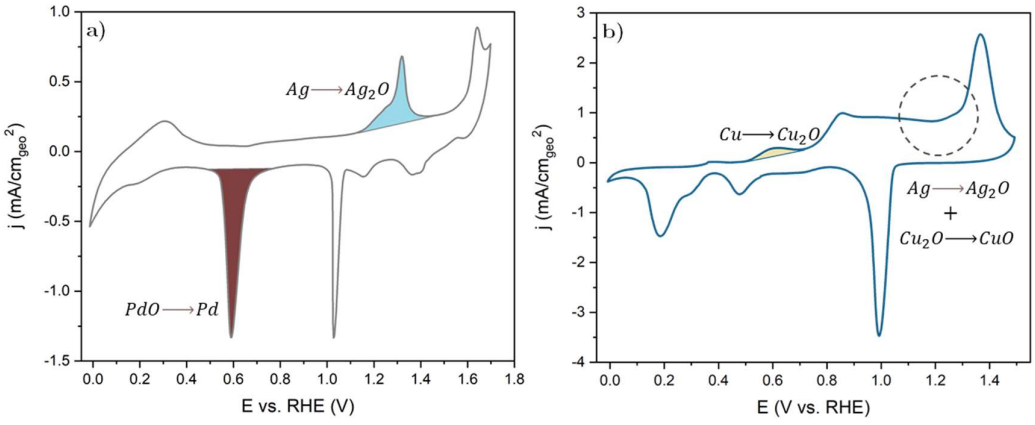

Figure 4.6 Cyclic voltammetries of (a) PdAg and (b) CuAg thin films at 50 mV/s in 0.1 M KOH with the Ag/Pd/Cu redox peaks used for ECSA determination. Although they have both been fabricated with the same Ag loading, they exhibit different Ag peak intensities due to different amount of surface Ag after potential cycling.

Capacitance

Non-faradaic currents arising from the EDL capacitance can also be used to calculate the ECSA, which is extracted from the dependence of the capacitive current (i_{DL}) on the scan rate ($\frac{dE}{dt}$) as:

$$ECSA = \frac{i_{DL}}{\frac{dE}{dt} C_M} \tag{4.17}$$

Thus, by plotting current vs. scan rate, the capacitance of the electrode is obtained, which can be converted to ECSA by dividing it by the specific capacitance found on the literature (C_M). For Pt, this value is usually reported to be 39.5 µF/cm^2 [130].

In this thesis, the methods described above have been applied for the ECSA determination of electrocatalysts, mainly for the two types of hydrogen polymer electrolyte fuel cells: the proton exchange membrane fuel cell (PEMFC) and the anion exchange membrane fuel cell (AEMFC), whose working principles and reaction mechanisms are explained below.

4.7 Proton-Exchange Membrane Fuel Cell (PEMFC)

Hydrogen PEM fuel cells are, without doubt, the most widely studied and used today, mainly for automotive applications thanks to its high energy density. The schematic diagram of the PEMFC working principle is shown in Fig. 4.7. In a PEMFC, hydrogen enters the flow field pattern, diffuses through the gas diffusion layer (GDL) and oxidizes in the anode catalyst layer. Protons generated from the hydrogen oxidation then travel through the acidic polymeric membrane to the cathode catalyst layer, where they react with oxygen that is being reduced to form water in the cathode. Compensating charge in the form of electrons then flows through the external circuit and provides the useful work done by the fuel cell. The overall PEMFC electrochemical reaction can be written:

Anode: $$H_2 \longrightarrow 2H^+ + 2e^- \tag{4.18}$$

Cathode: $$\frac{1}{2}O_2 + 2H^+ + 2e^- \longrightarrow H_2O \tag{4.19}$$

Overall: $$H_2 + \frac{1}{2}O_2 \longrightarrow H_2O \tag{4.20}$$

Since the electrochemical reactions required for the fuel cell to operate take place at the TPB in the catalyst layers, these are crucial for the good performance of the cell. The catalysts need to have contact with the electronic and the proton-conducting media, as

well as with hydrogen and oxygen. For this, a large-area catalyst support and a proton-conducting ionomer are needed. The support is usually carbon-based, which allows for high electric conductivity and provides favorable porosity with a suitable balance between catalyst utilization and good mass transport. Similarly, the right amount of ionomer is needed to provide ionic conductivity to all active sites. A good ionomer and carbon support performance, however, cannot guarantee a good reaction rate if the catalytic material does not provide the correct reactant conversion. Thus, efficient and stable electrocatalysts need to be developed if the full potential of PEMFC is meant to be exploited. Moreover, their cost also needs to be reduced for their widespread commercialization. The first step in the development of new inexpensive catalysts, however, needs the correct understanding of both the ORR and the HOR mechanisms.

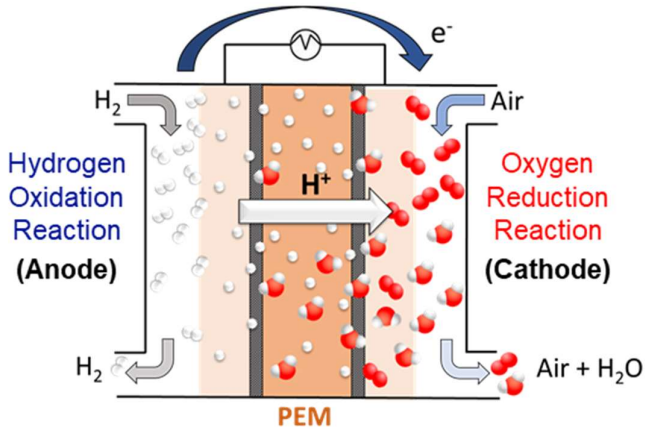

Figure 4.7 Schematic illustration of the PEMFC.

4.7.1 Oxygen Reduction Reaction (ORR)

As many other reactions, the oxygen reduction reaction (ORR) undergoes different pathways depending on the pH at which it occurs. In PEMFCs, which operate at low pH, the ORR is the largest single contributor to the potential loss of the fuel cell [131]. Thus, most of the research on PEMFC focuses on finding electrocatalysts more active than Pt, which is the current benchmark for this reaction in acidic media.

The ORR is a complex reaction to catalyze because it involves the transfer of 4 electrons and 4 protons to each O_2 molecule throughout a number of elementary steps, resulting in an exchange current density one order of magnitude lower than that of the HOR [40]. Moreover, the exact reaction mechanism is still not well understood, although it is believed to depend on the nature of the electrolyte, electrode and catalyst. In aqueous acidic solutions, there are two pathways through which the ORR may occur (at pH=0):

I) The direct 4-electron reduction pathway:

$$O_2 + 4H^+ + 4e^- \longrightarrow 2H_2O \qquad E°=1.23\ V \tag{4.21}$$

II) The 2-electron reduction pathway through H_2O_2:

$$O_2 + 2H^+ + 2e^- \longrightarrow H_2O_2 \qquad E°=0.70\ V \tag{4.22}$$

$$H_2O_2 + 2H^+ + 2e^- \longrightarrow 2H_2O \qquad E°=1.77\ V \tag{4.23}$$

Since generally the sluggish 2 electron pathway gives rise to a lower potential than the 4 electron one, the latter is preferred in hydrogen fuel cells. Moreover, the 2 electron pathway involves the formation of peroxide species, which is detrimental for the membrane [97].

Within a theoretical electrochemical framework, two possible ORR mechanisms are proposed for the 4 electron pathway: associative and dissociative mechanism [132]. In the associative mechanism, the pathway to form adsorbed O* intermediates proceed as follows:

$$O_{2(g)} + * \longrightarrow O_2^* \tag{4.24}$$

$$O_2^* + H^+ + e^- \longrightarrow HOO^* \tag{4.25}$$

$$HOO^* + H^+ + e^- \longrightarrow O^* + H_2O_{(l)} \tag{4.26}$$

while in the dissociative route, O* is formed by:

$$O_{2(g)} + 2 * \longrightarrow 2O^* \tag{4.27}$$

Lastly, OH* is formed and reduced to water in both mechanisms by:

$$O^* + H^+ + e^- \longrightarrow HO^* \tag{4.28}$$

$$HO^* + H^+ + e^- \longrightarrow H_2O_{(l)} + * \tag{4.29}$$

The specific reaction pathway mainly depends on the catalyst used and the potential applied. However, the ORR can be summarized as follows [45,133]:

i) O_2 surface adsorption.
ii) electron transfer to adsorbed O* species.
iii) dissociation of O=O bond.
iv) desorption of the OH- formed.

Among these steps, three are considered to be the rate-limiting steps: i), ii) and iii), which depend on the cathode material.

The state-of-the-art catalyst for PEMFC is either platinum or platinum alloys supported on carbon black. The high ORR activity is attributed to the balance between the relatively weak adsorption of the oxygen species intermediates (O^*, HO^*, HOO^*) and the rather strong adsorption of O_2 on adjacent Pt sites, which enables the O=O bond breakage [134]. Thus, since the stability of oxygenated species scales linearly with the oxygen binding energy, the latter can be used as a descriptor for the ORR on different metals [102]. As explained in Section 3.1, rate-limiting intermediates in a catalytic reaction should bind neither too weak nor too strong to the surface for optimum activity, which is illustrated by the volcano plot. For metals that bind oxygen intermediates too strongly, the reaction 4.26 is the RDS and, for the ones who bind intermediates too weakly, it is found that the reactions 4.24 and 4.27 are the RDS [135]. Pt is found on the "too strong" side of the oxygen intermediates binding of the volcano plot (Fig. 4.8) [132]. Thus, although Pt evidently has the highest activity for the ORR, an optimum catalyst should bind oxygen species approximately 0.1 eV weaker than Pt [132]. Furthermore, its high price and scarcity are additional motivations to reduce the amount of Pt used in the catalyst layer or, preferably, use Pt-free catalysts.

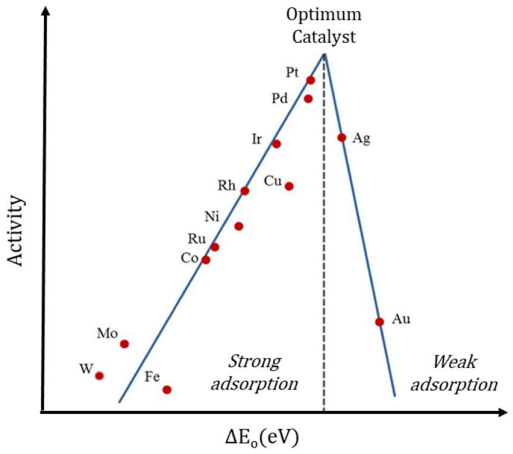

Figure 4.8 Volcano plot for the ORR activity on the oxygen binding energy for different catalysts. Data from [132].

The most common strategy to reduce Pt catalyst loading on the cathode is by alloying with other metal elements (often transition metals), such as Co, Ni, Fe, Ti, Cr, Ir or lanthanides [22,136–139], which can achieve higher intrinsic activities than pure Pt. The enhancement in the ORR activity has been attributed to different mechanisms, mainly ligand (electronic) and/or strain (structural) effects, that change the Pt electronic structure and thus the adsorption energy of reactants and intermediates. It has been proposed that structural effects may enhance the ORR by providing favorable active

sites for the dissociative adsorption of oxygen. This is caused by the insertion of a second metal with a larger atomic radius into the Pt lattice, which results in a compressive lattice strain and thus a decrease in the Pt-Pt distance [140]. Hence, when Pt is alloyed with metals of dissimilar radii, the greater the difference radii is, the more strain is induced. This has been extensively investigated with Pt-rare earth metals (REM) alloys, in which the REM is more thermodynamically favored to stay in the bulk, causing a compressive strain on the Pt surface layer and consequently increasing its activity [138,141–143]. On the other hand, alloying Pt with low d-orbital occupancy transition metals cause the Pt to share its d-orbital electrons with the unfilled d-orbital of the transition metal, tuning its d-band center [144,145]. This electronic effect is considered to be the most significant in determining the adsorption strength of oxygen intermediates. This has been investigated for Pt_3Ni and PtCu, among other Pt alloys [146,147]. However, the metallic transition metal alloys are often not very stable in acidic conditions, which leads to catalyst degradation [148]. For this reason, metal oxide catalysts have been investigated both as an alloying element with Pt or as a support in order to increase the stability of the catalyst layer. Other approaches involve switching to non-noble metal catalyst, such as M-N-C, where M corresponds to a non-PGM catalyst such as Fe or Co [149]. However, these are beyond the scope of this thesis, which focuses on Pt-REM alloys for the acidic ORR.

4.7.2 Hydrogen Oxidation Reaction (HOR)

In PEMFCs, most research has been focused on the development of cathode catalysts because the activation overpotential is mainly caused by the sluggish ORR kinetics. For this reason, much less attention has been paid to the anode reaction, in which Pt is also the most active catalyst. However, the HOR can also contribute to the PEMFC overpotential due to the high sensitivity of Pt towards CO impurities, which led to a vast research on CO-tolerant anode catalysts [150,151].

In acidic solution, the hydrogen oxidation is believed to be composed of two out of the three following steps (either Tafel-Volmer or Heyrovsky-Volmer):

Tafel $$H_2 + 2* \longrightarrow 2H* \tag{4.30}$$

Heyrovsky $$H_2 + * \longrightarrow H* + H^+ + e^- \tag{4.31}$$

Volmer $$H* \longrightarrow H^+ + e^- + * \tag{4.32}$$

Although the exact mechanism remains to be elucidated, the hydrogen adsorption is often considered to be the RDS in both the Tafel-Volmer and in the Heyrovsky-Volmer

pathways. Several studies have reported that the RDS are individually applicable only in limited potential ranges, with some claiming that the Tafel-Volmer route is the RDS at low potentials and it switches to the Heyrovsky-Volmer mechanism at higher potentials [152–154]. Nevertheless, other studies consider the Tafel-Volmer mechanism applicable at all operating potentials [155], while others consider the HOR on Pt as a structure-sensitive and temperature-dependent reaction [156].

Although Pt is the most active catalyst for HOR, there is a lack of consensus in the literature concerning the exchange current density values. The main discrepancy arises from kinetic data measured in RDE, in which the exchange current density obtained is too small by at least a factor of 20, bringing concerns on the actual mechanism controlling the reaction in Pt catalysts, i.e. kinetics vs. hydrogen diffusion [157]. Parallel to these studies, a lot of research has focused on the development of stable CO-tolerant electrocatalysts, mainly by alloying Pt with Ru, Ni, Fe or Sn [151].

4.8 Anion-Exchange Membrane Fuel Cell (AEMFC)

Alkaline fuel cells (AFCs) were the first fuel cell technology to be put into practical service, proving the feasibility of using hydrogen as a fuel, when it was first used in spacecraft in the 1960s [81]. AFCs were further extended into anion exchange membrane fuel cells (AEMFCs), the most recent fuel cell technology, where a solid electrolyte was used instead of liquid. This technology operates under the same principles as that of PEMFCs, its acidic analog, with the main difference of hydroxyl ions serving as charge carriers instead of protons. The schematic diagram of the PEMFC working principle is shown in Fig. 4.9. In an AEMFC, the oxygen from air diffuses through the GDL and is reduced on the cathode, thereby forming hydroxide anions. These ions are then transferred through the alkaline membrane electrolyte to the anode, on which oxidation of hydrogen into water takes place [40]. The overall PEMFC electrochemical reaction can be written as:

Anode: $$H_2 + 2OH^- \longrightarrow 2H_2O + 2e^- \tag{4.33}$$

Cathode: $$\frac{1}{2}O_2 + H_2O + 2e^- \longrightarrow 2OH^- \tag{4.34}$$

Overall: $$H_2 + \frac{1}{2}O_2 \longrightarrow H_2O \tag{4.35}$$

The main advantage of AEMFCs over PEMFCs relies on the alkaline electrolyte, whose milder conditions enables the possibility to use electrocatalysts free of noble metals, thereby opening the door for low-cost polymer electrolyte fuel cells. Furthermore, the

electrode kinetics of the cathode reduction are more facile in a high pH environment, which mitigates the activation overpotential attributed to the cathodic site [23]. Water flooding issues are also mitigated in AMEFCs compared to PEMFCs because the hydroxides and dragged water molecules generally migrate from the cathode to the anode, thereby suppressing hydrogen crossover [158]. They also present the advantage over AFCs of using an alkaline polymer electrolyte, which is less susceptible to carbonation issues that decrease the ionic conductivity, and avoids electrolyte leakage [159].

Nevertheless, AEMFCs have a few drawbacks compared to PEMFCs, mainly attributed to the nature of the electrolyte. A typical anion exchange membrane is composed of a polymer backbone with tethered cationic ion-exchange groups to facilitate the movement of free OH^- ions. However, the diffusion coefficient of hydroxide ions is approximately four times lower than that of the protons, which translates into conductivity issues. Although the carbonates precipitations are mitigated in AMEFCs due to cations being fixed to the membrane backbone, this also causes additional anion conductivity issues [159]. Besides, there are no commercially available anion-exchange membranes that are as efficient as Nafion® for PEMFCs. Last but not least, the lower AEMFC performance compared to PEMFCs has been attributed to a slower hydrogen oxidation in alkaline media, which evidences the need for highly active HOR catalysts as well as a good understanding of its mechanism at high pH [157].

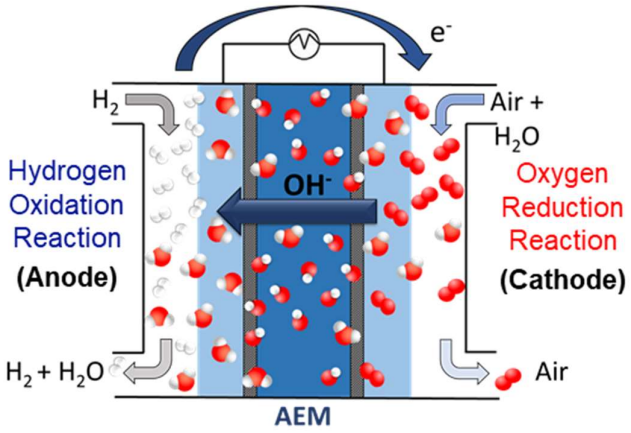

Figure 4.9 Schematic illustration of the AEMFC.

4.8.1 Oxygen Reduction Reaction (ORR)

Although the ORR kinetics in alkaline media is enhanced compared to acidic media, it is still far from being optimal and its exact sequence in AEMFC also remains to be elucidated. As in PEMFCs, the ORR is a multielectron reaction that undergoes two

different pathways that include a number of elementary steps involving different reaction intermediates, which slightly differ from those in acidic media [160]:

I) The direct 4 electron pathway, in which O_2 is directly reduced to OH^-:

$$O_2 + 2H_2O + 4e^- \longrightarrow 4OH^- \qquad E°=0.41\ V \tag{4.36}$$

II) The 2+2 electron pathway through HO2- intermediate:

$$O_2 + H_2O + 2e^- \longrightarrow HO_2^- + OH^- \qquad E°=-0.065\ V \tag{4.37}$$

$$HO_2^- + H_2O + 2e^- \longrightarrow 3OH^- \qquad E°=0.87\ V \tag{4.38}$$

The peroxide produced may also undergo disproportionation:

$$2HO_2^- \longrightarrow 2OH^- + O_2 \tag{4.39}$$

Thus, in alkaline media, the following intermediate species are formed: O^{2-}, O, OH^- and HO_2^-, whose stability regulate the activity of the ORR catalyst. Although the exact mechanism is still not well understood, it is known that the rate-determining step on metals such as Pt and Ag is the first electron transfer [161]:

$$O_{2(g)} + e^- \longrightarrow O_2^- \tag{4.40}$$

It is also known that the origin of the lower activation overpotential, i.e. higher voltage, in AEMFCs relies on the preferred formation of peroxide species in alkaline media, which desorb more easily than in their acidic analog [162]. The stabilization of HO_2^- due to its negative charge as opposed to its neutrality in acid solutions is believed to be the reason behind the more facile kinetics at high pH. Moreover, the dependence of the ORR on the pH was also explained by the presence of spectator species adsorbed on the catalyst surface, which at low pH block the active sites and lower the adsorption energy of the intermediates, thereby decreasing the overall reaction rate [163].

The decrease of the overpotential with increasing pH is one of the main factors permitting the use of Pt-free catalysts for the ORR in alkaline media, including noble metals, non-noble metals and metal-free catalysts [161]. Although the performance of Pt catalysts does not compensate their price, it remains the most commonly used and active catalyst for the ORR in alkaline conditions. Hence, considerable efforts have been devoted to decrease Pt content while maintaining a high ORR activity [24,164,165]. These Pt-based catalysts have lower Pt loadings and increased activity and stability relative to bulk Pt, mainly due to: i) strain effects that reduce the Pt-Pt bond distance and thus favor the oxygen adsorption, ii) d-coupling effects that lower the d-band center of the 5d-orbital when alloying with transition metals such as Ni, Co or Cr and iii) the

presence of surface oxide layers such as perovskites that enhance the covalency of the metal-oxygen bond [163,166,167].

With the need for comparatively cheap materials in AEMFCs, a number of substitutes to Pt have been considered, mainly in the PGM because they all promote the 4 electron pathway in alkaline media [166]. Pd and Ag-based electrocatalysts are more abundant noble metals than Pt that exhibit promising ORR activity via various modification methods. Pd has a similar electronic configuration to Pt and presents an optimum balance between the O=O bond breaking and the OH^- formation [168]. Moreover, Pd exhibits higher activity in alkaline than in acidic solutions due to a decrease in the anion poisoning effect in alkaline solutions [169]. However, its highly occupied d-orbital results in a too strong binding of oxygenated species, for which alloying with other transition metals is needed if the O binding energy is meant to be weakened. 3d transition metals are widely employed to enhance the catalytic activity of Pd catalysts, such as Cu, Ni, Fe and Co, which is highly dependent on the composition and structure of the alloy [166,168,170,171]. Ag has also been considered to substitute Pt in the cathode. The ORR in Ag surfaces occurs through 2 and 4 electron pathways depending on the surface morphology and oxidation state [161]. As opposed to Pd, Ag binds oxygen adsorbates too weakly, for which alloying with 3d metals is also needed, being Pd a good candidate due to its strong bonding to adsorbed intermediate species [172].

Among non-noble metal ORR catalysts, Fe, Co, and Mn are the most widely studied. Manganese oxides represent an attractive inexpensive and active catalysts towards the ORR in alkaline media, especially MnO_2 and Mn_3O_4 [160]. Their higher activity has been attributed to the mediation process involving the reduction of Mn(IV) to Mn(III), followed by the electron transfer from Mn(III) to oxygen. However, the ORR activity of MnO_2 was found to vary depending on the crystalline structure, with amorphous manganese oxides providing more active sites [173]. Mn oxides led to a new approach of electrocatalyst bifunctionality, in which one catalyst is used for the reduction of O_2 through the formation of HO_2^- and is subsequently reduced to OH^- by MnO_2, leading to a 4 electron transfer [174].

4.8.2 Hydrogen Oxidation Reaction (HOR)

In the PEMFC anode, platinum is an excellent HOR electrocatalyst. Nevertheless, in alkaline conditions the exchange current density for HOR on Pt is slowed by approximately three order of magnitude [175]. Despite the reduced activity of Pt for HOR in alkaline electrolytes and its price, Pt is still the most commonly used anode catalyst for hydrogen AEMFCs, for which considerable amounts of Pt are still needed [176].

The correct understanding of the HOR mechanism at high pH is a cornerstone in the development of inexpensive catalysts. Thus, tailoring of new alkaline HOR electrocatalysts rely on the thorough understanding of the reaction mechanism. Similar to that in acid, the HOR is normally believed to proceed through the combination of the following steps (either Tafel-Volmer or Heyrovsky-Volmer) [177]:

Tafel $$H_2 + 2* \longrightarrow 2H_{ad} \tag{4.41}$$

Heyrovsky $$H_2 + OH^- + * \longrightarrow H_{ad} + H_2O + e^- \tag{4.42}$$

Volmer $$H_{ad} + OH^- \longrightarrow * + H_2O + e^- \tag{4.43}$$

As seen, the Tafel step, i.e. dissociative adsorption of H_2 without electron transfer, is the same as in acidic media. However, the exact mechanism of the Heyrovsky and Volmer steps remains under considerable debate so far [178]. The Heyrovsky step can be described as the electron transfer from H_2 to the catalyst, either by OH^- or OH_{ad}. Similarly, the Volmer step, i.e. the discharge of the adsorbed hydrogen, can also occur *via* OH^- or OH_{ad} [177]. Thus, the different beliefs can be classified into two categories: HOR pathway with OH^- in solution and HOR pathway with OH_{ad} on the electrocatalyst surface. However, the hydrogen atom desorption (Volmer step), is widely viewed as the rate-determining step.

Two descriptors governing the HOR activity of electrocatalysts have been proposed depending on whether the HOR pathway is assumed to rely on OH^- or OH_{ad}. One descriptor is the hydrogen binding energy (HBE), in which only OH^- from solution is involved in the alkaline HOR. It is therefore suggested that, in strong base, the HOR mechanism does not change except that the Heyrovsky or Volmer step are followed by the fast recombination of H^+ and the abundant OH^- in the electrolyte, and thus the HBE governs the HOR activities in the full range of pHs [179]. In this way, it is suggested that the OH^- in solution affects the HOR activities through tuning the HBE, although they do not directly participate in the reactions through adsorption [180]. This hypothesis is widely demonstrated on Pt and Pt alloys, for which it has been claimed that the rate-determining step is the Volmer step and that the HBE is the unique and

sole descriptor for the HOR in alkaline electrolytes [181–184]. Others, however, describe the HBE as the *dominant* descriptor in HOR on PGMs, although other factors such as oxophilicity may also play a secondary role [185,186]. It has been reported that the HBEs of PGMs increase with increasing pH, and that the high HBEs in alkaline conditions are the underlying reason for the sluggish HOR [179,184]. Thus, when alloying Pt with other metals such as Ru, the HBE is weakened by down-shifting the d-band center of Pt through either structural or electronic effects, which leads to an enhanced HOR [187,188].

The other descriptor is the oxophilicity, i.e. the tendency of a certain element to abstract an oxygen atom from another molecule, in which adsorbed OH is involved. This hypothesis arose from the apparent beneficial effect of an added oxophilic metal in facilitating the hydrogen desorption (i.e. the assumed RDS), which has been interpreted as *bifunctional* activity. Thus, according to this hypothesis, alloying dissimilar metals in which one is a surface site with high affinity towards H_{ad} (M_A), and the other is an oxophilic metal that binds OH reversibly (M_B), results in a lowering of the energy barrier of the Volmer step and thus an enhanced HOR in alkaline media [189]. This process takes place on a bifunctional catalyst surface as follows:

$$H_2 + M_A \longrightarrow 2M_A - H_{ad} \tag{4.44}$$

$$OH^- + M_B \longrightarrow M_B - OH_{ad} + e^- \tag{4.45}$$

$$M_A - H_{ad} + M_B - OH_{ad} \longrightarrow H_2O + M_A + M_B \tag{4.46}$$

According to this model, the reason for slower HOR kinetics at high pH relies on the competitivity between H and OH for adsorption on active sites, which is dominated by OH due to its high concentration in alkaline electrolytes. Hence, with the aim to provide different adsorption sites and thus avoid competitivity, alloying of oxophilic metals with others with optimal HBE have been widely investigated for different morphologies, mainly involving bimetallic alloys such as PdNi [168,170,171,189]. For these alloys, it is yet not clear if the addition of a second metal results in an enhanced HOR through added oxophilicity or by tuning the HBE of the first metal. So far, however, there is no direct evidence that OH adsorption occurs at potentials near the HOR reversible potential, which is essential for this proposed mechanism [190].

Many examples have been provided for the beneficial effects of alloying to the HOR rate in alkaline media, either through electronic and structural effects modifying the HBE of PGMs or by added oxophilicity. Nonetheless, examples providing the existence of both mechanisms have also been given, which seems to be the most feasible occurrence. In summary, identifying the exact alkaline HOR pathway is indispensable for tailoring new highly-active inexpensive HOR electrocatalysts.

5. Model Electrodes

Fuel cell electrodes are complex materials, usually containing several components that contribute to overall performance, i.e. activity, selectivity and stability. The structure of a ready-to-use electrode is rather complicated, with a variable carbon support porosity and non-uniform Pt-site distributions. Additionally, the catalyst layer interface is a high transport and kinetic site where a variety of species (water, gas, protons/hydroxides, and electrons) shuttle at different rates and through different mechanisms. For this reason, in order to deconvolute the interplay of different components or factors, such as the catalyst active site, from the observed performance, is a challenging task. Hence, being able to study a very small amount of material and reactants at the surface of these complex materials is utmost importance, as well as the differentiation of its surface from its bulk. This requires employment of surface sensitive techniques and a variation in the complexity of the catalysts to isolate the contribution of each component. Thus, only by systematically adding complexity to a simple system, the ultimate real system may be approached. Model systems are well-defined systems that have been modified and structurally simplified in order to isolate the contribution from one or a few phenomena that are important for the real (and complex) system and thus allow for the investigation of performance-determining parameters separately in detail (Fig. 5.1). By improving control over parameters such as operating conditions, reactions and surface variability, the impact of several performance-controlling factors can be detangled from the fundamental dynamics, thereby allowing for the elucidation of the underlying mechanisms. In this work, different well-defined thin-film model electrodes have been fabricated and characterized (both physically and electrochemically) in order to analyze specific and selected mechanisms that describe the catalyst behavior.

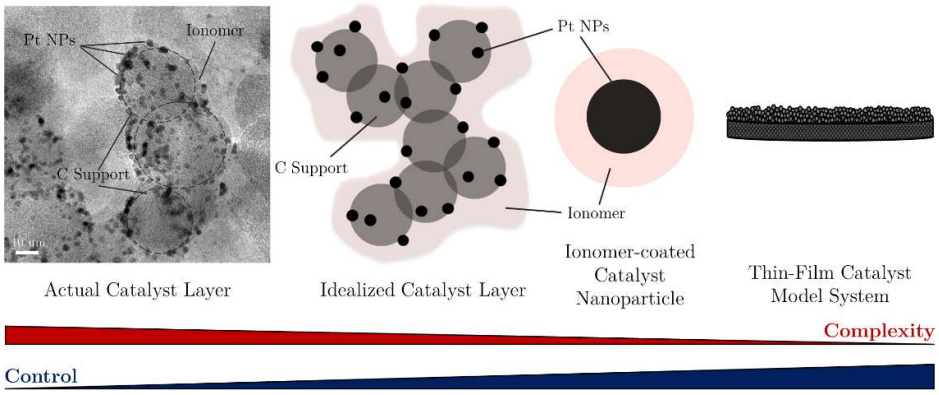

Figure 5.1 Schematic illustration of the role of model systems as a way of simplifying complexity while improving control of highly complex heterogeneous catalytic systems.

Physical vapor deposition (PVD) covers a range of thin-film deposition techniques. PVD processes involve individual atoms or clusters, which are not usually found in the gas phase, that are removed from a solid source and collide on a solid surface where atoms stick and form a film. The means to remove atoms or clusters from the source can occur through either sputtering (magnetron or ion beam), which utilizes energetic ions colliding with a target to sputter target material, or evaporation (thermal resistive and e-beam), which relies on heating a solid source material past its vaporization temperature. For this process to occur, an ultra-high vacuum (UHV) is needed to create the necessary mean free path for the vaporized metal to reach the substrate.

5.1 Fabrication

Since the complex structure of supported metal catalysts usually hinders the connection between macroscopic effects and microscopic processes at the surface, simpler structures are often preferred. Hence, the fabrication methods used for the sample preparation are critical to aim at fundamental questions about the correlation between structure and properties of catalytic materials. The methods used for the fabrication of model electrodes are critical because a high catalytic activity relies on very fine and well dispersed catalyst particles, for which planar structures are preferred. Besides, a model electrode should also ensure a high degree of reproducibility and maximized mass activity in order to provide a reliable comparison between different catalyst materials. Physically deposited thin-film model electrodes fulfill all the above-mentioned requirements. Thus, in this work, thin-films have been fabricated by physical deposition techniques, such as evaporation and sputtering, which allow for high control of the composition and thickness that ensure minimal structural variation between samples. Thin-films have

been deposited on both glassy carbon substrates (to be evaluated in Rotating Disk Electrode) and on conventional GDLs which are evaluated in single cell AEMFC.

5.1.1. E-beam Physical Vapor Deposition

E-beam PVD (a form of thermal evaporation in vacuum) uses a high-voltage electron beam directed by a magnetic field to focus a large amount of energy into the evaporation source found in a water-cooled holder. The high-energy beam produces a very high temperature in the metal target, which allows the metal to be vaporized. The vaporized metal atoms or clusters then diffuse through an evacuated chamber and impinge on a solid surface used as a substrate, at which they condensate and form a thin-film (Fig. 5.2) [94,191].

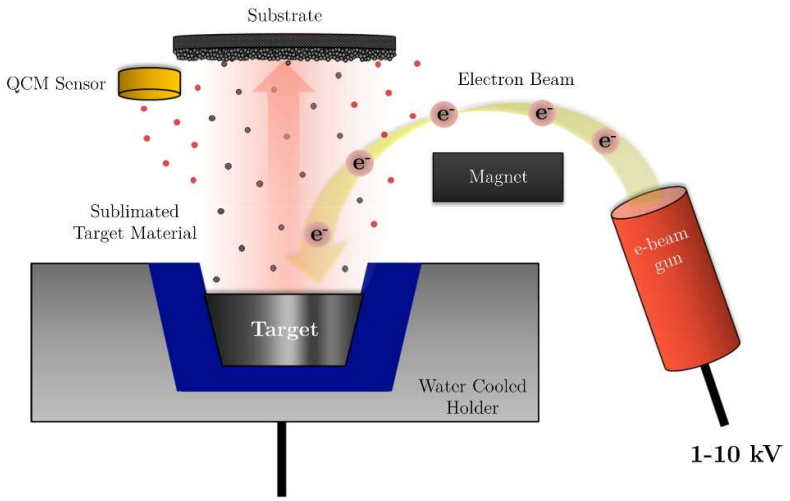

Figure 5.2 Schematic illustration of e-beam physical vapor deposition (PVD).

E-beam PVD can be used even on metals with high melting points, without compromising uniformity or material utilization. Moreover, this technique also presents the advantage of good directionality and low level of impurities, which are essential for the fabrication of well-defined model electrodes. Nonetheless, e-beam PVD also exhibits a few drawbacks that might affect the properties of ideal thin-films. Since thin-films are formed as a result of the much lower temperature of the substrate on which they are being deposited at low deposition rates, they usually have a smaller grain size than the bulk materials [191]. The impact energy in PVD is generally rather low, which might result in low adhesion of evaporated films. Furthermore, this technique is not suited for depositing alloy thin-films because each alloying element has a different temperature-vapor pressure relation, which leads to different evaporation rates and thus a difficult control of the alloy composition [94]. Alternatively, it is also possible to evaporate two materials subsequently and anneal at a certain temperature to form the desired alloy.

However, the surface composition of the resulting alloy is often difficult to reproduce and other physical deposition techniques are used in order to obtain uniform and well-controlled alloy thin-films.

5.1.2 DC Magnetron Sputtering

As opposed to e-beam PVD, magnetron sputtering is a plasma-based technique that employs magnetron sputtering sources that use electric and magnetic fields to confine a plasma (typically composed of positively charged Ar particles) close to the surface of the source, or target material. The confined plasma collides with the negatively charge target material (cathode), thereby causing the ejection of atom clusters from the metal target (Fig. 5.3). These ejected atoms then travel through the UHV chamber under a magnetic field and are deposited onto the substrate material (anode) [191,192].

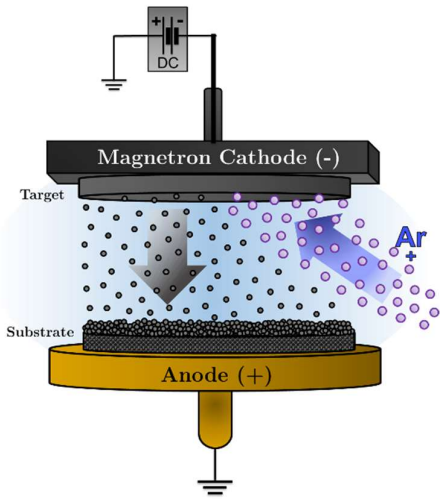

Figure 5.3 Schematic illustration of DC magnetron sputtering.

This method produces good film quality and uniformity, as well as very strong adhesion. Moreover, DC magnetron sputtering exhibits the highest scalability among all the physical deposition methods, which is very advantageous for industry applications [191,193]. More importantly, this method is very suitable for fabrication of alloy thin-films with compositions very close to that of the alloy target, either by placing clips of the alloying metal on top of the metal to be alloyed, by using an alloy target or by sputtering from multiple alloys.

Although both evaporation and DC sputtering are well-established and commonly used methods for thin film fabrication with high reproducibility and uniformity, the different conditions in which they operate results in thin films of slightly different properties. Since e-beam PVD vaporizes the target material, the evaporated metal target clusters

are usually larger than those ejected by the Ar plasma in DC magnetron sputtering (Fig. 5.4). Moreover, the presence of Ar atoms in the sputtering chamber also decreases the unidirectionality of the sputtered material due to collisions with plasma, which translates to a higher coverage in porous materials. Hence, since a full coverage can be achieved with less amount of material, DC sputtering is more suitable for material coating with the minimum amount of target material (Fig. 5.3c).

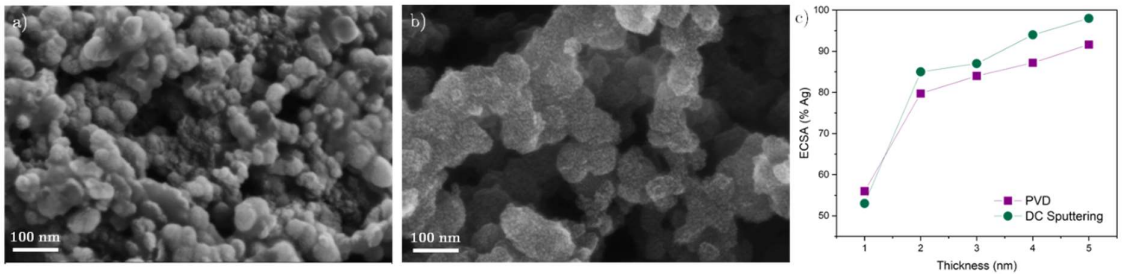

Figure 5.4 SEM images taken at 5 kV of Pt 3 nm (a) sputtered and (b) evaporated on a GDL. (c) ECSA % of Ag of the total surface area of sputtered and deposited Ag onto a Pd thin film.

5.2 Electrochemical Characterization

5.2.1 Rotating Disk Electrode (RDE) and Rotating Ring Disk Electrode (RRDE)

In order to study electron transfer kinetics of HOR and ORR electrocatalysts and evaluate their catalytic activity, convective systems like the rotating disk electrode (RDE) are used. The RDE allows for the screening of catalysts under constant reactant flux and steady state. In this hydrodynamic technique, the mass transfer to the electrode surface is faster and more controllable than in case of stationary electrodes, where mass transport is governed solely by diffusion and migration. Thus, by setting an enhanced and well-defined mass transport, kinetic information such as rate constants, electron transfer coefficients and symmetry factors can be obtained [31,32]. In this work, RDE is the main tool to evaluate the performance of electrocatalysts.

The RDE is used in a conventional three electrode set-up, with a counter electrode, reference electrode and the disk of the RDE as working electrode, which consists of a circular conductive disk (5 mm diameter) embedded in an insulating PTFE sheath. The disk itself is generally made of catalytic material deposited onto glassy carbon, which are both conductive. The electrode rotates with a defined constant velocity, adjusted by the attached motor, around the rotating axis, which is perpendicular to the electrode surface (Fig. 5.5). The rotating disk then drags the electrolyte at its surface along with it and the centrifugal force propels the solution outwards in a radial direction, which

increases with increasing rotation rate (ω) [32,33]. This results in a laminar flow of solution towards and across the electrode of which rate can be controlled by rotation speed.

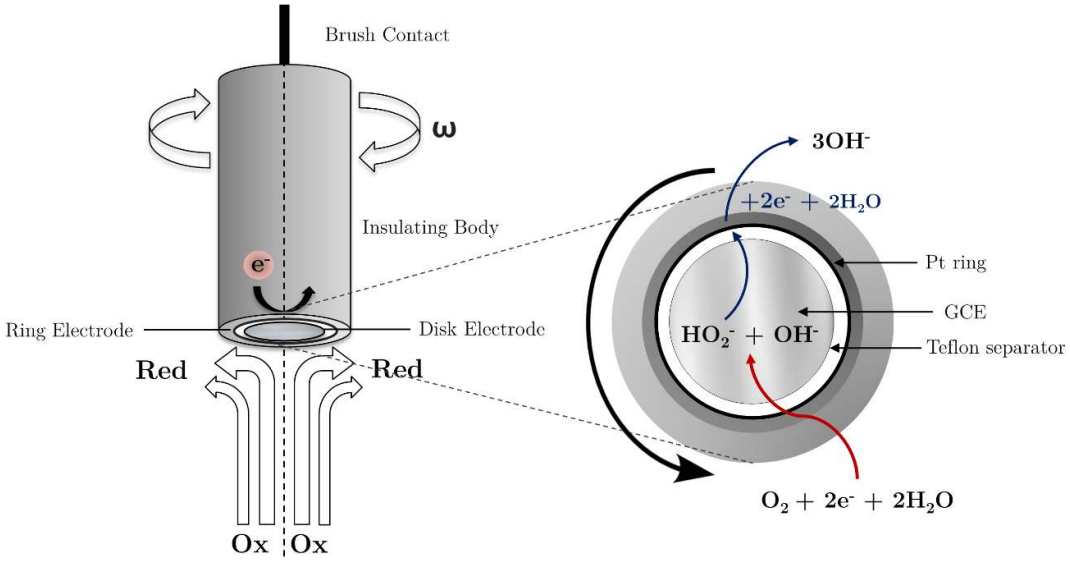

Figure 5.5 Schematic illustration of a rotating ring disk electrode (RRDE) and the radial flow of electrolyte during a reduction reaction (left), together with the ring detection of the peroxide generated by incomplete O_2 reduction in alkaline media (right).

Diffusion, convection and migration are the processes by which reactants are transported to the electrode surface. In a stagnant electrolyte, the dominant mechanism is diffusion, which induces limitations in the obtention of kinetic data of planar electrodes because the current in the kinetic region is dominated by mass transport, which is increasing with time. Forced convection can be applied in order to enhance mass transport, which is particularly important when dissolved gases with low solubility are used as reactants, such as in the ORR and HOR. Under forced convection, the net mass transport and thus the current is governed by the diffusion of reactants through the diffusion layer [31,33]. Hence, since the thickness of the diffusion layer is determined by the rotation speed, the current is also controlled by convection. The current density measured at the electrode surface is inversely proportional to the thickness of the double layer (δ), which is expressed by Fick's law [31]:

$$j = nF\frac{D}{\delta}(c_0 - c^*) \tag{5.1}$$

where n is the number of moles of electrons transferred in the half reaction, F is the Faraday constant (C/mol), D is the diffusion constant, c_0 the concentration of reactants in the bulk and c^* is the concentration of reactants at the surface. High rotation speeds result in very thin diffusion layer thicknesses and, as a consequence, each species that

arrive at the electrode surface are immediately converted (i.e. oxidized or reduced), leading to a surface concentration equal to zero. Eq. 5.1 can then be simplified to:

$$j = nF\frac{D}{\delta}c_0 \tag{5.2}$$

which relates the thickness of the diffusion layer to the current generated under convection. The relation between δ and the rotation speed (ω) of the electrode is expressed by an equation developed by Levich [32]:

$$\delta = 1.61D^{\frac{1}{3}}\nu^{\frac{1}{6}}\omega^{-\frac{1}{2}} \tag{5.3}$$

where ν is the kinematic viscosity of the electrolyte (cm^2/s). According to Eq. 5.3, the thickness of the diffusion layer of a chosen system depends only on the rotation rate. By combining Eq. 5.2 and 5.3, the *Levich equation* for the diffusion limited current density (j_L) using RDE is obtained:

$$j_d = 0.62nFc_0D^{\frac{2}{3}}\nu^{-\frac{1}{6}}\omega^{\frac{1}{2}} \tag{5.4}$$

where the value of 0.62 is used when using rotation units of radians per second.

Before reaching the mass transport controlled regime, the current is also affected by the reaction kinetics in the so-called *mixed region*. Thus, in order to analyze the kinetics in this region, the kinetic and the diffusion current densities must be deconvoluted so they can be determined separately by:

$$\frac{1}{j} = \frac{1}{j_k} + \frac{1}{j_d} \tag{5.5}$$

where j_k and j_d are the kinetic and the diffusion-limited current density respectively. The diffusion-limited current can easily be determined from the diffusion region of the polarization curve at high overpotentials and the kinetic current density can be quantified by plotting $1/j$ vs. $1/j_d$, in which j_k corresponds to the intercept of the plot with the y axis. Kinetic parameters, such as the electron transfer coefficient (n), can be obtained by rearranging Eq. 5.4 and 5.5, which gives the *Koutecky-Levich equation* [38]:

$$\frac{1}{j} = \frac{1}{j_k} + \frac{1}{0.62nFc_0D^{\frac{2}{3}}\nu^{-\frac{1}{6}}\omega^{\frac{1}{2}}} \tag{5.6}$$

By plotting $1/j$ vs. $\omega^{-\frac{1}{2}}$, a straight line is obtained, whose slope is used to determine kinetic parameters expressed in the Levich Equation [32,33].

As explained in Sections 4.7.1 and 4.8.1, when oxygen is reduced by an electrocatalysts, hydroperoxide (HO_2^-) by-product may be produced, which is unwanted because of its

harmfulness to the membrane and because indicates the incomplete O_2 reduction and thus less current generated [194]. Since it allows for the study of the kinetics of slow electron transfer and electrochemical reaction mechanisms, the rotating ring disk electrode (RRDE) is an essential tool to investigate electrocatalyzed multi-electron reactions such as the ORR. The RRDE consists of an RDE with a second independently-controlled working electrode (ring electrode) concentric to the disc and separated by a non-conductive barrier (Fig. 5.5). Because of the laminar flow generated during rotation, the hydrodynamic fluid flows from the disk over the ring, where the products from the half-reaction at the disk are detected as they are swept. The limiting current at the ring($i_{ring,l}$) is given by:

$$i_{ring,l} = 0.62nF\pi(r_3^3 - r_2^3)^{2/3}D^{2/3}\omega^{1/2}\nu^{-1/6}C_0 \tag{5.7}$$

Where r_2 and r_3 are the inner and outer radii respectively.

As in RDE, by varying the rotation rate it is possible to determine electrochemical reaction rates if and when it is in the proper kinetic regime. Furthermore, the average fraction of hydroperoxide produced during ORR ($\%\, HO_2^-$), as well as the average number of electrons involved during the process (n) over the potential range, can be determined by:

$$\%\, HO_2^- = 200x\frac{I_r/N}{I_d + I_r/N} \tag{5.8}$$

$$n = 4x\frac{I_d}{I_d + I_r/N} \tag{5.9}$$

Where I_d is the disk current, I_r the ring current and N the current collection efficiency, which represents the fraction of species from the disk that arrived on the ring. This parameter depends only on hydrodynamics and on the ring-disk electrode geometry and can be either calculated experimentally or provided by the supplier.

Even though RRDE does exhibit several limitations that will be explained below, this technique is widely used for preliminary screening of catalyst electrochemical behavior. By using cyclic voltammetry, for instance, information regarding the structure and composition of a catalyst surface can easily be obtained. Fig. 5.6a shows the CV of three different thin films: Pd, Ni and PdNi annealed. As observed, whereas the alloy resulting from annealing of Ni and Pd thin films barely exhibits any observable Ni features, the peaks characteristic of Pd in PdNi are significantly different than those for pure Pd. Firstly, although only Pd is active for hydrogen adsorption, the annealed PdNi alloy exhibits a larger hydrogen adsorption/desorption region (between 0.05 and 0.4 V vs. RHE), which is attributed to the alloying effect that results in a lattice spacing increase and hence may facilitate the hydrogen absorption into the metal lattice [195]. Secondly,

the anodic peaks emerging at 0.7-0.8 V in the Pd sample correspond to the chemisorption of OH^- ions on Pd and is not present for the PdNi sample, indicating different oxygen affinities in PdNi. The reduction peak at 0.7 V is attributed to the reduction of Pd(II) compounds during the cathodic sweep and, as seen, the Pd(II) reduction takes place at slightly different potentials for pure Pd and for PdNi. As expected, PdNi shows a lower amount of charge involved on the Pd(II) reduction, indicating less amount of surface Pd, which can be quantified according to the method described in Section 4.6. More importantly, the reduction peak for PdNi is shifted negatively with respect to pure Pd, which suggests that the electronic structure of surface Pd in PdNi is affected by the Ni in the alloy below the surface (Paper II). Hence, a great deal of electrocatalyst surface information can be extracted in RDE from simply scanning the potential.

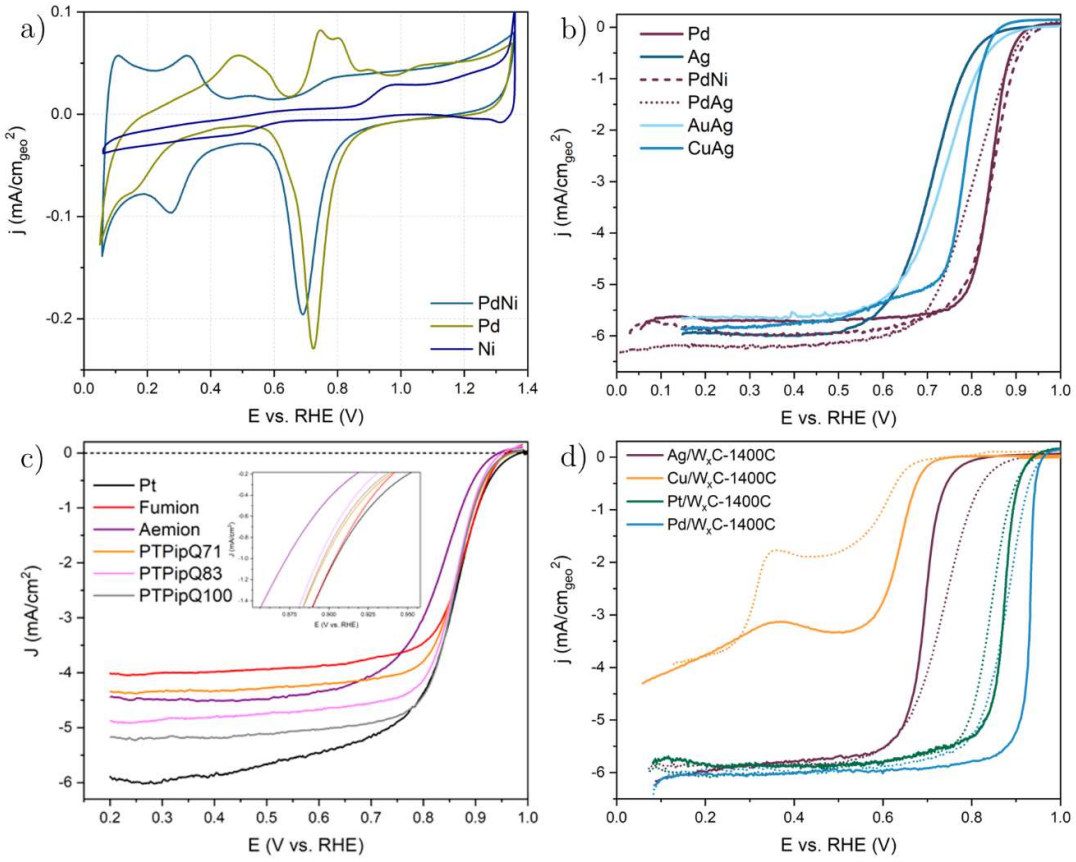

Figure 5.6 Examples of electrochemical screening of electrocatalysts by means of RDE: (a) Cyclic voltammetries of Pd, Ni and PdNi annealed at 500 °C thin films in 0.1 M KOH at 50 mV/s. (b) ORR polarization curves of Pd, Ag and Pd and Ag bimetallic thin films in KOH 0.1 M at 50 mV/s. (c) ORR testing of different alkaline ionomers drop-casted on Pt and their kinetic activities at ~0.9 V. (d) ORR activity of noble metals supported on WxC annealed at 1400 °C in inert atmosphere with the respective pure metals (dashed lines) in 0.1 M KOH.

The RDE is also a well-established tool to evaluate the catalyst performance towards catalyzing electrochemical reactions. By recording the current generated upon applied potential in O_2-saturated electrolytes, different alloyed thin films can be evaluated

towards their ORR activity in alkaline media. Fig. 5.6b shows ORR polarization curves of Pd, Ag and several of their alloys. As shown, the alloying metal plays a major role in the catalytic properties of the resulting alloyed thin film. Whereas the addition of Ni to Pd gives rise to a slight ORR activity improvement at low overpotentials due to electronic effects, the addition of Ag does not result in any improvement compared to pure Pd. Given that Ag is more active than Ni towards catalyzing the ORR in alkaline media, this decay in Pd ORR activity when Ag is introduced is attributed to a degree of alloying in PdAg that is insufficient to improve Pd intrinsic activity. However, the addition of Cu and Au to a Ag thin film does exhibit a better ORR activity, which is attributed to ligand and strain effects respectively (Paper III). Thus, the mere addition of two metals together is not enough to result in an observable catalytic enhancement.

The relation between ionomer structure and catalyst kinetic and transport properties can also be evaluated in RDE (Fig. 5.6c). The effect on Pt ORR activity of two commercial ionomers and three lab-synthesized ionomers were characterized by means of ORR polarization curves in KOH. The trend in ORR activities at both kinetic and mass-transport regimes were in very good agreement with what has been reported in the literature. At low overpotentials, the ionomer ion exchange capacity (IEC) plays a crucial role because an incomplete removal of the halide counter-ion will most likely result in active-site blocking, which match the trend observed at 0.9 V (inset) [196,197]. At high overpotentials, instead, the presence of phenol may lower the local pH and thus affect OH^- transport [198,199], which is evidenced by the agreement between the ionomer phenyl content and their activities in the mass transport region.

Alloying of two or more metals is not the only strategy that can be adopted to improve catalyst intrinsic activity. The employment of carbon-based supports, such as tungsten carbide (W_xC), has been proven to improve Pt intrinsic activity in alkaline media [200–202]. To further investigate the enhancement mechanism, 3 nm of four different noble metals were evaporated onto a WxC support annealed at 1400 °C in H_2 atmosphere (Fig. 5.6d). Except for Ag, the ORR polarization curves showed a remarkable improvement of the ORR activity for all W_xC-supported metals compared to the respective pure metals. Thus, given that all three metals exhibiting an ORR enhancement are located on the left side of the Volcano plot (Fig. 4.8), we inferred that the improvement observed for Pt, Pd and Cu could be attributed to a synergetic effect induced by the support that weakens the oxygen binding energy of these metals and thus results in an optimal adsorption of oxygen intermediates. More importantly, this results evidence the

beneficial effect of using supports to optimize catalyst utilization while improving their intrinsic activity, which translates to a major cathode catalyst cost reduction.

As proven above, the RDE technique is a widely popular and well-establish approach to evaluate the electrocatalyst performance. The following assets add to the advantages previously described: (i) the small amount of catalyst needed for the measurement, (ii) the unnecessary use of expensive fuel cell stations, and (iii) the straightforward and well-stablish test protocols compared to other setups. However, for the investigation of benchmarked ORR catalyst, a wide range of varying activities has been reported [148]. The discrepancies between RDE measurements mainly arise due to the use of different electrolytes, a non-optimal catalyst layer and/or different testing protocols. Moreover, RDE measurements are inherent to limited mass transport, low current densities, and less understanding of potentials at kinetic region [203]. Even though the reliability of RDE testing has considerably improved due to several best practice studies [108,112,148,204], its poor reactant mass transport, low current densities and idealized catalysts on solid substrates hinder the extrapolation of catalyst performance in ready-to-use systems. Thus, since the RDE provides conditions quite different from those in a real fuel cell, the measurement of electrocatalytic activity under more relevant operating conditions are highly needed.

5.2.2 Fuel Cell Measurements in Membrane Electrode Assembly (MEA)

The membrane electrode assembly (MEA) is a suitable choice for measuring model electrodes under conditions similar to those in an actual fuel cell, e.g. high reactant mass transport. The MEA is the heart of a polymer exchange fuel cell, i.e. PEMFC or AEMFC, and it consists of two catalytically active electrodes that form the anode and the cathode, and a polymer exchange electrolyte, forming a three-layer structure (Fig. 5.7). However, the real electrode in real MEAs is very complicated to fabricate and complex to analyze, which makes the catalyst study and development very challenging. At the same time, the conditions in in the RDE are not the same as in the fuel cell and thus the catalyst evaluation is not ideal. An MEA model system relies between those, which can be seen as a combination of both. Thus, by using PVD fabrication methods on gas diffusion electrode (GDE) materials, is it possible to evaluate catalyst performance in a real fuel cell environment while having most of the advantages from thin-film fabrication. Similar to an actual MEA, the MEA model system also contains electrodes that facilitate transport of products and reactants through the setup, ions through the

membrane, and electrons to and from the current collectors. However, despite the more realistic conditions, the evaluation of catalyst performance in MEA configurations still lack a well-established testing protocol that needs to be widely implemented if a reliable comparison of fuel cell catalysts is meant to be conducted.

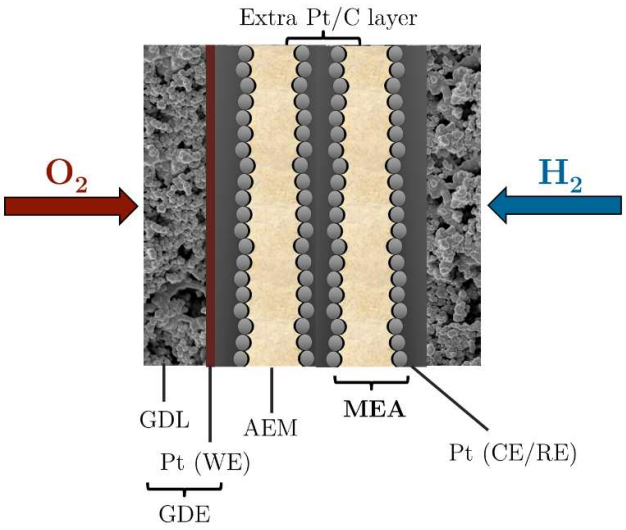

Figure 5.7 Schematic illustration of the double-MEA setup using Pt nanoparticles as catalyst.

In this work, a double-MEA configuration developed at the department of Applied Electrochemistry at KTH was employed for both Pt-REM thin film performance evaluation and investigation of Pt and Pt_3Y aging under realistic conditions. In this setup, an extra Pt/C -membrane layer is introduced between the membrane and the combined CE/RE. Oxygen and hydrogen react on this extra Pt/C layer to form water, thereby reducing the amount of permeating gases and thus cross-over effects (Fig. 5.7). Regardless of the protocol followed for the evaluation of electrocatalytic performances in this system, consistency and rigorousness in electrochemical measurements can ensure reproducible and reliable comparison of electrocatalysts evaluated in this configuration (Fig. 5.8).

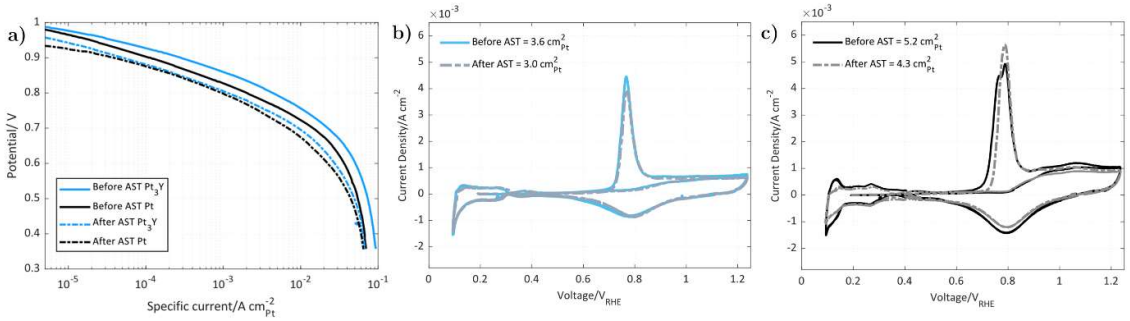

Figure 5.8 (a) Non-IR corrected steady-state ORR polarization curves of Pt and Pt_3Y thin films before and after accelerated stress test (AST) between 0.6 and 1.4 V_{RHE} in acidic media indicating the superior activity of Pt_3Y; and CO stripping profiles of (a) Pt and (b) Pt_3Y before and after AST to track ECSA changes.

5.2.3 Gas Diffusion Electrodes (GDE)

Despite the advantages of MEA systems over RDE techniques, comparison of different MEA studies is often challenging due to discrepancies in operating conditions and different measuring protocols. Hence, techniques combining the advantages of RDE, i.e. simplicity and comparability, with the realistic operating conditions of MEA systems are needed to elucidate the effects of catalyst layer parameters on fuel cell reactions. Gas diffusion electrode (GDE) half-cell setups have recently emerged as crucial tools to bridge the gap between fundamental and actual fuel cell electrocatalyst research [205]. These half-cell setups are capable of mimicking a fuel cell single electrode and, as opposed to RDE, exhibit the advantage of catalyst performance evaluation at realistic current densities without mass-transport limitations, thereby resembling the catalyst performance in MEA systems [206]. Hence, GDE setups also allow for a reliable evaluation of catalyst layer stability and selectivity under relevant mass transport conditions.

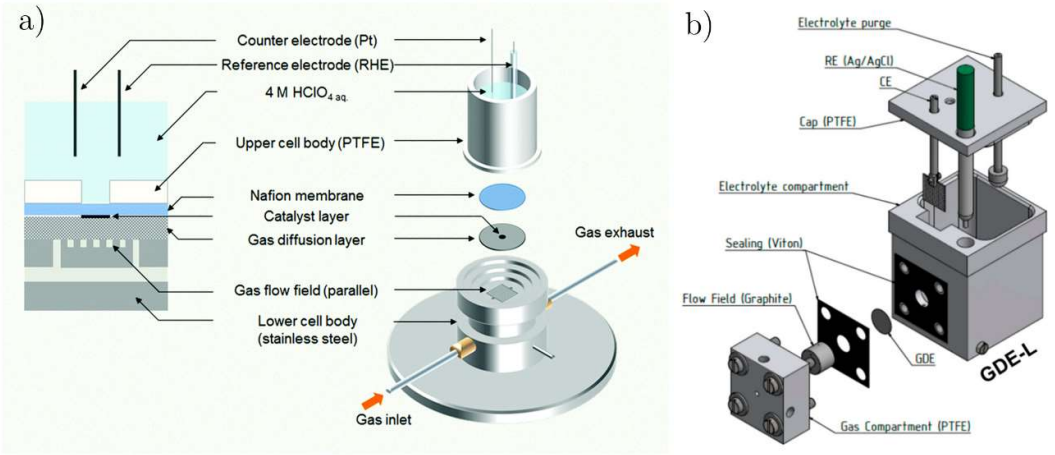

Figure 5.9 Schematic representations of GDE half-cell setups used for the inter-lab comparison. Reproduced from Ref. [206] with permission from the Royal Society of Chemistry.

In this work, we have compared the GDE setup of Masanori et al. [206] (Fig. 5.8a) with the GDE of Ehelebe et al. [207] (Fig. 5.9b) with different thicknesses of sputtered Pt_3Y and Pt on a GDL as ORR catalyst (Fig. 5.10), from which it was concluded that, even for non-benchmarked catalysts, the GDE approach indeed possesses the potential to reach standard fundamental testing within a lab-scale. However, similarly to RDE and MEA testing, it has been reported that a reliable comparability between GDE systems can only be achieved if: (i) similar (or equal) electrochemical protocols are utilized, and (ii) a homogeneous catalyst layer is used regardless of the geometric surface area [205].

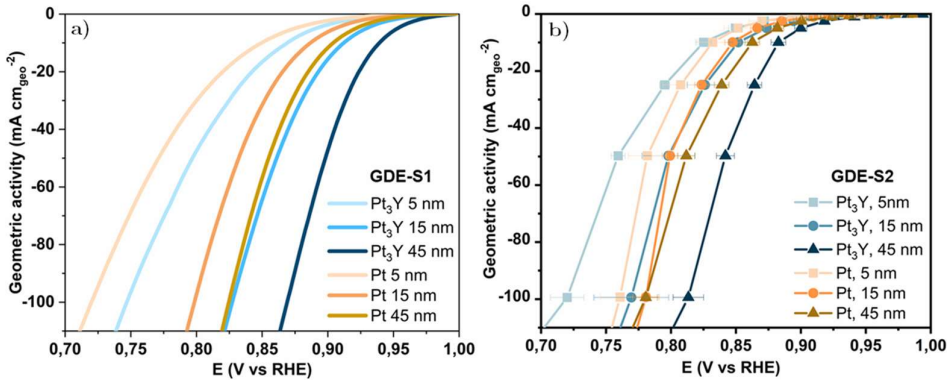

Figure 5.10 ORR geometric activities of 5, 15, and 45 nm sputtered Pt and Pt_3Y measured in the GDE from (a) Masanori et al. [206] through potentiodynamic measurements and from (b) Ehelebe et al. [207] through galvanostatic measurements.

5.3 Physical Characterization

5.3.1 X-ray Photoelectron Spectroscopy

X-ray Photoelectron Spectroscopy (XPS) is a surface-sensitive technique that is used for qualitative and semi-quantitative analysis of the elements within a material, as well as their chemical state and the density of electronic states. Since it gives information about the chemical state of the material components, it is also called Electron Spectroscopy for Chemical Analysis (ECSA). The possibility to estimate the chemical composition and chemical state of elements, together with a small probing depth, makes XPS an important method for catalysts physical characterization [208].

The basic principle of XPS is based on energetic X-rays kicking out core electrons of an atom, whose energy is measured in an electron analyzer and compared to a reference library, such as Handbook of X-ray Photoelectron Spectroscopy [209]. Therefore, an XPS instrument consists of three critical components: the X-ray source, the electron energy analyzer and the detector. The X-ray source is composed of filaments that emit electrons, which are accelerated towards their respective anodes at 10-15 keV and bring about emission of X-rays. The choice of the anode material determines the energy of the X-rays emitted, which depends on the of surface analysis required. The most commonly used X-ray sources are Mg and Al due to their narrow full width at half maximum (FWHM), relatively high energy and intensity. The X-rays are then filtered by a monochromator and irradiated onto the material to be analyzed, which emits electrons whose kinetic energies are differentiated by the electron energy analyzer to allow for element identification. The material analyzed should be metallic and have a reasonably high melting point because the emission current creates a lot of heat on the material. The electrons are then accelerated to a certain energy (pass energy) and enter the detector, where they induce a detectable current that is registered by the detector itself.

Depending on the energy of the electrons, they will have different trajectories and can thus be differentiated for elemental identification [208,210].

In XPS, surface atoms are differentiated by tracing back the energy of the detected electrons to retrieve the kinetic energy of the incident electrons. This energy, together with the energy of the X-ray line, enables the calculation of the binding energy of the electrons (E_{BE}) by [208]:

$$E_{BE} = h\nu - E_k - \phi_{sp} \tag{5.10}$$

Thus, for an electron kicked out with a photon energy $h\nu$, it has to overcome the binding energy (E_{BE}) and the spectrometer work function (ϕ_{sp}) in order to reach the detector with a kinetic energy E_k (Fig. 5.11). However, the kinetic energy of the electron in vacuum, i.e. in the XPS chamber, could be descried as:

$$E_{k-XPS} = h\nu - E_{BE} - \phi_s \tag{5.11}$$

where ϕ_s is the work function of the sample. Since both the sample and the analyzer are grounded, the contact potential between the two metals accelerates or decelerates the electron so that, at the end:

$$E_k - \phi_{sp} = E_{k-XPS} - \phi_s \tag{5.12}$$

Eq. 5.10 can now be written as [208]:

$$E_{BE} = h\nu - E_{k-XPS} - \phi_{sp} \tag{5.13}$$

which is how the instrument derives the binding energy of a certain ejected electron. To detect the electrons, ultra-high vacuum (UHV) is needed to ensure that photoelectrons can travel from the sample to the detector without significant scattering [210]. Moreover, high vacuum is also needed to keep the surface of the sample clean, otherwise the surface can adsorb monolayers of hydrocarbons and water and the XPS signal can be stemmed from this contamination.

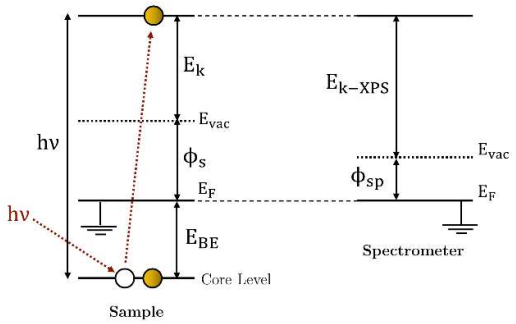

Figure 5.11 Schematic band diagram showing the energy of the photoemission process.

As far as every chemical element has a characteristic XPS spectrum, the chemical composition of a sample can be identified by the photoelectron energy. The position of a certain core-level photoelectron depends on the surrounding atoms. However, different binding energies in the same element in different chemical compounds might also be observed due to several reasons: difference in the oxidation state, different lattice parameters, *etc.* Thus, the binding energy shift due to the atomic environment effect, the so-called *chemical shift*, arises from different phenomena. In oxide samples, for instance, the strong electronegative oxygen atoms attract electron density, which causes the increase of the binding energy of core electrons and thus shifts the core-level energy peak to higher binding energies. In fact, binding to any atom with a higher electronegativity will result in a withdraw of electron density and thus a chemical shift towards higher binding energies. Other phenomena that might be seen in an XPS spectrum is *satellite peaks*, which appear at lower binding energies of the peak and are caused by the irradiation with the non-chromatic source. Moreover, *ghost peaks* arising from imperfections of the X-ray source might also be observed. Electrons that suffered an energy loss during the travel to the detector also give rise to XPS peaks, which include: *Auger peaks* and plasmon-loss features. Auger peaks emerge when an inner level hole is refilled by a more energetic electron from an outer level, which results in the emission of another electron from the outer energy level and a peak at very high binding energies is observed. Plasmon-losses originate from discreet energy losses and are observed at higher binding energies than the core-level photoelectron peak due to the interaction of the plasma oscillation of the outer shell with the photoelectron. In addition, some elements exhibit a spin-orbit splitting resulting in two peaks for p, d and f states, the so-called *spin-orbital coupling*. The ratio between the two peaks are different for each orbital shell (*p*, *d* and *f*) and the separation between the coupling states is characteristic of each element [208,209].

The shape and intensity of a core-level photoelectron peak are used for the qualitative and quantitative analysis of the sample constituents, which depend on the peak type as well as on the nature of the sample. Several components that overlap each other can be observed in a peak due to the coexistence of all the phenomena explained above. For this, deconvolution of each contribution is needed if each chemical state is meant to be quantified. The peak shape is usually well-defined by a Gauss-Lorentz profile for insulators and semiconductors, and by the Doniach-Sunjic line shape for metals. Moreover, the background arising from inelastically scattered photoelectrons should also be subtracted for the appropriate determination of the peak intensity and thus its quantification. Different background shapes can be used to better evaluate the line shape and stoichiometry, i.e. linear, Shirley or Tougaard, whose use depends on the nature of the photoelectron peak [208,211]. Lastly, XPS peaks should be calibrated to account for

differences between the Fermi level of the spectrometer and the sample, which results in photoelectron kinetic energies differing from the actual value. The most common calibration peak is carbon 1s at a binding energy of 284.8 eV because every sample surface has a trace of adventitious carbon, i.e. carbon contamination.

Information from XPS beyond the surface can be obtained by performing a non-destructive depth profiling by means of synchrotron radiation XPS (SRXPS), which is carried out by tunning the excitation photon energy [208]. Similarly, angular resolved photoelectron spectroscopy (ARXPS) also allows for measuring a depth profile by tunning the angle between the perpendicular to the sample surface and the direction of the photoelectron detection, thereby changing the probing depth. Hence, different probing depths allow to track changes in electronic structure at different sample depths (Fig. 5.12a), thereby enabling the correlation between the electronic structure of the outermost layers (i.e. active in catalyzing the redox reaction) with their specific activities at a certain potential (Fig. 12b).

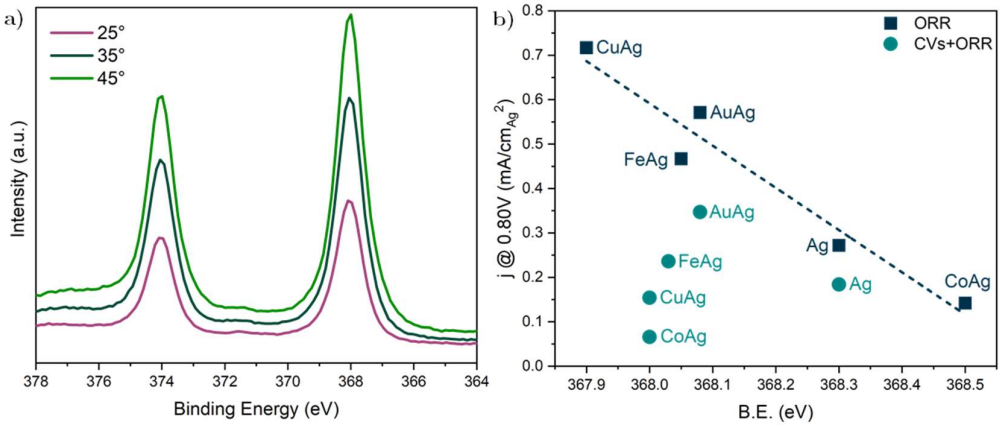

Figure 5.12 (a) Ag 3d XPS spectra of a Ag-covered Au thin film measured at different incident angles showing how the effect induced by the underlying Au on Ag binding energy attenuates when going to lower incident angles, i.e. far from the Au-Ag interfaces. (b) correlation between Ag binding energy (Ag 3d3/2) of different Ag-based bimetallic thin films after ORR testing measured at 25° and their ORR specific activity at 0.80 V_{RHE} in 0.1 M KOH.

In a lab XPS, depth profiling may also be obtained by destructive ion etching. By using an ion beam (usually Ar) to etch the layers of the surface or surface contamination, subsurface information can be revealed. The surface is etched by scanning an ion beam over an area of the sample (usually in the range of µm) and, after the etch cycle, an XPS spectrum is recorded from the surface of the sample. Thus, combining a sequence of ion gun etch cycles with XPS analysis provides both qualitative and quantitative information about the elemental composition throughout the sample, as well as the sample thickness.

5.3.2 Scanning Electron Microscopy/Energy-dispersive X-ray Spectroscopy (SEM/EDX)

Electron microscopy is a technique used to determine the size and shape of materials, as well as give information of the internal structure due to the different possible interactions between the electron beam and material. The interaction of the electron beam with a sample atom gives rise to, among others, back-scattered electrons (BSE) and emitted secondary electrons (SE) (Fig. 5.13), which are both used in scanning electron microscopy (SEM) to obtain information about the surface topography and composition. Moreover, the interaction between matter and an electron beam also produces characteristic X-rays, which might be used in energy-dispersive X-ray spectroscopy (EDX) for elemental analysis and chemical characterization of a sample [212].

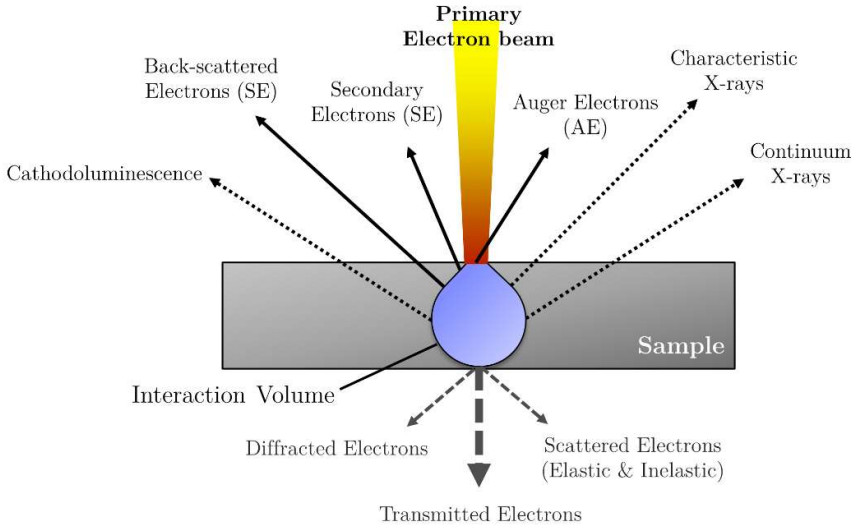

Figure 5.13 Electron-matter interaction volume and types of signal generated.

SEM is a type of electron microscopy that is used for imaging of samples by scanning them with a focused beam of electrons (typically 0.2-40 keV) and recording both the BSE and the SE emitted. BSE correspond to those electrons from the electron beam that have been bounced back out of the sample and, in contrast, low-energy SE are produced when electrons knock into atoms of the sample and displace electrons from the sample itself. The detection of these electrons allows for the investigation of the structure, morphology and crystallite size, as well as for determining surface defects. However, different elements show characteristic differences for backscattered electron energies, making some elements more distinguishable in images taken at the same accelerating voltage and magnification (Fig. 5.14). The BSE produced by the elastic scattering of electrons can also be collected in a different detector and, in combination with the

evaluation of the characteristic X-rays, qualitative and quantitative elemental analysis can be obtained by EDX, which is an integrated characteristic of the SEM [212,213].

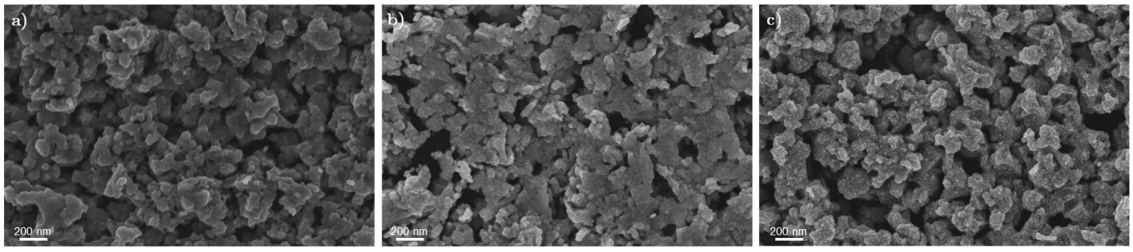

Figure 5.14 SEM images using backscattered electrons at 5 kV of (a) Cu, (b) Pd and (c) Ag 3 nm sputtered onto a W_xC 40 nm support annealed at 1400 °C on GC.

5.3.3 X-ray Diffraction (XRD)

XRD is a very suitable tool to identify the crystalline phases of model electrodes by means of lattice structural parameters. Since the interplanar spacing is characteristic of the material lattice parameter, this technique can also be used to identify the crystal lattice specific to a certain material. XRD relies on the emission of X-rays of wavelength λ onto a surface, which will result in constructive interference if the radiation is scattered in a mirror-like reflection by the material surface crystallinity. The cases in which constructive X-ray interference is found in specular geometry is described by the *Bragg's law* [214]:

$$n\lambda = 2d_{hkl}sin\theta \tag{5.14}$$

Where n is an integer number of the wavelength, λ is the X-rays wavelength, d_{hkl} the interplanar spacing between crystal atomic layers where h, k and l are *Miller* indices and θ is the angle between the incident beam and the sample surface (Fig. 5.15). Thus, according to Eq. 5.14, the path length of the diffracted X-rays has to differ by n for the interference to be constructive.

Hence, by shining X-rays onto samples at various angles, information on the crystal structure can be obtained through interference patterns. Whereas the structure of single crystal samples can be determined by a particular pattern at certain 2θ values, the crystalline domains of polycrystalline samples are randomly oriented and give rise to multiple diffraction peaks. However, for thin film model electrodes on GCs, the surface area is often not enough to generate a significant signal-to-noise ratio with the given thickness and Gracing Incidence-XRD (GI-XRD) is required.

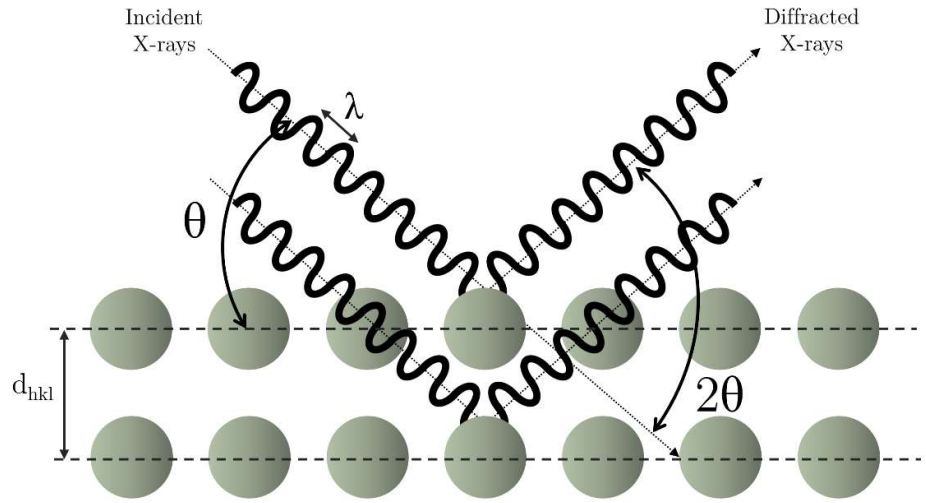

Figure 5.15 Visualization of Bragg's law and the constructive interface on the lattice planes of crystals.

Besides crystal structure determination and crystal phases identification, XRD can also be used to determine whether the electronic effects described in Chapter 3 are due to strain or ligan effects. Positive shifts of XRD peaks towards higher 2θ values result in a negative strain relative to the unalloyed sample (i.e. compressive strain), whereas a negative shift indicates a positive strain (i.e. tensile strain). Since the nature of the lattice strain can be used to predict the change in the d-band of an alloyed metal (Section 3.1.1.), enthalpy of alloy formation and metals radii can assist the rational design of electrocatalysts. However, it should also be mentioned that, although certain strain is expected when incorporating a metal with dissimilar radius, for some alloyed systems (e.g. Pt-REM) the opposite desired strain is observed due to a more thermodynamically favorable rearrangement of the overlayer [66,215].

6. Summary, Conclusions and Outlook

The main long-term goal of my project is to investigate the catalytic activity and stability of electrocatalysts for both the hydrogen oxidation reaction and the oxygen reduction reaction in PEMFC and AEMFC with the aim to develop the next generation of efficient, durable and inexpensive catalysts for low-temperature hydrogen fuel cells. The work presented here represents the first progress towards achieving this goal.

6.1 Summary of Appended Papers

In **Paper I**, the electrocatalytic activity towards the oxygen reduction reaction (ORR) of thin-films of Pt and rare earth metals (REM) alloys (Pt_3Y, Pt_5Gd and Pt_5Tb) was evaluated in a membrane electrode assembly (MEA) of a PEMFC. The cathode thin-film electrodes were fabricated by deposition onto a gas diffusion layer (GDL) using DC magnetron sputtering and they were subsequently acid-treated to obtain a Pt overlayer covering the Pt-REM alloy bulk. Formation of a protective Pt skin over the Pt-REM alloy was confirmed by EDX and XPS/SRXPS, which was measured for as-sputtered, acid-treated and fuel cell measured samples. The thin-film catalysts performance was evaluated in a fuel cell environment by means of polarization curves in O_2/H_2. As the key result, it was found that the acid-treated alloys of Pt_3Y and Pt_5Gd catalysts show a specific activity enhancement of 2.5 times compared to pure Pt, and a 2.0 enhancement for acid-treated Pt_5Tb. The activity enhancement in Pt-REM alloys was attributed to a lattice strain effect caused by the underlying alloy on the Pt skin, which was found to be thicker for Pt_5Tb and thus the reason for its lower electroactivity. This study demonstrates the beneficial effects of alloying Pt with REM, which can lead to more active and less expensive catalysts compared to today's PEMFCs.

In **Paper II**, electronic effects on both the HOR and the ORR for PdNi thin-film alloys were evaluated in alkaline media. The bimetallic alloys were fabricated by means of

physical vapor deposition (PVD) and were subsequently annealed at different temperatures to induce the formation of different surface compositions. The samples were then acid-treated to remove Ni species on the surface and form a Pd overlayer, and both these and as-annealed samples were evaluated in RDE for HOR and ORR by means of polarization curves. Elemental surface composition and structure were evaluated by XPS and SEM respectively, which revealed different surface constituents at different temperatures, as well as a grain size dependent on temperature. It was found that, whereas the addition of surface Ni was beneficial for the HOR, the ORR activity showed an overall enhancement in acid-treated samples. The evaluation of the HOR activity and its correlation with the Hydrogen Binding Energy (HBE) of Pd provided clarifications on the HOR mechanism by confirming the HBE as the main descriptor of this reaction in alkaline media. Moreover, given the Tafel slopes obtained, the Volmer step was proposed as the rate-determining step in the HOR. The ORR, conversely, showed that electronic effects resulted in the largest enhancement when Ni was placed in the subsurface rather than on the surface, which induced an electronic effect that caused a shift of the d-band center of Pd and thus a weaker adsorption of oxygenated species.

The beneficial or detrimental effect of the alloying metal on the ORR catalytic activity of Ag-based alloyed thin films in alkaline media was investigated in **Paper III**. Four different Ag bimetallic samples were fabricated by means of DC magnetron sputtering, in which 4 nm Ag thin layer was sputtered onto Co, Cu, Au and Fe thin films. The ORR electrochemical performance was then evaluated in the RRDE setup for both as sputtered samples and samples in which cyclic voltammetries (CVs) were run prior to ORR, which induces different changes in their surface compositions depending on the underlying metal. The surface (and subsurface) composition, as well as the degree of alloying, were studied by AR-XPS, XRD and CVs, which provided insights on the surface structure before and after CVs and ORR. The surface structure and composition were then related to their ORR performance in terms of both H_2O_2 production, ORR kinetics, and electron transfer coefficients, which evidenced the different roles of the alloying metal in terms of oxophilicity, structural defects, and electronic structure. Since the ORR activity enhancements in different bimetallic samples were attributed to different causes, this was used to obtain a better mechanistic understanding of the ORR in alkaline conditions and thus facilitate future AEMFC ORR electrocatalyst rational design.

In **Paper IV**, the activity of three different thicknesses of both Pt and Pt_3Y thin films in acidic media was evaluated in two gas diffusion electrode (GDE) half-cell setups in order to bridge the gap between activity discrepancies in fundamental and applied Pt-Y catalyst research. As in both RDE and MEA model systems, the GDE measurements

revealed the better ORR performance of Pt_3Y thin films compared to Pt in terms of both geometric and specific activities, which singled out the 45 nm sample as the best performing thickness. In mass activities, however, the most optimal catalyst utilization was found to be in 5 nm Pt_3Y, which outperformed every other thin film. Furthermore, XPS, TEM and EDX physical characterization provided proof of the Pt-skeleton structure formed upon Pt_3Y acid treatment, whose strained Pt has long been speculated to be the reason behind the ORR enhancement in Pt-REM alloys. This paper evidenced the beneficial effect, in terms of cost and activity, of alloying Pt with Y to enhance Pt intrinsic activity, as well as the successful usage of GDE setups as a lab-scale setup to evaluate thin film catalysts under relevant (and realistic) fuel cell conditions.

A better understanding of the cathode kinetics in alkaline conditions was provided by evaluating a Pt thin film electrode in an operating AEMFC in **Paper V**. A 2D evaporated Pt on a gas diffusion layer (GDL) was assembled in an optimized double-MEA setup and ORR polarization curves at different O_2 partial pressures were recorded. It was found that the O_2 partial pressure had a significant negative effect on the system open circuit voltage, maximum current density and cell voltage, as expected. A rapidly increasing Tafel slope with increasing overpotential, as well as the constant slope at voltages above 0.80 V_{RHE}, were observed, which was explained by a theoretical model. The model considered an associative mechanism where both charge and proton transfer steps are deconvoluted, which pinpointed the proton transfer as the rate-determining step in the ORR in alkaline media. Moreover, a decrease in the apparent reaction order with respect to O_2 was observed when going to larger overpotentials, which was indicative of a potential-dependent rate-determining step. The theoretical model developed in this study is of great importance for fast-screening the intrinsic ORR activity of catalysts at relevant fuel cell conditions, which exhibits a substantial potential to assist in the design of the new generation of AMEFC electrocatalysts.

Electrocatalysts for the alkaline analog of the PEMFC, the AEMFC, were studied in **Paper VI**, in which different radiation-induced chemically synthesized AgNi structured nanoparticles were evaluated for their activity towards the ORR in alkaline conditions. Two types of bimetallic AgNi nanocatalysts were synthesized by γ-radiation induced synthesis: Ag@Ni core-shells and Ag/Ni heterostructures. The structural and compositional analyses were carried out by microscopy (TEM, HRTEM and HAADF-STEM), diffraction (XRD) and spectroscopy (XPS and EDS). The electrochemical characterization by RDE was used to evaluate the ORR activity, which for both structures was shown to be higher than their monometallic counterparts. Both alloy samples exhibited a very similar ORR enhancement, which was attributed to a ligand effect originating from the Ag-Ni interface for Ag@Ni, and to both a lattice strain effect

and the presence of oxidized Ni species for Ag/Ni. Thus, in this paper, the study of the ORR performance was correlated with the nature of the electronic effects induced in the nanoparticles as a result of both ligand and structural effects.

In **Paper VII**, the well-reported superior performance of Pt_3Y thin films with respect to Pt was evaluated in terms of long-term stability under severe potential cycling in acidic conditions. The electrochemical stability of Pt_3Y thin films sputtered onto a GDL was investigated in relevant PEMFC conditions provided by a double-MEA, which was carried out by an accelerated stress test (AST). The aging test consisted of 3600 potential cycles between 0.6 and 1.5 V_{RHE} at 1 V/s scan rate, which was selected to induce both Pt and carbon corrosion and thus submit the electrode to severely harsh conditions. By recording ORR polarization curves before and after the AST, as well as CO-stripping to track ECSA changes, a decrease in specific activity was observed for both Pt and Pt_3Y thin films. Whereas EDX and XPS quantification revealed a rather constant bulk and surface composition upon aging, deconvolution of Pt-4f XPS spectra indicated the presence of a pure Pt-like Pt in the Pt_3Y sample after the AST, thereby evidencing the change in Pt electronic structure despite the presence of bulk Y. The XPS spectra did not show any significant changes in the electronic structure of the pure Pt sample. However, SEM images showed a major change in morphology after aging in both samples, which was more pronounced in the pure Pt sample and was therefore considered the major reason behind its activity decrease. Overall, it was concluded from Paper VII that Pt_3Y thin films are, at least, as stable as Pt.

The effect of the solvent ratio when drop-casting alkaline ionomers onto catalyst layers was investigated in **Paper VIII**. Since the interactions between ionomer and thin film model electrodes/catalysts is critical to determine the performance of the catalyst, different ratios of DMSO:IPA used for preparing an ink of PTPiPQ83, a poly(arylene piperidinium)-based ionomer recently synthesized at Lund University, were studied in terms of both morphology and both HOR and ORR electrochemical performance. It was found that the morphology of the ionomer, as well as the ionomer/Pt thin film interaction, is highly dependent on the dispersion of ionomer in various solvent ratios. Structural changes of the PTPiPQ83 concerning solvent ratio were investigated by SEM and FIB-TEM images, which showed different ionomer morphologies attributed to different drying processes due to different solvent ratios. The RDE testing of PTPiPQ83-modified Pt electrodes revealed that ionomer binding to Pt promotes higher ORR and HOR activity, which corroborate well with the morphological studies. Among all five different ratios tested, 10:90 solvent ratio dispersed PTPiPQ 83 capped Pt showed higher geometric and specific activity among all solvent ratios.

6.2 Conclusions and Outlook

This project has focused on the development of electrocatalysts for low-temperature hydrogen fuel cells, whose rational development is currently hindered by the lack of mechanistic understanding. A versatile platform to study model system catalysts was built to allow for reliable comparison among catalytic materials. Different catalyst model systems were fabricated by means of physical methods and were tested for their electrochemical activity and stability towards catalyzing fuel cell reactions in both acidic and alkaline media. With the aim to reveal the insights behind their electrochemical behavior, their electrochemical performance was then related to their composition and structure by *ex situ* physical characterization, mainly consisting of spectroscopy, electron microscopy and X-ray diffraction methods. Moreover, different systems with different testing conditions were used with the intention of linking property measurements in well-defined model systems to real fuel cell performance metrics. Overall, this study aimed to provide new insights for a more tailored electrocatalyst design and thus facilitate the correct implementation of the new generation of low-temperature fuel cells.

Whereas the methods and techniques employed in this work provided enough tools to uncover the mechanistic understanding of fuel cell half electrochemical reactions, there are a few elements that should be implemented if the actual electrocatalytic performance is meant to deciphered. Firstly, although *ex situ* characterization was successfully used to investigate catalytic surface composition, structure and morphology before and after testing, catalytic systems are often highly dependent on the system conditions. Thus, the use of *in situ* techniques to track surface changes upon applied potential would greatly boost the electrocatalyst research. Secondly, whereas different electrochemical setups and model systems were utilized to prove tunable variables and surface-specific parameters that are critical for system scale design, the ideal environment provided by the widely-used RDE setup is not sufficient to detangle the multitude of factors that impact the electrode performance from the fundamental underlying dynamics. Hence, in order to develop fundamental understanding of factors that result in a given electrocatalytic performance, systems that mimic actual fuel cell phenomena should be more integrated in electrocatalyst fundamental research.

Beyond this thesis work, the upcoming steps should focus on the fabrication and characterization, both physical and electrochemical, of thoroughly tailored electrocatalysts. However, more importantly, the design of model catalysts should be oriented towards elucidating the mechanisms through which the HOR and ORR are enhanced. For this, we have currently several pathways that could potentially be taken in order to find the new state-of-the-art catalysts for both PEMFCs and AEMFCs.

One route that this project could take is based on deconvoluting the interplay between electronic effects, which are generally responsible for the enhanced activity of the catalysts already studied in this work. For this, rigorously fabricated thin film model systems with well-defined structures should be evaluated for both the HOR and ORR in order to pinpoint the exact effect responsible for the enhancement in both reactions, which will be correlated with their atomic distribution and thus their electronic environment. In this way, future catalysts can be carefully tailored in order to obtain the highest possible electroactivity. To have a better understanding of the structure and morphology effects on the catalytic activity, the HOR and ORR activity of thin-films fabricated by physical methods should be compared to the catalyst with the same composition but different structures fabricated by chemical methods by our collaborators.

Parallel to the evaluation of catalysts in our platform, physically-fabricated catalytic materials with the same composition and structure should also be evaluated in a membrane electrode assembly (MEA) model system. By studying their HOR and ORR performance in conditions more relevant for fuel cells, their performance can then be extrapolated to that in a real fuel cell, which is the original aim of this work. Thus, by establishing a relation between different model systems, the influence of the reaction conditions can be elucidated, which is of crucial importance for the development of the new generation of efficient and inexpensive catalysts. In this context, the interaction between the catalysts and the other components in a fuel cell is essential to predict their behavior under real-life operation. For this, different ionomers used for ionic and reactants transport should also be also evaluated in combination with our electrocatalysts, which will provide a further comprehension of both the ionomer and the catalyst performance. Moreover, since non-noble metals have the potential to outperform the currently benchmarked fuel cell catalysts while majorly reducing their cost, the use of catalyst supports to increase their specific activity and reduce catalyst loading is a route that should be exploited.

7. Acknowledgements

The work presented in this thesis was carried out at the Division of Chemical Physics at the Department of Physics, Chalmers University of Technology, Göteborg, Sweden from October 2018 through January 2023.

This work is financially supported by the Sweden Foundation for Strategic Research (*Stiftelsen för Strategisk Forskning*, SSF).

I would like to thank, first and foremost, my supervisor Björn Wickman, for his guidance and optimism, his patience, for putting his trust in me and for pushing me instead of pulling me back. You always offered opportunities to explore and develop to become an independent researcher, for which I am very grateful.

I would also like to thank my office and lab mate (and technically also co-supervisor) Rosemary Brown for all her guidance in those first steps and for all her patience when doing so. You are greatly missed.

I would also like to acknowledge all the help and support I received from the external collaborators at KTH and Lund University, from both professors and PhD students, who provided me with many opportunities to explore the research field we are in and to grow as a scientist.

A big thanks also to my examiner Henrik Grönbeck for all the help, support and discussions in a very relaxed and professional environment.

A huge thanks to everyone in the Division of Chemical Physics, current and former members, for creating a very nice, comfortable and professional work environment. Despite the times we are living, the environment at the Division makes it definitely worth to work here.

Thanks also to Lasse Urholm, Lars Hellberg and Lennart Norberg for always providing great, quick and generous support whenever it was needed.

Last but not least, I would like to thank my family for an unconditional and constant support. To all my great friends from Barcelona, Alió, DTU and all the ones across Europe, as well as all the new friends I made here in Göteborg. You all constantly reminded me who I am and what made me arrive until here. You truly make my life easier.

Gràcies!

Bibliography

[1] G.W.Y. Melillo, J.M., T.C. Richmond, Climate change impacts in the United States: The third National Climate Assessment, U.S. Glob. Chang. Res. Progr. (2014).

[2] European Comission, A European Green Deal, (2021). https://ec.europa.eu/info/strategy/priorities-2019-2024/european-green-deal_en.

[3] EUREC, 2030: A binding 45% renewable energy target, (2020). https://eurec.be/2030-a-binding-45-renewable-energy-target/.

[4] W.M. Haynes; David R. Lide, ed., CRC Handbook of Chemistry and Physics, 92nd ed., CRC Press, 2011.

[5] G. Cipriani, V. Di Dio, F. Genduso, D. La Cascia, R. Liga, R. Miceli, G. Ricco Galluzzo, Perspective on hydrogen energy carrier and its automotive applications, Int. J. Hydrogen Energy. 39 (2014) 8482–8494. https://doi.org/10.1016/j.ijhydene.2014.03.174.

[6] S.E. Hosseini, M.A. Wahid, Hydrogen production from renewable and sustainable energy resources: Promising green energy carrier for clean development, Renew. Sustain. Energy Rev. 57 (2016) 850–866. https://doi.org/10.1016/j.rser.2015.12.112.

[7] R.M. Navarro, M.A. Peña, J.L.G. Fierro, Hydrogen production reactions from carbon feedstocks: Fossil fuels and biomass, Chem. Rev. 107 (2007) 3952–3991. https://doi.org/10.1021/cr0501994.

[8] C. Xiang, K.M. Papadantonakis, N.S. Lewis, Principles and implementations of electrolysis systems for water splitting, Mater. Horizons. 3 (2016) 169–173. https://doi.org/10.1039/c6mh00016a.

[9] P. Nikolaidis, A. Poullikkas, A comparative overview of hydrogen production processes, Renew. Sustain. Energy Rev. 67 (2017) 597–611. https://doi.org/10.1016/j.rser.2016.09.044.

[10] T. Nguyen, Z. Abdin, T. Holm, W. Mérida, Grid-connected hydrogen production via large-scale water electrolysis, Energy Convers. Manag. 200 (2019) 112108. https://doi.org/10.1016/j.enconman.2019.112108.

[11] A. Buttler, H. Spliethoff, Current status of water electrolysis for energy storage, grid balancing and sector coupling via power-to-gas and power-to-liquids: A review, Renew. Sustain. Energy Rev. 82 (2018) 2440–2454. https://doi.org/10.1016/j.rser.2017.09.003.

[12] S. Fang, D. Bresser, S. Passerini, Transition Metal Oxide Anodes for Electrochemical Energy Storage in Lithium- and Sodium-Ion Batteries, Adv. Energy Mater. 10 (2020). https://doi.org/10.1002/aenm.201902485.

[13] M. Cakici, K.R. Reddy, F. Alonso-Marroquin, Advanced electrochemical energy storage supercapacitors based on the flexible carbon fiber fabric-coated with uniform coral-like MnO2 structured electrodes, Chem. Eng. J. 309 (2017) 151–158. https://doi.org/10.1016/j.cej.2016.10.012.

[14] Y. Wang, D.F. Ruiz Diaz, K.S. Chen, Z. Wang, X.C. Adroher, Materials, technological status, and fundamentals of PEM fuel cells – A review, Mater. Today. 32 (2020) 178–203. https://doi.org/10.1016/j.mattod.2019.06.005.

[15] H. Lohse-Busch, K. Stutenberg, M. Duoba, X. Liu, A. Elgowainy, M. Wang, T. Wallner, B. Richard, M. Christenson, Automotive fuel cell stack and system

efficiency and fuel consumption based on vehicle testing on a chassis dynamometer at minus 18 °C to positive 35 °C temperatures, Int. J. Hydrogen Energy. 45 (2020) 861–872. https://doi.org/10.1016/j.ijhydene.2019.10.150.

[16] Y. Wang, K.S. Chen, J. Mishler, S.C. Cho, X.C. Adroher, A review of polymer electrolyte membrane fuel cells: Technology, applications, and needs on fundamental research, Appl. Energy. 88 (2011) 981–1007. https://doi.org/10.1016/j.apenergy.2010.09.030.

[17] U.S. Department of Energy, DOE Technical Targets for Fuel Cell Systems and Stacks for Transportation Applications, Internet Publlication. (2017). https://www.energy.gov/eere/fuelcells/doe-technical-targets-fuel-cell-systems-and-stacks-transportation-applications.

[18] C.J. Yang, An impending platinum crisis and its implications for the future of the automobile, Energy Policy. 37 (2009) 1805–1808. https://doi.org/10.1016/j.enpol.2009.01.019.

[19] T. Abdel-Baset, T. Benjamin, R. Borup, K.E. Martin, N. Garland, S. Hirano, J. Kopasz, B. Lakshmanmn, D. Masten, M. Mehall, D. Myers, D. Papageorgopoulos, W. Podolski, T. Trabold, B. Vermeersch, J. Waldecker, The. US Deparment of Energy (DOE). Energy Efficiency and Renewable Energy https://energy.gov/eere/fuelcells/doe-technical-targets-polymer-electrolyte-membrane-fuel-cell-components, (2017) 30. https://doi.org/10.2172/1220127.

[20] M. Breitwieser, M. Klingele, B. Britton, S. Holdcroft, R. Zengerle, S. Thiele, Improved Pt-utilization efficiency of low Pt-loading PEM fuel cell electrodes using direct membrane deposition, Electrochem. Commun. 60 (2015) 168–171. https://doi.org/10.1016/j.elecom.2015.09.006.

[21] L. Ye, Y. Gao, S. Zhu, J. Zheng, P. Li, J.P. Zheng, A Pt content and pore structure gradient distributed catalyst layer to improve the PEMFC performance, Int. J. Hydrogen Energy. 42 (2017) 7241–7245. https://doi.org/10.1016/j.ijhydene.2016.11.002.

[22] V. Čolić, A.S. Bandarenka, Pt Alloy Electrocatalysts for the Oxygen Reduction Reaction: From Model Surfaces to Nanostructured Systems, ACS Catal. 6 (2016) 5378–5385. https://doi.org/10.1021/acscatal.6b00997.

[23] D.R. Dekel, Review of cell performance in anion exchange membrane fuel cells, J. Power Sources. 375 (2018) 158–169. https://doi.org/10.1016/j.jpowsour.2017.07.117.

[24] Q. He, E.J. Cairns, Review—Recent Progress in Electrocatalysts for Oxygen Reduction Suitable for Alkaline Anion Exchange Membrane Fuel Cells, J. Electrochem. Soc. 162 (2015) F1504–F1539. https://doi.org/10.1149/2.0551514jes.

[25] S. Gu, R. Cai, T. Luo, Z. Chen, M. Sun, Y. Liu, G. He, Y. Yan, A soluble and highly conductive ionomer for high-performance hydroxide exchange membrane fuel cells, Angew. Chemie - Int. Ed. 48 (2009) 6499–6502. https://doi.org/10.1002/anie.200806299.

[26] Gerard Montserrat-Sisó, Electrocatalyst materials for low-temperature hydrogen fuel cells, Chalmers University of Technology, 2021.

[27] D.B. Hibbert, Introduction to electrochemistry, 1st ed., THE MACMILLAN PRESS LTD, 1993. https://doi.org/10.1007/978-1-349-22721-1.

[28] E.I. Ortiz-Rivera, A.L. Reyes-Hernandez, R.A. Febo, Understanding the history of fuel cells, 2007 IEEE Conf. Hist. Electr. Power, HEP 2007. 2 (2007) 117–122. https://doi.org/10.1109/HEP.2007.4510259.

[29] S. Petrovic, Basic Electrochemistry Concepts, 2021. https://doi.org/10.1007/978-3-030-61562-8_2.

[30] John Simpson; Edmund Weiner, Oxford English Dictionary: The definitive record of the English language, 3rd ed., Oxford University Press, 2018. https://www.oed.com/.

[31] W.V. Carl H. Hamann, Andrew Hamnet, Electrochemistry, 2nd Editio, WILEY-VCH, 2007.

[32] A.J.B. and L.R. M. Faulkner, Electrochemical Methods: Fundamentals and Applications, 2nd Editio, John Wiley & Sons, Ltd., 2001.

[33] D. Pletcher, A First Course in Electrode Processes, 2nd Editio, RSC Publishing, 2009.

[34] J. Staszak-Jirkovský, R. Subbaraman, D. Strmcnik, K.L. Harrison, C.E. Diesendruck, R. Assary, O. Frank, L. Kobr, G.K.H. Wiberg, B. Genorio, J.G. Connell, P.P. Lopes, V.R. Stamenkovic, L. Curtiss, J.S. Moore, K.R. Zavadil, N.M. Markovic, Water as a Promoter and Catalyst for Dioxygen Electrochemistry in Aqueous and Organic Media, ACS Catal. 5 (2015) 6600–6607. https://doi.org/10.1021/acscatal.5b01779.

[35] D. Strmcnik, K. Kodama, D. Van Der Vliet, J. Greeley, V.R. Stamenkovic, N.M. Marković, The role of non-covalent interactions in electrocatalytic fuel-cell reactions on platinum, Nat. Chem. 1 (2009) 466–472. https://doi.org/10.1038/nchem.330.

[36] A.J.B. and L.R. MFaulkner, Electrochemical Methods, 2nd Ed, John Wiley & Sons, Ltd., 2001.

[37] M. Favaro, B. Jeong, P.N. Ross, J. Yano, Z. Hussain, Z. Liu, E.J. Crumlin, Unravelling the electrochemical double layer by direct probing of the solid/liquid interface, Nat. Commun. 7 (2016) 1–8. https://doi.org/10.1038/ncomms12695.

[38] Richard G. Compton and Craig E. Banks, Understanding Voltammetry, 3rd Editio, World Scientific Publishing Europe, 2018.

[39] A.J.B. and L.R. MFaulkner, Electrochemichal Methods, 2nd Editio, John Wiley & Sons, Ltd., 2001.

[40] Andrew L. Dicks; David A.J. Rand, Fuel Cell Systems Explained, 3rd Editio, 2018.

[41] J. Wisniak, The History of Catalysis. From the Beginning to Nobel Prizes, Educ. Quim. 21 (2010) 60–69. https://doi.org/10.1016/S0187-893X(18)30074-0.

[42] R. Winderlich, J.M. Moore, JONS JAKOB BERZELIUS, (1852).

[43] A. Camia, Birth of the catalytic concept, Catal. Letters. 67 (2000) 1–4. https://doi.org/10.1023/a:1016622806065.

[44] E. Auer, A. Freund, J. Pietsch, T. Tacke, Carbons as supports for industrial precious metal catalysts, Appl. Catal. A Gen. 173 (1998) 259–271. https://doi.org/10.1016/S0926-860X(98)00184-7.

[45] Z.W. Chen, L.X. Chen, Z. Wen, Q. Jiang, Understanding electro-catalysis by using density functional theory, Phys. Chem. Chem. Phys. 21 (2019) 23782–23802. https://doi.org/10.1039/c9cp04430b.

[46] C.J.H. Jacobsen, Novel class of ammonia synthesis catalysts, Chem. Commun. (2000) 1057–1058. https://doi.org/10.1039/b002930k.

[47] R.J. Farrauto, R.M. Heck, Catalytic converters: State of the art and perspectives, Catal. Today. 51 (1999) 351–360. https://doi.org/10.1016/S0920-5861(99)00024-3.

[48] IUPAC, Compendium of Chemical Terminology—The "Gold Book," 2nd Editio, Blackwell Scientific Publications, Oxford. (2006-), 1997.

[49] J. Heveling, Heterogeneous catalytic chemistry by example of industrial applications, J. Chem. Educ. 89 (2012) 1530–1536. https://doi.org/10.1021/ed200816g.

[50] I. Chorkendorff and J. W. Niemantsverdriet, Concepts of Modern Catalysis and kinetics, 3rd Editio, John Wisley & Sons, 2017.

[51] K. Taylor, Nitric oxide catalysis in automotive exhaust systems, Catal. Rev. 35 (1993) 457–481. https://doi.org/10.1080/01614949308013915.

[52] J.K. Nørskov, T. Bligaard, A. Logadottir, S. Bahn, L.B. Hansen, M. Bollinger, H. Bengaard, B. Hammer, Z. Sljivancanin, M. Mavrikakis, Y. Xu, S. Dahl, C.J.H. Jacobsen, Universality in heterogeneous catalysis, J. Catal. 209 (2002) 275–278. https://doi.org/10.1006/jcat.2002.3615.

[53] A.J. Medford, A. Vojvodic, J.S. Hummelshøj, J. Voss, F. Abild-Pedersen, F. Studt, T. Bligaard, A. Nilsson, J.K. Nørskov, From the Sabatier principle to a predictive theory of transition-metal heterogeneous catalysis, J. Catal. 328 (2015) 36–42. https://doi.org/10.1016/j.jcat.2014.12.033.

[54] A.S. Bandarenka, E. Ventosa, A. Maljusch, J. Masa, W. Schuhmann, Techniques and methodologies in modern electrocatalysis: evaluation of activity, selectivity and stability of catalytic materials, Analyst. 139 (2014) 1274–1291. https://doi.org/10.1039/c3an01647a.

[55] C.C.L. McCrory, S. Jung, I.M. Ferrer, S.M. Chatman, J.C. Peters, T.F. Jaramillo, Benchmarking Hydrogen Evolving Reaction and Oxygen Evolving Reaction Electrocatalysts for Solar Water Splitting Devices, J. Am. Chem. Soc. 137 (2015) 4347–4357. https://doi.org/10.1021/ja510442p.

[56] I. Technical Services, Fuel Cell Handbook, Seventh Ed, U.S. Department of Energy. National Energy Technology Laboratory., 2004.

[57] J. He, N.J.J. Johnson, A. Huang, C.P. Berlinguette, Electrocatalytic Alloys for CO2 Reduction, ChemSusChem. 11 (2018) 48–57. https://doi.org/10.1002/cssc.201701825.

[58] A.S. Bandarenka, M.T.M. Koper, Structural and electronic effects in heterogeneous electrocatalysis: Toward a rational design of electrocatalysts, J. Catal. 308 (2013) 11–24. https://doi.org/10.1016/j.jcat.2013.05.006.

[59] Z.W. She, J. Kibsgaard, C.F. Dickens, I. Chorkendorff, J.K. Nørskov, T.F. Jaramillo, Combining theory and experiment in electrocatalysis: Insights into materials design, Science (80-.). 355 (2017). https://doi.org/10.1126/science.aad4998.

[60] J. Pal, T. Pal, Faceted metal and metal oxide nanoparticles: Design, fabrication and catalysis, Nanoscale. 7 (2015) 14159–14190. https://doi.org/10.1039/c5nr03395k.

[61] S. Kabir, T. Van Cleve, S. Khandavalli, S. Medina, S. Pylypenko, S. Mauger, M. Ulsh, K.C. Neyerlin, Toward Optimizing Electrospun Nanofiber Fuel Cell Catalyst Layers: Microstructure and Pt Accessibility, ACS Appl. Energy Mater. 4 (2021) 3341–3351. https://doi.org/10.1021/acsaem.0c03073.

[62] J. Marie, R. Chenitz, M. Chatenet, S. Berthon-Fabry, N. Cornet, P. Achard, Highly porous PEM fuel cell cathodes based on low density carbon aerogels as Pt-support: Experimental study of the mass-transport losses, J. Power Sources. 190 (2009) 423–434. https://doi.org/10.1016/j.jpowsour.2009.01.047.

[63] D. Kunwar, S. Zhou, A. Delariva, E.J. Peterson, H. Xiong, X.I. Pereira-Hernández, S.C. Purdy, R. Ter Veen, H.H. Brongersma, J.T. Miller, H. Hashiguchi, L. Kovarik, S. Lin, H. Guo, Y. Wang, A.K. Datye, Stabilizing High Metal Loadings of Thermally Stable Platinum Single Atoms on an Industrial Catalyst Support, ACS Catal. 9 (2019) 3978–3990.

https://doi.org/10.1021/acscatal.8b04885.

[64] S. Samad, K.S. Loh, W.Y. Wong, T.K. Lee, J. Sunarso, S.T. Chong, W.R. Wan Daud, Carbon and non-carbon support materials for platinum-based catalysts in fuel cells, Int. J. Hydrogen Energy. 43 (2018) 7823–7854. https://doi.org/10.1016/j.ijhydene.2018.02.154.

[65] H. Jin, C. Guo, X. Liu, J. Liu, A. Vasileff, Y. Jiao, Y. Zheng, S.Z. Qiao, Emerging Two-Dimensional Nanomaterials for Electrocatalysis, Chem. Rev. 118 (2018) 6337–6408. https://doi.org/10.1021/acs.chemrev.7b00689.

[66] I.E.L. Stephens, A.S. Bondarenko, U. Grønbjerg, J. Rossmeisl, I. Chorkendorff, Understanding the electrocatalysis of oxygen reduction on platinum and its alloys, Energy Environ. Sci. 5 (2012) 6744–6762. https://doi.org/10.1039/c2ee03590a.

[67] S.A. Park, H. Lim, Y.T. Kim, Enhanced Oxygen Reduction Reaction Activity Due to Electronic Effects between Ag and Mn3O4 in Alkaline Media, ACS Catal. 5 (2015) 3995–4002. https://doi.org/10.1021/acscatal.5b00495.

[68] H.E. Hoster, O.B. Alves, M.T.M. Koper, Tuning adsorption via strain and vertical ligand effects, ChemPhysChem. 11 (2010) 1518–1524. https://doi.org/10.1002/cphc.200900500.

[69] X. Wang, Y. Orikasa, Y. Takesue, H. Inoue, M. Nakamura, T. Minato, N. Hoshi, Y. Uchimoto, Quantitating the lattice strain dependence of monolayer Pt shell activity toward oxygen reduction, J. Am. Chem. Soc. 135 (2013) 5938–5941. https://doi.org/10.1021/ja312382h.

[70] B. Hammer, J.K. Nørskov, Electronic factors determining the reactivity of metal surfaces, Surf. Sci. 343 (1995) 211–220. https://doi.org/10.1016/0039-6028(96)80007-0.

[71] A. Nilsson, L.G.M. Pettersson, B. Hammer, T. Bligaard, C.H. Christensen, J.K. Nørskov, The electronic structure effect in heterogeneous catalysis, Catal. Letters. 100 (2005) 111–114. https://doi.org/10.1007/s10562-004-3434-9.

[72] J.K. Nørskov, F. Abild-Pedersen, F. Studt, T. Bligaard, Density functional theory in surface chemistry and catalysis, Proc. Natl. Acad. Sci. U. S. A. 108 (2011) 937–943. https://doi.org/10.1073/pnas.1006652108.

[73] Y. Guo, M. Wang, Q. Zhu, D. Xiao, D. Ma, Ensemble effect for single-atom, small cluster and nanoparticle catalysts, Nat. Catal. 5 (2022) 766–776. https://doi.org/10.1038/s41929-022-00839-7.

[74] G. Montserrat-Sisó, B. Wickman, PdNi thin films for hydrogen oxidation reaction and oxygen reduction reaction in alkaline media, Electrochim. Acta. 420 (2022). https://doi.org/10.1016/j.electacta.2022.140425.

[75] B. Zhu, Advantages of intermediate temperature solid oxide fuel cells for tractionary applications, J. Power Sources. 93 (2001) 82–86. https://doi.org/10.1016/S0378-7753(00)00564-4.

[76] D. Bloch, Miniature fuel cells for portable applications, Low-Power Electron. Des. 106 (2004) 44-1-44–20. https://doi.org/10.1201/9781420039559.ch44.

[77] B.D. McNicol, D.A.J. Rand, K.R. Williams, Fuel cells for road transportation purposes - Yes or no?, J. Power Sources. 100 (2001) 47–59. https://doi.org/10.1016/S0378-7753(01)00882-5.

[78] K. Sopian, W.R. Wan Daud, Challenges and future developments in proton exchange membrane fuel cells, Renew. Energy. 31 (2006) 719–727. https://doi.org/10.1016/j.renene.2005.09.003.

[79] W.R. Grove, On a Gaseous Voltaic Battery, (1842).

[80] W. Grove, On Voltic Series and the Combination of Gases by Platinum, (1838).

[81] J.M. Andújar, F. Segura, Fuel cells: History and updating. A walk along two centuries, Renew. Sustain. Energy Rev. 13 (2009) 2309–2322. https://doi.org/10.1016/j.rser.2009.03.015.

[82] Marc. T.M. Koper, Fuel Cell Catalysis: A Surface Science Approach, 1st Editio, Andrzej Wieckowski, 2009.

[83] A. Larminie, J., & Dicks, 2 - Efficiency and Open Circuit Voltage, in: Fuel Cell Syst. Explain., Second Edi, John Wiley & Sons, Ltd., 2003.

[84] G. Sasikumar, J.W. Ihm, H. Ryu, Optimum Nafion content in PEM fuel cell electrodes, Electrochim. Acta. 50 (2004) 601–605. https://doi.org/10.1016/j.electacta.2004.01.126.

[85] J. Chlistunoff, B. Pivovar, Effects of Ionomer Morphology on Oxygen Reduction on Pt, J. Electrochem. Soc. 162 (2015) F890–F900. https://doi.org/10.1149/2.0661508jes.

[86] Y. Zhou, H. Yu, F. Xie, Y. Zhao, X. Sun, D. Yao, G. Jiang, J. Geng, Z. Shao, Improving cell performance for anion exchange membrane fuel cells with FeNC cathode by optimizing ionomer content, Int. J. Hydrogen Energy. (2022). https://doi.org/10.1016/j.ijhydene.2022.11.057.

[87] N. Chen, Y.M. Lee, Anion exchange polyelectrolytes for membranes and ionomers, Prog. Polym. Sci. 113 (2021) 101345. https://doi.org/10.1016/j.progpolymsci.2020.101345.

[88] A. Hermann, T. Chaudhuri, P. Spagnol, Bipolar plates for PEM fuel cells: A review, Int. J. Hydrogen Energy. 30 (2005) 1297–1302. https://doi.org/10.1016/j.ijhydene.2005.04.016.

[89] B. Viswanathan, M.A. Scibioh, Fuel Cells: Principles and Applications, (2007) 494.

[90] H.W. Langmi, J. Ren, N.M. Musyoka, Nanomaterials for Fuel Cell Catalysis, 2016. http://link.springer.com/10.1007/978-3-319-29930-3.

[91] R.M. Ormerod, Solid oxide fuel cells, Chem. Soc. Rev. 32 (2003) 17–28. https://doi.org/10.1039/b105764m.

[92] N. Sammes, R. Bove, K. Stahl, Phosphoric acid fuel cells: Fundamentals and applications, Curr. Opin. Solid State Mater. Sci. 8 (2004) 372–378. https://doi.org/10.1016/j.cossms.2005.01.001.

[93] M. Neergat, A.K. Shukla, A high-performance phosphoric acid fuel cell, J. Power Sources. 102 (2001) 317–321. https://doi.org/10.1016/S0378-7753(01)00766-2.

[94] San Ping Jiang and Pei Kang Shen, Nanostructured and Advanced Materials for Fuel Cells, 1st Editio, CRC Press Taylor & Francis Group, 2017.

[95] R. Borup, J. Meyers, B. Pivovar, Y.S. Kim, R. Mukundan, N. Garland, D. Myers, M. Wilson, F. Garzon, D. Wood, P. Zelenay, K. More, K. Stroh, T. Zawodzinski, J. Boncella, J.E. McGrath, M. Inaba, K. Miyatake, M. Hori, K. Ota, Z. Ogumi, S. Miyata, A. Nishikata, Z. Siroma, Y. Uchimoto, K. Yasuda, K.I. Kimijima, N. Iwashita, Scientific aspects of polymer electrolyte fuel cell durability and degradation, Chem. Rev. 107 (2007) 3904–3951. https://doi.org/10.1021/cr050182l.

[96] C. Francia, V.S. Ijeri, S. Specchia, P. Spinelli, Estimation of hydrogen crossover through Nafion® membranes in PEMFCs, J. Power Sources. 196 (2011) 1833–1839. https://doi.org/10.1016/j.jpowsour.2010.09.058.

[97] S.A. Vilekar, R. Datta, The effect of hydrogen crossover on open-circuit voltage in polymer electrolyte membrane fuel cells, J. Power Sources. 195 (2010) 2241–

2247. https://doi.org/10.1016/j.jpowsour.2009.10.023.

[98] E. Alonso, F.R. Field, R.E. Kirchain, Platinum availability for future automotive technologies, Environ. Sci. Technol. 46 (2012) 12986–12993. https://doi.org/10.1021/es301110e.

[99] M.L.C.M. Henckens, P.P.J. Driessen, E. Worrell, Metal scarcity and sustainability, analyzing the necessity to reduce the extraction of scarce metals, Resour. Conserv. Recycl. 93 (2014) 1–8. https://doi.org/10.1016/j.resconrec.2014.09.012.

[100] N. Dubouis, A. Grimaud, The hydrogen evolution reaction: From material to interfacial descriptors, Chem. Sci. 10 (2019) 9165–9181. https://doi.org/10.1039/c9sc03831k.

[101] A.B. Anderson, O2 reduction and CO oxidation at the Pt-electrolyte interface. The role of H2O and OH adsorption bond strengths, Electrochim. Acta. 47 (2002) 3759–3763. https://doi.org/10.1016/S0013-4686(02)00346-8.

[102] I.E.L. Stephens, A.S. Bondarenko, L. Bech, I. Chorkendorff, Oxygen Electroreduction Activity and X-Ray Photoelectron Spectroscopy of Platinum and Early Transition Metal Alloys, ChemCatChem. 4 (2012) 341–349. https://doi.org/10.1002/cctc.201100343.

[103] C. Wei, S. Sun, D. Mandler, X. Wang, S.Z. Qiao, Z.J. Xu, Approaches for measuring the surface areas of metal oxide electrocatalysts for determining their intrinsic electrocatalytic activity, Chem. Soc. Rev. 48 (2019) 2518–2534. https://doi.org/10.1039/c8cs00848e.

[104] S. Trasatti, O.A. Petrii, International Union of Pure and Applied Chemistry Physical Chemistry Division Commission on Electrochemistry: Real Surface Area Measurements in Electrochemistry, Pure Appl. Chem. 63 (1991) 711–734. https://doi.org/10.1351/pac199163050711.

[105] T. Biegler, D.A.J. Rand, R. Woods, Limiting oxygen coverage on platinized platinum; Relevance to determination of real platinum area by hydrogen adsorption, J. Electroanal. Chem. 29 (1971) 269–277. https://doi.org/10.1016/S0022-0728(71)80089-X.

[106] R. Sharma, S. Gyergyek, S.M. Andersen, Critical thinking on baseline corrections for electrochemical surface area (ECSA) determination of Pt/C through H-adsorption/H-desorption regions of a cyclic voltammogram, Appl. Catal. B Environ. 311 (2022) 121351. https://doi.org/10.1016/j.apcatb.2022.121351.

[107] A.M. Chaparro, A.J. Martín, M.A. Folgado, B. Gallardo, L. Daza, Comparative analysis of the electroactive area of Pt/C PEMFC electrodes in liquid and solid polymer contact by underpotential hydrogen adsorption/desorption, Int. J. Hydrogen Energy. 34 (2009) 4838–4846. https://doi.org/10.1016/j.ijhydene.2009.03.053.

[108] K. Shinozaki, J.W. Zack, R.M. Richards, B.S. Pivovar, S.S. Kocha, Oxygen Reduction Reaction Measurements on Platinum Electrocatalysts Utilizing Rotating Disk Electrode Technique, J. Electrochem. Soc. 162 (2015) F1144–F1158. https://doi.org/10.1149/2.1071509jes.

[109] V. Čolić, J. Tymoczko, A. Maljusch, A. Ganassin, W. Schuhmann, A.S. Bandarenka, Experimental Aspects in Benchmarking of the Electrocatalytic Activity, ChemElectroChem. 2 (2015) 143–149. https://doi.org/10.1002/celc.201402295.

[110] S. Moniri, T. Van Cleve, S. Linic, Pitfalls and best practices in measurements of the electrochemical surface area of platinum-based nanostructured electrocatalysts, J. Catal. 345 (2017) 1–10. https://doi.org/10.1016/j.jcat.2016.11.018.

[111] R. Wreland Lindström, K. Korstdottir, G. Lindbergh, Active Area Determination for Porous Pt-Electrodes Used in PEM Fuel Cells: Temperature and Humidity Effects, ECS Meet. Abstr. MA2009-02 (2009) 1016–1016. https://doi.org/10.1149/ma2009-02/10/1016.

[112] C. Wei, R.R. Rao, J. Peng, B. Huang, I.E.L. Stephens, M. Risch, Z.J. Xu, Y. Shao-Horn, Recommended Practices and Benchmark Activity for Hydrogen and Oxygen Electrocatalysis in Water Splitting and Fuel Cells, Adv. Mater. 31 (2019) 1–24. https://doi.org/10.1002/adma.201806296.

[113] D.F. Van Der Vliet, C. Wang, D. Li, A.P. Paulikas, J. Greeley, R.B. Rankin, D. Strmcnik, D. Tripkovic, N.M. Markovic, V.R. Stamenkovic, Unique electrochemical adsorption properties of Pt-skin surfaces, Angew. Chemie - Int. Ed. 51 (2012) 3139–3142. https://doi.org/10.1002/anie.201107668.

[114] R. Chattot, I. Martens, M. Scohy, J. Herranz, J. Drnec, F. Maillard, L. Dubau, Disclosing Pt-Bimetallic Alloy Nanoparticle Surface Lattice Distortion with Electrochemical Probes, ACS Energy Lett. 5 (2020) 162–169. https://doi.org/10.1021/acsenergylett.9b02287.

[115] E.G. Ciapina, S.F. Santos, E.R. Gonzalez, Electrochemical CO stripping on nanosized Pt surfaces in acid media: A review on the issue of peak multiplicity, J. Electroanal. Chem. 815 (2018) 47–60. https://doi.org/10.1016/j.jelechem.2018.02.047.

[116] E. Herrero, L.J. Buller, H.D. Abruña, Underpotential deposition at single crystal surfaces of Au, Pt, Ag and other materials, Chem. Rev. 101 (2001) 1897–1930. https://doi.org/10.1021/cr9600363.

[117] W. Zhao, K. Huang, Q. Zhang, H. Wu, L. Gu, K. Yao, Y. Shen, Y. Shao, In-situ synthesis, operation and regeneration of nanoporous silver with high performance toward oxygen reduction reaction, Nano Energy. 58 (2019) 69–77. https://doi.org/10.1016/j.nanoen.2019.01.021.

[118] X. Wu, F. Chen, N. Zhang, Y. Lei, Y. Jin, A. Qaseem, R.L. Johnston, Activity Trends of Binary Silver Alloy Nanocatalysts for Oxygen Reduction Reaction in Alkaline Media, Small. 13 (2017) 1–8. https://doi.org/10.1002/smll.201603387.

[119] F. He, N. Xia, Y. Zheng, H. Fan, D. Ma, X. Hu, Boosting Oxygen Electroreduction over Strained Silver, ACS Appl. Mater. Interfaces. 12 (2020) 57134–57140. https://doi.org/10.1021/acsami.0c17973.

[120] T. Van Cleve, E. Gibara, S. Linic, Electrochemical Oxygen Reduction Reaction on Ag Nanoparticles of Different Shapes, ChemCatChem. 8 (2016) 256–261. https://doi.org/10.1002/cctc.201500899.

[121] K.J. Stevenson, D.W. Hatchett, H.S. White, Influence of surface defect structure on the underpotential deposition of Pb monolayers at Ag(111), Langmuir. 12 (1996) 494–499. https://doi.org/10.1021/la950509l.

[122] Y. Bonfil, M. Brand, E. Kirowa-Eisner, Characteristics of subtractive anodic stripping voltammetry of Pb and Cd at silver and gold electrodes, Anal. Chim. Acta. 464 (2002) 99–114. https://doi.org/10.1016/S0003-2670(02)00489-0.

[123] S.D. Giri, A. Sarkar, Estimating surface area of copper powder: A comparison between electrochemical, microscopy and laser diffraction methods, Adv. Powder Technol. 29 (2018) 3520–3526. https://doi.org/10.1016/j.apt.2018.09.034.

[124] E. Kirowa-Eisner, Y. Bonfil, D. Tzur, E. Gileadi, Thermodynamics and kinetics of upd of lead on polycrystalline silver and gold, J. Electroanal. Chem. 552 (2003) 171–183. https://doi.org/10.1016/S0022-0728(03)00181-5.

[125] T. Mittermeier, A. Weiß, H.A. Gasteiger, F. Hasché, Monometallic Palladium for Oxygen Reduction in PEM Fuel Cells: Particle-Size Effect, Reaction Mechanism, and Voltage Cycling Stability, J. Electrochem. Soc. 164 (2017) F1081–F1089.

https://doi.org/10.1149/2.0561712jes.

[126] A. Holewinski, J.C. Idrobo, S. Linic, High-performance Ag-Co alloy catalysts for electrochemical oxygen reduction, Nat. Chem. 6 (2014) 828–834. https://doi.org/10.1038/nchem.2032.

[127] A. Visintin, J.C. Canullo, W.E. Triaca, A.J. Arvia, Changes in real surface area, crystallographic orientation and morphology of platinum electrodes caused by periodic potential treatments: phenomenological approach, J. Electroanal. Chem. 239 (1988) 67–89. https://doi.org/10.1016/0022-0728(88)80270-5.

[128] M. Vega-Cartagena, E.M. Flores-Vélez, G.S. Colón-Quintana, D.A. Blasini Pérez, M.A. De Jesús, C.R. Cabrera, Silver-Palladium Electrodeposition on Unsupported Vulcan XC-72R for Oxygen Reduction Reaction in Alkaline Media, ACS Appl. Energy Mater. 2 (2019) 4664–4673. https://doi.org/10.1021/acsaem.9b00038.

[129] W. Wang, J.Q. Chen, Y.R. Tao, S.N. Zhu, Y.X. Zhang, X.C. Wu, Flowerlike Ag-Supported Ce-Doped Mn3O4 Nanosheet Heterostructure for a Highly Efficient Oxygen Reduction Reaction: Roles of Metal Oxides in Ag Surface States, ACS Catal. 9 (2019) 3498–3510. https://doi.org/10.1021/acscatal.8b04943.

[130] Cynthia G. Zoski, ed., Handbook of Electrochemistry, Elsevier B.V. and Science Press, 2007. https://doi.org/https://doi.org/10.1016/B978-0-444-51958-0.X5000-9.

[131] G.S. Harzer, J.N. Schwämmlein, A.M. Damjanović, S. Ghosh, H.A. Gasteiger, Cathode Loading Impact on Voltage Cycling Induced PEMFC Degradation: A Voltage Loss Analysis, J. Electrochem. Soc. 165 (2018) F3118–F3131. https://doi.org/10.1149/2.0161806jes.

[132] J.K. Nørskov, J. Rossmeisl, A. Logadottir, L. Lindqvist, J.R. Kitchin, T. Bligaard, H. Jónsson, Origin of the overpotential for oxygen reduction at a fuel-cell cathode, J. Phys. Chem. B. 108 (2004) 17886–17892. https://doi.org/10.1021/jp047349j.

[133] E. Zamburlini, K.D. Jensen, I.E.L. Stephens, I. Chorkendorff, M. Escudero-Escribano, V. Čolić, A.S. Bandarenka, O. Ozturk, O.K. Ozdemir, I. Ulusoy, A.S. Ahsen, E. Slavcheva, N.M. Marković, T.J. Schmidt, V. Stamenković, P.N. Ross, M. Wesselmark, B. Wickman, C. Lagergren, G. Lindbergh, Oxygen Reduction Reaction on Pt and Pt Bimetallic Surfaces: A Selective Review, Electrochim. Acta. 111 (2013) 152–159. https://doi.org/10.1016/j.electacta.2013.07.108.

[134] A.J. Appleby, Electrocatalysis of aqueous dioxygen reduction, J. Electroanal. Chem. 357 (1993) 117–179. https://doi.org/10.1016/0022-0728(93)80378-U.

[135] V. Viswanathan, H.A. Hansen, J. Rossmeisl, J.K. Nørskov, Universality in oxygen reduction electrocatalysis on metal surfaces, ACS Catal. 2 (2012) 1654–1660. https://doi.org/10.1021/cs300227s.

[136] N.M. Marković, T.J. Schmidt, V. Stamenković, P.N. Ross, Oxygen Reduction Reaction on Pt and Pt Bimetallic Surfaces: A Selective Review, Fuel Cells. 1 (2001) 105–116. https://doi.org/10.1002/1615-6854(200107)1:2<105::aid-fuce105>3.3.co;2-0.

[137] O. Ozturk, O.K. Ozdemir, I. Ulusoy, A.S. Ahsen, E. Slavcheva, Effect of Ti sublayer on the ORR catalytic efficiency of dc magnetron sputtered thin Pt films, Int. J. Hydrogen Energy. 35 (2010) 4466–4473. https://doi.org/10.1016/j.ijhydene.2010.02.077.

[138] E. Zamburlini, K.D. Jensen, I.E.L. Stephens, I. Chorkendorff, M. Escudero-Escribano, Benchmarking Pt and Pt-lanthanide sputtered thin films for oxygen electroreduction: fabrication and rotating disk electrode measurements,

Electrochim. Acta. 247 (2017) 708–721.
https://doi.org/10.1016/j.electacta.2017.06.146.

[139] M. Wesselmark, B. Wickman, C. Lagergren, G. Lindbergh, The impact of iridium on the stability of platinum on carbon thin-filmmodel electrodes, Electrochim. Acta. 111 (2013) 152–159.
https://doi.org/10.1016/j.electacta.2013.07.108.

[140] M.K. Min, J. Cho, K. Cho, H. Kim, Particle size and alloying effects of Pt-based alloy catalysts for fuel cell applications, Electrochim. Acta. 45 (2000) 4211–4217.
https://doi.org/10.1016/S0013-4686(00)00553-3.

[141] J.N. Schwämmlein, G.S. Harzer, P. Pfändner, A. Blankenship, H.A. El-Sayed, H.A. Gasteiger, Activity and Stability of Carbon Supported Pt x Y Alloys for the ORR Determined by RDE and Single-Cell PEMFC Measurements , J. Electrochem. Soc. 165 (2018) J3173–J3185.
https://doi.org/10.1149/2.0221815jes.

[142] N. Lindahl, E. Zamburlini, L. Feng, H. Grönbeck, M. Escudero-Escribano, I.E.L. Stephens, I. Chorkendorff, C. Langhammer, B. Wickman, High Specific and Mass Activity for the Oxygen Reduction Reaction for Thin Film Catalysts of Sputtered Pt3Y, Adv. Mater. Interfaces. 4 (2017) 1–9.
https://doi.org/10.1002/admi.201700311.

[143] P. Malacrida, M. Escudero-Escribano, A. Verdaguer-Casadevall, I.E.L. Stephens, I. Chorkendorff, Enhanced activity and stability of Pt-La and Pt-Ce alloys for oxygen electroreduction: The elucidation of the active surface phase, J. Mater. Chem. A. 2 (2014) 4234–4243. https://doi.org/10.1039/c3ta14574c.

[144] V. Stamenkovic, B.S. Mun, K.J.J. Mayrhofer, P.N. Ross, N.M. Markovic, J. Rossmeisl, J. Greeley, J.K. Nørskov, Changing the activity of electrocatalysts for oxygen reduction by tuning the surface electronic structure, Angew. Chemie - Int. Ed. 45 (2006) 2897–2901. https://doi.org/10.1002/anie.200504386.

[145] F.H.B. Lima, J. Zhang, M.H. Shao, K. Sasaki, M.B. Vukmirovic, E.A. Ticianelli, R.R. Adzic, Catalytic activity - d-band center correlation for the O2 reduction reaction on platinum in alkaline solutions, J. Phys. Chem. C. 111 (2007) 404–410. https://doi.org/10.1021/jp065181r.

[146] I.E.L. Stephens, A.S. Bondarenko, F.J. Perez-Alonso, F. Calle-Vallejo, L. Bech, T.P. Johansson, A.K. Jepsen, R. Frydendal, B.P. Knudsen, J. Rossmeisl, I. Chorkendorff, Tuning the activity of Pt(111) for oxygen electroreduction by subsurface alloying, J. Am. Chem. Soc. 133 (2011) 5485–5491.
https://doi.org/10.1021/ja111690g.

[147] V.R. Stamenkovic, B. Fowler, B.S. Mun, G. Wang, P.N. Ross, C.A. Lucas, N.M. Markovic, Improved oxygen reduction activity on Pt3Ni(111) via increased surface site availability, Science (80-.). 315 (2007) 493–497.
https://doi.org/10.1126/science.1135941.

[148] H.A. Gasteiger, S.S. Kocha, B. Sompalli, F.T. Wagner, Activity benchmarks and requirements for Pt, Pt-alloy, and non-Pt oxygen reduction catalysts for PEMFCs, Appl. Catal. B Environ. 56 (2005) 9–35.
https://doi.org/10.1016/j.apcatb.2004.06.021.

[149] G. Wu, K.L. More, C.M. Johnston, P. Zelenay, High-performance electrocatalysts for oxygen reduction derived from polyaniline, iron, and cobalt, Science (80-.). 332 (2011) 443–447. https://doi.org/10.1126/science.1200832.

[150] L.J. Wan, Lattice-confined Ru clusters for hydrogen oxidation reaction with high CO-tolerance, Sci. China Chem. 63 (2020) 1169–1170.
https://doi.org/10.1007/s11426-020-9774-3.

[151] S.J. Lee, S. Mukerjee, E.A. Ticianelli, J. McBreen, Electrocatalysis of CO

tolerance in hydrogen oxidation reaction in PEM fuel cells, Electrochim. Acta. 44 (1999) 3283–3293. https://doi.org/10.1016/S0013-4686(99)00052-3.

[152] M. Wesselmark, B. Wickman, C. Lagergren, G. Lindbergh, Hydrogen oxidation reaction on thin platinum electrodes in the polymer electrolyte fuel cell, Electrochem. Commun. 12 (2010) 1585–1588. https://doi.org/10.1016/j.elecom.2010.08.037.

[153] S.A. Vilekar, I. Fishtik, R. Datta, Kinetics of the Hydrogen Electrode Reaction, J. Electrochem. Soc. 157 (2010) B1040. https://doi.org/10.1149/1.3385391.

[154] B. Babić, J. Gulicovski, L. Gajić-Krstajić, N. Elezović, V.R. Radmilović, N. V. Krstajić, L.M. Vračar, Kinetic study of the hydrogen oxidation reaction on sub-stoichiometric titanium oxide-supported platinum electrocatalyst in acid solution, J. Power Sources. 193 (2009) 99–106. https://doi.org/10.1016/j.jpowsour.2008.11.142.

[155] S. Chen, A. Kucernak, Electrocatalysis under conditions of high mass transport: Investigation of hydrogen oxidation on single submicron Pt particles supported on carbon, J. Phys. Chem. B. 108 (2004) 13984–13994. https://doi.org/10.1021/jp048641u.

[156] N.M. Marković, B.N. Grgur, P.N. Ross, Temperature-dependent hydrogen electrochemistry on platinum low-index single-crystal surfaces in acid solutions, J. Phys. Chem. B. 101 (1997) 5405–5413. https://doi.org/10.1021/jp970930d.

[157] W. Sheng, H.A. Gasteiger, Y. Shao-Horn, Hydrogen Oxidation and Evolution Reaction Kinetics on Platinum: Acid vs Alkaline Electrolytes, J. Electrochem. Soc. 157 (2010) B1529. https://doi.org/10.1149/1.3483106.

[158] S. Gottesfeld, D.R. Dekel, M. Page, C. Bae, Y. Yan, P. Zelenay, Y.S. Kim, Anion exchange membrane fuel cells: Current status and remaining challenges, J. Power Sources. 375 (2018) 170–184. https://doi.org/10.1016/j.jpowsour.2017.08.010.

[159] J.R. Varcoe, R.C.T. Slade, Prospects for alkaline anion-exchange membranes in low temperature fuel cells, Fuel Cells. 5 (2005) 187–200. https://doi.org/10.1002/fuce.200400045.

[160] X. Ge, A. Sumboja, D. Wuu, T. An, B. Li, F.W.T. Goh, T.S.A. Hor, Y. Zong, Z. Liu, Oxygen Reduction in Alkaline Media: From Mechanisms to Recent Advances of Catalysts, ACS Catal. 5 (2015) 4643–4667. https://doi.org/10.1021/acscatal.5b00524.

[161] A. Qaseem, F. Chen, X. Wu, R.L. Johnston, Pt-free silver nanoalloy electrocatalysts for oxygen reduction reaction in alkaline media, Catal. Sci. Technol. 6 (2016) 3317–3340. https://doi.org/10.1039/c5cy02270c.

[162] M.T. Ergül, L. Türker, I. Eroğlu, An investigation on the performance optimization of an alkaline fuel cell, Int. J. Hydrogen Energy. 22 (1997) 1039–1045. https://doi.org/10.1016/s0360-3199(96)00244-3.

[163] J. Stacy, Y.N. Regmi, B. Leonard, M. Fan, The recent progress and future of oxygen reduction reaction catalysis: A review, Renew. Sustain. Energy Rev. 69 (2017) 401–414. https://doi.org/10.1016/j.rser.2016.09.135.

[164] M.G. Hosseini, P. Zardari, Electrocatalytical study of carbon supported Pt, Ru and bimetallic Pt-Ru nanoparticles for oxygen reduction reaction in alkaline media, Appl. Surf. Sci. 345 (2015) 223–231. https://doi.org/10.1016/j.apsusc.2015.03.146.

[165] K.D. Jensen, J. Tymoczko, J. Rossmeisl, A.S. Bandarenka, I. Chorkendorff, M. Escudero-Escribano, I.E.L. Stephens, Elucidation of the Oxygen Reduction Volcano in Alkaline Media using a Copper–Platinum(111) Alloy, Angew. Chemie - Int. Ed. 57 (2018) 2800–2805. https://doi.org/10.1002/anie.201711858.

[166] C.R. Raj, A. Samanta, S.H. Noh, S. Mondal, T. Okajima, T. Ohsaka, Emerging new generation electrocatalysts for the oxygen reduction reaction, J. Mater. Chem. A. 4 (2016) 11156–11178. https://doi.org/10.1039/c6ta03300h.

[167] Z.F. Pan, L. An, T.S. Zhao, Z.K. Tang, Advances and challenges in alkaline anion exchange membrane fuel cells, Prog. Energy Combust. Sci. 66 (2018) 141–175. https://doi.org/10.1016/j.pecs.2018.01.001.

[168] L. Zhang, Q. Chang, H. Chen, M. Shao, Recent advances in palladium-based electrocatalysts for fuel cell reactions and hydrogen evolution reaction, Nano Energy. 29 (2016) 198–219. https://doi.org/10.1016/j.nanoen.2016.02.044.

[169] M. Shao, Palladium-based electrocatalysts for hydrogen oxidation and oxygen reduction reactions, J. Power Sources. 196 (2011) 2433–2444. https://doi.org/10.1016/j.jpowsour.2010.10.093.

[170] M. Wang, W. Zhang, J. Wang, D. Wexler, S.D. Poynton, R.C.T. Slade, H. Liu, B. Winther-Jensen, R. Kerr, D. Shi, J. Chen, PdNi hollow nanoparticles for improved electrocatalytic oxygen reduction in alkaline environments, ACS Appl. Mater. Interfaces. 5 (2013) 12708–12715. https://doi.org/10.1021/am404090n.

[171] L. Chen, H. Guo, T. Fujita, A. Hirata, W. Zhang, A. Inoue, M. Chen, Nanoporous PdNi bimetallic catalyst with enhanced electrocatalytic performances for electro-oxidation and oxygen reduction reactions, Adv. Funct. Mater. 21 (2011) 4364–4370. https://doi.org/10.1002/adfm.201101227.

[172] J.A. Zamora Zeledón, M.B. Stevens, G.T.K.K. Gunasooriya, A. Gallo, A.T. Landers, M.E. Kreider, C. Hahn, J.K. Nørskov, T.F. Jaramillo, Tuning the electronic structure of Ag-Pd alloys to enhance performance for alkaline oxygen reduction, Nat. Commun. 12 (2021) 1–9. https://doi.org/10.1038/s41467-021-20923-z.

[173] F. Cheng, Y. Su, J. Liang, Z. Tao, J. Chen, MnO2-based nanostructures as catalysts for electrochemical oxygen reduction in alkaline media, Chem. Mater. 22 (2010) 898–905. https://doi.org/10.1021/cm901698s.

[174] I. Roche, E. Chaînet, M. Chatenet, J. Vondrák, Carbon-supported manganese oxide nanoparticles as electrocatalysts for the Oxygen Reduction Reaction (ORR) in alkaline medium: Physical characterizations and ORR mechanism, J. Phys. Chem. C. 111 (2007) 1434–1443. https://doi.org/10.1021/jp0647986.

[175] P.J. Rheinländer, J. Herranz, J. Durst, H.A. Gasteiger, Kinetics of the Hydrogen Oxidation/Evolution Reaction on Polycrystalline Platinum in Alkaline Electrolyte Reaction Order with Respect to Hydrogen Pressure, J. Electrochem. Soc. 161 (2014) F1448–F1457. https://doi.org/10.1149/2.0501414jes.

[176] P. Rheinlander, S. Henning, J. Herranz, H.A. Gasteiger, Comparing Hydrogen Oxidation and Evolution Reaction Kinetics on Polycrystalline Platinum in 0.1 M and 1 M KOH, ECS Trans. 50 (2013) 2163–2174. https://doi.org/10.1149/05002.2163ecst.

[177] Y. Cong, B. Yi, Y. Song, Hydrogen oxidation reaction in alkaline media: From mechanism to recent electrocatalysts, Nano Energy. 44 (2018) 288–303. https://doi.org/10.1016/j.nanoen.2017.12.008.

[178] L. Su, D. Gong, Y. Jin, D. Wu, W. Luo, Recent advances in alkaline hydrogen oxidation reaction, J. Energy Chem. 66 (2022) 107–122. https://doi.org/10.1016/j.jechem.2021.07.015.

[179] W. Sheng, Z. Zhuang, M. Gao, J. Zheng, J.G. Chen, Y. Yan, Correlating hydrogen oxidation and evolution activity on platinum at different pH with measured hydrogen binding energy, Nat. Commun. 6 (2015) 6–11. https://doi.org/10.1038/ncomms6848.

[180] E.S. Davydova, S. Mukerjee, F. Jaouen, D.R. Dekel, Electrocatalysts for

Hydrogen Oxidation Reaction in Alkaline Electrolytes, ACS Catal. 8 (2018) 6665–6690. https://doi.org/10.1021/acscatal.8b00689.

[181] J. Ohyama, D. Kumada, A. Satsuma, Improved hydrogen oxidation reaction under alkaline conditions by ruthenium-iridium alloyed nanoparticles, J. Mater. Chem. A. 4 (2016) 15980–15985. https://doi.org/10.1039/c6ta05517f.

[182] J. Huang, P. Li, S. Chen, Quantitative Understanding of the Sluggish Kinetics of Hydrogen Reactions in Alkaline Media Based on a Microscopic Hamiltonian Model for the Volmer Step, J. Phys. Chem. C. 123 (2019) 17325–17334. https://doi.org/10.1021/acs.jpcc.9b03639.

[183] S. Lu, Z. Zhuang, Investigating the Influences of the Adsorbed Species on Catalytic Activity for Hydrogen Oxidation Reaction in Alkaline Electrolyte, J. Am. Chem. Soc. 139 (2017) 5156–5163. https://doi.org/10.1021/jacs.7b00765.

[184] J. Durst, A. Siebel, C. Simon, F. Hasché, J. Herranz, H.A. Gasteiger, New insights into the electrochemical hydrogen oxidation and evolution reaction mechanism, Energy Environ. Sci. 7 (2014) 2255–2260. https://doi.org/10.1039/c4ee00440j.

[185] L. fan Shen, B. an Lu, X. ming Qu, J. yu Ye, J. ming Zhang, S. hu Yin, Q. hui Wu, R. xiang Wang, S. yu Shen, T. Sheng, Y. xia Jiang, S. gang Sun, Does the oxophilic effect serve the same role for hydrogen evolution/oxidation reaction in alkaline media?, Nano Energy. 62 (2019) 601–609. https://doi.org/10.1016/j.nanoen.2019.05.045.

[186] J. Zheng, W. Sheng, Z. Zhuang, B. Xu, Y. Yan, Universal dependence of hydrogen oxidation and evolution reaction activity of platinum-group metals on pH and hydrogen binding energy, Sci. Adv. 2 (2016) 1–9. https://doi.org/10.1126/sciadv.1501602.

[187] J. Hu, K.A. Kuttiyiel, K. Sasaki, C. Zhang, R.R. Adzic, Determination of Hydrogen Oxidation Reaction Mechanism Based on Pt−H ad Energetics in Alkaline Electrolyte , J. Electrochem. Soc. 165 (2018) J3355–J3362. https://doi.org/10.1149/2.0471815jes.

[188] Y. Wang, G. Wang, G. Li, B. Huang, J. Pan, Q. Liu, J. Han, L. Xiao, J. Lu, L. Zhuang, Pt-Ru catalyzed hydrogen oxidation in alkaline media: Oxophilic effect or electronic effect?, Energy Environ. Sci. 8 (2015) 177–181. https://doi.org/10.1039/c4ee02564d.

[189] M. Alesker, M. Page, M. Shviro, Y. Paska, G. Gershinsky, D.R. Dekel, D. Zitoun, Palladium/nickel bifunctional electrocatalyst for hydrogen oxidation reaction in alkaline membrane fuel cell, J. Power Sources. 304 (2016) 332–339. https://doi.org/10.1016/j.jpowsour.2015.11.026.

[190] M.T.M. Koper, Hydrogen electrocatalysis: A basic solution, Nat. Chem. 5 (2013) 255–256. https://doi.org/10.1038/nchem.1600.

[191] S.M. Rossnagel, Thin film deposition with physical vapor deposition and related technologies, J. Vac. Sci. Technol. A Vacuum, Surfaces, Film. 21 (2003) S74–S87. https://doi.org/10.1116/1.1600450.

[192] I. Safi, Recent aspects concerning DC reactive magnetron sputtering of thin films: A review, Surf. Coatings Technol. 127 (2000) 203–218. https://doi.org/10.1016/s0257-8972(00)00566-1.

[193] Y.S. Jung, J.Y. Seo, D.W. Lee, D.Y. Jeon, Influence of DC magnetron sputtering parameters on the properties of amorphous indium zinc oxide thin film, Thin Solid Films. 445 (2003) 63–71. https://doi.org/10.1016/j.tsf.2003.09.014.

[194] X.X. Wang, V. Prabhakaran, Y. He, Y. Shao, G. Wu, Iron-Free Cathode Catalysts for Proton-Exchange-Membrane Fuel Cells: Cobalt Catalysts and the

Peroxide Mitigation Approach, Adv. Mater. 31 (2019) 1–18. https://doi.org/10.1002/adma.201805126.

[195] J. Greeley, M. Mavrikakis, Surface and subsurface hydrogen: Adsorption properties on transition metals and near-surface alloys, J. Phys. Chem. B. 109 (2005) 3460–3471. https://doi.org/10.1021/jp046540q.

[196] A. Kongkanand, M.F. Mathias, The Priority and Challenge of High-Power Performance of Low-Platinum Proton-Exchange Membrane Fuel Cells, J. Phys. Chem. Lett. 7 (2016) 1127–1137. https://doi.org/10.1021/acs.jpclett.6b00216.

[197] M. Roca-Ayats, M.D. Roca-Moreno, M. V. Martínez-Huerta, Optimization of alkaline catalytic inks for three-electrode electrochemical half-cell measurements, Int. J. Hydrogen Energy. 41 (2016) 19656–19663. https://doi.org/10.1016/j.ijhydene.2016.06.168.

[198] E.J. Park, S. Maurya, A.S. Lee, D.P. Leonard, D. Li, J.Y. Jeon, C. Bae, Y.S. Kim, How does a small structural change of anode ionomer make a big difference in alkaline membrane fuel cell performance?, J. Mater. Chem. A. 7 (2019) 25040–25046. https://doi.org/10.1039/c9ta10157h.

[199] D. Li, H.T. Chung, S. Maurya, I. Matanovic, Y.S. Kim, Impact of ionomer adsorption on alkaline hydrogen oxidation activity and fuel cell performance, Curr. Opin. Electrochem. 12 (2018) 189–195. https://doi.org/10.1016/j.coelec.2018.11.012.

[200] A.R.B. Levy, M. Boudart, S. Science, N. Series, N. Aug, Platinum-Like Behavior of Tungsten Carbide in Surface Catalysis Published by : American Association for the Advancement of Science Stable URL : http://www.jstor.com/stable/1736506 Platinum-Like Behavior of Tungsten Carbide in Surface Cat, 181 (1973) 547–549.

[201] N.R. Elezović, B.M. Babić, L. Gajić-Krstajić, P. Ercius, V.R. Radmilović, N. V. Krstajić, L.M. Vračar, Pt supported on nano-tungsten carbide as a beneficial catalyst for the oxygen reduction reaction in alkaline solution, Electrochim. Acta. 69 (2012) 239–246. https://doi.org/10.1016/j.electacta.2012.02.105.

[202] H. Meng, P.K. Shen, Tungsten carbide nanocrystal promoted Pt/C electrocatalysts for oxygen reduction, J. Phys. Chem. B. 109 (2005) 22705–22709. https://doi.org/10.1021/jp054523a.

[203] A. Ly, T. Asset, P. Atanassov, Integrating nanostructured Pt-based electrocatalysts in proton exchange membrane fuel cells, J. Power Sources. 478 (2020) 228516. https://doi.org/10.1016/j.jpowsour.2020.228516.

[204] Y. Garsany, O.A. Baturina, K.E. Swider-Lyons, S.S. Kocha, Experimental methods for quantifying the activity of platinum electrocatalysts for the oxygen reduction reaction, Anal. Chem. 82 (2010) 6321–6328. https://doi.org/10.1021/ac100306c.

[205] K. Ehelebe, N. Schmitt, G. Sievers, A.W. Jensen, A. Hrnjić, P. Collantes Jiménez, P. Kaiser, M. Geuß, Y.P. Ku, P. Jovanovič, K.J.J. Mayrhofer, B. Etzold, N. Hodnik, M. Escudero-Escribano, M. Arenz, S. Cherevko, Benchmarking Fuel Cell Electrocatalysts Using Gas Diffusion Electrodes: Inter-lab Comparison and Best Practices, ACS Energy Lett. 7 (2022) 816–826. https://doi.org/10.1021/acsenergylett.1c02659.

[206] M. Inaba, A.W. Jensen, G.W. Sievers, M. Escudero-Escribano, A. Zana, M. Arenz, Benchmarking high surface area electrocatalysts in a gas diffusion electrode: Measurement of oxygen reduction activities under realistic conditions, Energy Environ. Sci. 11 (2018) 988–994. https://doi.org/10.1039/c8ee00019k.

[207] K. Ehelebe, D. Seeberger, M.T.Y. Paul, S. Thiele, K.J.J. Mayrhofer, S. Cherevko, Evaluating Electrocatalysts at Relevant Currents in a Half-Cell: The

Impact of Pt Loading on Oxygen Reduction Reaction, J. Electrochem. Soc. 166 (2019) F1259–F1268. https://doi.org/10.1149/2.0911915jes.

[208] Paul van der Heide, X-ray Photoelectron Spectrocopy: An Introduction to Principles and Practices, John Wiley & Sons, Ltd., 2012.

[209] and K.D.B. J. F. Moulder, W. F. Stickle, P. E. Sobol, Handbook of x-ray photoelectron spectroscopy: a reference book of standard spectra for indentification and interpretation of XPS data, 1995.

[210] S. Hiifner, Photoelectron Spectroscopy: Principles and Applications, 3rd Editio, Springer US, 2003.

[211] J. Schnadt, J. Knudsen, N. Johansson, Present and new frontiers in materials research by ambient pressure x-ray photoelectron spectroscopy, J. Phys. Condens. Matter. 32 (2020). https://doi.org/10.1088/1361-648X/ab9565.

[212] Scanning Electron Microscopy 1928 – 1965 *, 17 (1995) 175–185.

[213] K.C.A. Smith, C.W. Oatley, The scanning electron microscope and its fields of application, Br. J. Appl. Phys. 6 (1955) 391–399. https://doi.org/10.1088/0508-3443/6/11/304.

[214] G.E.M. Jauncey, The Scattering of X-Rays and Bragg's Law, Proc. Natl. Acad. Sci. 10 (1924) 57–60. https://doi.org/10.1073/pnas.10.2.57.

[215] M. Escudero-Escribano, A. Verdaguer-Casadevall, P. Malacrida, U. Grønbjerg, B.P. Knudsen, A.K. Jepsen, J. Rossmeisl, I.E.L. Stephens, I. Chorkendorff, Pt5Gd as a highly active and stable catalyst for oxygen electroreduction, J. Am. Chem. Soc. 134 (2012) 16476–16479. https://doi.org/10.1021/ja306348d.